Junior Professor for Machine Learning on Graphs

RWTH AACHEN UNIVERSITY

The present work was submitted to the Machine Learning on Graphs Group at the Chair of Computer Science 6, RWTH Aachen University

A Theoretical and Empirical Investigation into the Equivalence of Graph Neural Networks and the Weisfeiler-Leman Algorithm

From the Faculty of Mathematics, Physics, and Computer Science approved for the purpose of obtaining the academic degree of Bachelor of Sciences.

Eric Tillmann Bill

Supervisor:
Prof. Dr. rer. nat. Christopher Morris

Machine Learning on Graphs Group
RWTH Aachen University

August, 2023

Abstract

Graphs are omnipresent data structures that model complex relationships in diverse fields, ranging from social networks and biological systems to recommendation engines and knowledge graphs. The inherent flexibility of graph data presents a challenge for machine learning, as it lacks the constraints found in other data formats like images and text. In recent years, Graph Neural Networks (GNNs) have emerged as a promising approach for analyzing graphs, showing exceptional empirical performance in various tasks. However, while their theoretical expressiveness has been studied thoroughly, a comprehensive understanding of the representations they learn remains limited.

This thesis addresses the need to gain deeper insights into the representations learned by GNNs. To this end, we introduce a novel framework named 1-WL+NN, which combines the Weisfeiler-Leman algorithm (1-WL) with a feedforward neural network. The 1-WL+NN framework serves as a powerful tool to study GNNs by enabling a comparison of their learned representations.

Empirical experiments conducted on various datasets reveal intriguing findings. Firstly, 1-WL+NN models achieve comparable performance to GNN models and even outperform them on certain datasets. Secondly, 1-WL+NN models tend to exhibit more pronounced overfitting, attributed to the expressive nature of the 1-WL algorithm. Both 1-WL+NN and GNN models primarily rely on the information computed by a single iteration of the 1-WL algorithm, suggesting a trade-off between expressiveness and efficiency. Additionally, graph representations inferred by GNN models demonstrate better linear separability and clustering compared to 1-WL+NN models.

In conclusion, this thesis contributes to the understanding of GNN representations and highlights the potential of the 1-WL+NN framework as an analysis tool. The empirical insights gained from our experiments shed light on the inner workings of GNN models, paving the way for further advancements in graph representation learning research.

Acknowledgements

I want to express my gratitude to the people who helped me throughout this thesis. Their support and guidance made a huge difference, and I am genuinely thankful for their assistance.

First and foremost, I am extremely grateful for my esteemed supervisors, Christopher Morris and Luis Müller. Together, they formed a great team that not only introduced me to this captivating research field but also provided me with a research question that aligns perfectly with my passion. Their valuable insights, constant encouragement, and belief in my abilities have been the driving force behind this thesis.

In particular, I want to thank Christopher for his dedication and generosity in sharing his time and knowledge despite his commitments as a full-time professor. His responsiveness to my questions, provision of supplementary materials, and flexibility for meetings were invaluable throughout the entire thesis.

Additionally, I want to thank Luis Müller for being a sort of mentor for me. His guidance on best practices for empirical investigations in this research field, creative ideas for experiment setups along with his thorough proofreading and constructive feedback, have significantly enhanced the academic rigor of this work.

The most fruitful moments of this journey were undoubtedly the countless meetings with both Christopher and Luis. Through these discussions, we explored the progress of my thesis, addressed theoretical limitations in the proofs, and delved into intermediate empirical results and their interpretations. Each interaction left me with renewed motivation, making the overall pursuit of this thesis a challenging yet profoundly enjoyable experience.

I also want to thank the RWTH Aachen High Performance Computing cluster for providing the necessary computational resources for my experiments. Without these resources, the research goals of my thesis would not have been possible.

Lastly, I want to thank my parents and family for their unwavering support throughout my studies. Their encouragement means a lot to me and has been a great source of motivation.

Contents

1. Introduction

This work aims to shed light on the representations learned by Graph Neural Networks. In this section, we will discuss the prevalence of graphs and the crucial role GNNs play in analyzing them. We will delve into the methods we use to gain insights and highlight the significance of our approach. Lastly, we will provide an overview of the structure of this work.

1.1. Motivation

Graphs are ubiquitous in various fields of life. Despite not always being explicitly identified as such, the graph data model's flexibility and simplicity make it an effective tool for modeling a diverse range of data. Examples of graph modeling applications include unexpected instances, such as modeling text or images as a graph, as well as more complex instances like chemical molecules, citation networks, or connectivity encodings of the World Wide Web Morris et al. [2020], Scarselli et al. [2009].

Although machine learning has achieved remarkable success with image classification (e.g., Zoph et al. [2018], He et al. [2016]) and text generation (e.g., Radford et al. [2019], Brown et al. [2020]) in the last decade, the lack of a significant breakthrough in machine learning for graphs can be attributed to the graph data model's inherent flexibility and simplicity. While, for example, an image classifier constrains its input data to be a grid-like image or a text generator expects its input to be a linear sequence of words, machine learning models working on graphs cannot leverage any constraints on the format or size of their input graphs without limiting their generality.

To put this flexibility of the graph data model into perspective and give an idea of how ubiquitous graphs are in various fields, we refer back to the examples of image classifiers and text generators and demonstrate how seemingly natural the graph data model can encode their input data. For example, images can be encoded by a graph, such that each pixel of the image corresponds to a node in the graph holding its color value, and each node is connected to its neighboring pixel nodes. Similarly, for sequential data like text files, one can encode a directed graph where each word in this file is represented as a node with the word as a feature and connected outgoingly to the next following word. See Figure 1.1 for an illustrative example of these encodings.

In recent years, a significant amount of research has been conducted to investigate Graph Neural Networks (GNNs). Among the most promising approaches are those utilizing the message-passing architecture, which was introduced by Scarselli et al. [2009] and Gilmer et al. [2017]. Empirically, this framework has demonstrated strong performance across various applications Kipf and Welling [2017], Hamilton et al. [2017], Xu et al. [2019]. However, its expressiveness is limited, as has been proved by the works of Morris et al. [2019], as well as Xu et al. [2019]. These works establish a connection to the Weisfeiler-Leman[1] algorithm (1-WL), originally proposed

[1]Based on https://www.iti.zcu.cz/wl2018/pdf/leman.pdf, we will use the spelling "Leman" here, as requested by A. Leman, the co-inventor of the algorithm.

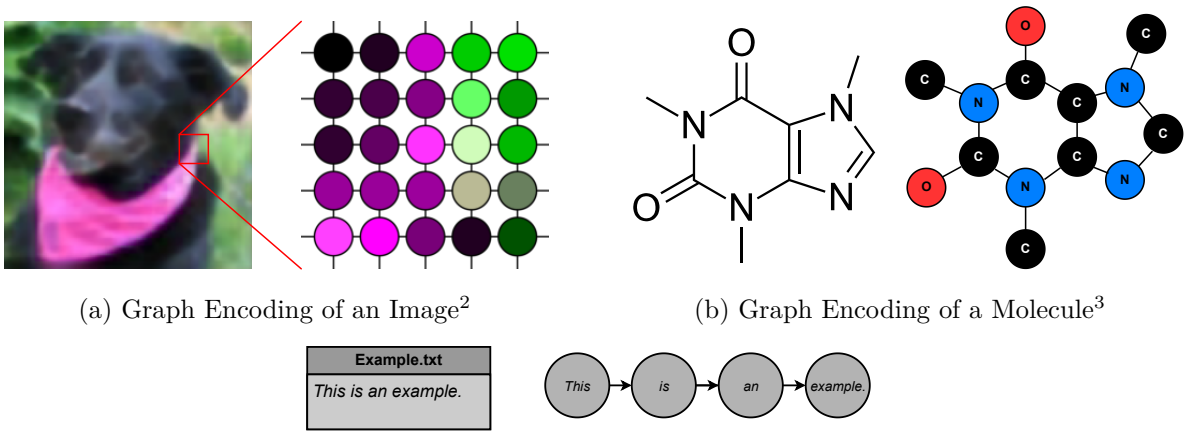

(a) Graph Encoding of an Image[2]

(b) Graph Encoding of a Molecule[3]

(c) Graph Encoding of a Text File.

Figure 1.1.: An overview of three examples of how graphs can be used to encode information across different domains. For each example, the conventional domain-specific encodings are visualized on the left, while on the right, we showcase how a graph can encode the same information. Note that these examples are just a sample; in actual practice, more detailed encodings are usually utilized to capture additional information.[4]

by Weisfeiler and Leman [1968] as a simple heuristic for the graph isomorphism problem. In particular, it has been proven that a GNN based on the message-passing architecture can, at most, be as good as the 1-WL algorithm in distinguishing non-isomorphic graphs. Furthermore, the 1-WL method demonstrates numerous similarities with the fundamental workings of the GNN architecture. It is, therefore, commonly believed that both methods are, to some extent, equivalent in their capacity to capture information in a graph.

Despite the remarkable empirical performance of GNNs, particularly compared to conventional graph kernel functions Morris et al. [2020], and the theoretical understanding of their ability to distinguish non-isomorphic graphs, there remains a limited understanding of the learned representations that drive this empirical success. This work aims to delve into these representations, seeking deeper insights into the factors contributing to the efficacy of GNNs.

1.2. Methodology and Contributions

In this work, we introduce a novel framework we coined "1-WL+NN," which involves applying the 1-WL algorithm to an input graph and further processing the resulting information using a feedforward neural network. Thereby, we obtain a trainable framework suited for all kinds of graph-related tasks, such as graph classification, node regression, and more. We will prove that both frameworks, 1-WL+NN and GNN, are theoretically equivalent, such that each function computed by a 1-WL+NN model can also be computed by a GNN model and vice versa.

The key characteristic of this novel framework lies in its contrasting learning behavior compared to GNNs. A 1-WL+NN model computes a maximally informative representation of

[2]The image of a dog is from the CIFAR-10 collection made available by Krizhevsky et al. [2009].
[3]The illustration of the skeletal formula of caffeine is taken from https://commons.wikimedia.org.
[4]All graphics were created using the free open source platform https://www.draw.io.

its input graph through the 1-WL algorithm, while the feedforward neural network then learns to extract the essential information from this representation to make accurate predictions. In contrast, a GNN operates the other way around, first learning to compute good representations of a graph effectively and then utilizing this knowledge for making predictions. Despite these differences in learning behaviors, both methods can compute the same functions, making their empirical performance comparison highly intriguing.

To gain deeper insights into the representations learned by GNNs, we conduct various empirical experiments, comparing both frameworks on multiple datasets. This exploration allows us to better understand the capabilities and limitations of GNNs and shed light on the effectiveness of the 1-WL+NN framework as a tool for studying graph neural networks.

Maybe continue from here a bit more

1.3. Outline

For ease of readability, we split this work into two parts. The first part investigates and establishes the theoretical equivalence between the frameworks of 1-WL+NN and GNNs. In contrast, the second part presents our different experiments and their empirical results, in which we use the 1-WL+NN framework to analyze the representation learned by a GNN.

In detail, in Chapter 2, we will discuss related work, milestones in GNNs over the past decade, essential properties of the 1-WL algorithm, and a subset of interesting connections between GNNs and the 1-WL algorithm.

Afterward, we will start with Part I, which begins with Chapter 3. Here, we will introduce formal definitions for both frameworks, as well as a set of notations we will use throughout the theoretical part. Preceding, in Chapter 4, we will introduce and prove two theorems that each present a connection between both frameworks and combined prove the equivalence of both frameworks.

The second part is dedicated to our empirical experiments. We begin with Chapter 5, explaining the experimental setup and our experiment choices. In detail, we will discuss the choice of benchmarking datasets, GNN models, and 1-WL+NN models, along with an explanation of our general testing procedure. In Chapter 6, we present the results of our experiments and delve into further analyses of certain aspects of GNN and 1-WL+NN models. In particular, we will investigate the representations computed by GNNs and try to infer common patterns that occurred across multiple datasets. Finally, the thesis concludes with a final discussion in Chapter 7, where we summarize our findings, address the limitations of this work, and offer recommendations for future research.

2. Background and Related Work

In this chapter, we will briefly introduce the foundation of our research by explaining the origins of the two frameworks, mentioning important recent advances, and providing a brief overview of the connections between them.

2.1. Weisfeiler-Leman Algorithm

The (1-dimensional) Weisfeiler-Leman algorithm (1-WL), proposed by Weisfeiler and Leman [1968], was initially designed as a simple heuristic for the *graph isomorphism problem*, but due to its interesting properties, its simplicity, and its good performance, the 1-WL algorithm gained much attention from researchers across many fields. One of the most noticeable properties is that the algorithm color codes the nodes of the input graph in such a way that in each iteration, each color encodes a learned local substructure.

This algorithm functions by assigning the same color to all nodes that meet two criteria: 1) they already share the same color, and 2) each color appears equally often in the set of the node's direct neighbors. The algorithm continues until the number of colors changes in each iteration. For determining whether two graphs are non-isomorphic, the heuristic is applied to both graphs simultaneously. The heuristic concludes that the graphs are non-isomorphic as soon as the number of occurrences of a color differs between them. We present a more formal definition of the algorithm in the following part in Section 3.4.

Since the *graph isomorphism problem* is difficult to solve due to the best known complete algorithm only running in deterministic quasipolynomial time (Babai [2016]), the 1-WL algorithm, running in deterministic polynomial time, cannot solve the problem completely. Moreover, Cai et al. [1992] constructed counterexamples of non-isomorphic graphs that the heuristic fails to distinguish, e.g., see Figure 3.2. However, following the work of Babai and Kucera [1979], this simple heuristic is still quite powerful and has a very low probability of failing to distinguish non-isomorphic graphs when both graphs are uniformly chosen at random as the number of nodes tends to infinity.

To overcome the limited expressiveness of the 1-WL algorithm, it has been generalized to the k-dimensional Weisfeiler-Leman algorithm (k-WL) by Babai [1979, 2016], as well as Immerman and Lander [1990][5]. This version works with k-tuples over the k-ary Cartesian product of the set of nodes. Interestingly, this created a hierarchy for the expressiveness of determining non-isomorphism, such that for all $k \in \mathbb{N}$ there exists a pair of non-isomorphic graphs that can be distinguished by the $(k+1)$-WL but not by the k-WL (Cai et al. [1992]).

[5] In Babai [2016] on page 27, László Babai explains that he, together with Rudolf Mathon, first introduced this algorithm in 1979. He adds that the work of Immerman and Lander [1990] introduced this algorithm independently of him.

2.2. Graph Neural Networks

The idea of leveraging machine learning techniques, previously proven effective in various domains, for graph-related tasks has been a well-established topic in the literature for the past decades. However, researchers faced challenges in effectively adapting these techniques to graphs of diverse sizes and complexities in the early stages. Notably, the works by Sperduti and Starita [1997], Scarselli et al. [2008], and Micheli [2009] were the first prominent examples of successful applications in this regard.

However, it was not until the emergence of more advanced models that the scientific community truly recognized the significance and potential of Graph Neural Networks (GNNs). Noteworthy among these advancements were the work of Duvenaud et al. [2015], who introduced a differentiable approach for generating unique fingerprints of arbitrary graphs, as well as Li et al. [2015], who applied gated recurrent units to capture graphs of various sizes, while Atwood and Towsley [2016] utilized diffusional convolutions for the same purpose. Of particular significance, however, were the contributions of Bruna et al. [2013], Defferrard et al. [2016] and Kipf and Welling [2017], which extended the concept of convolution from its traditional application on images to the domain of arbitrary graphs.

After the early success of these GNN models, Gilmer et al. [2017] introduced a unified architecture for GNNs. The authors observed a recurring pattern in how information is exchanged and processed among many of these works, including many mentioned in the paragraph above. Leveraging these observations, Gilmer et al. [2017] devised the message-passing architecture as a generalized framework for GNNs. Models using this architecture can be referred to as Message-Passing-Neural-Network (MPNN); however, throughout this thesis, we will use the term GNN and MPNN interchangeably, as the focus of this thesis is solely on the message-passing architecture. This architecture uses the input graph as its basis for computation and computes new node features for the graph in each layer. The computation of each new node feature involves aggregating all the features of the neighboring nodes and the node's own feature. After applying each layer of a GNN model, a representation of the entire graph is obtained by applying a pooling function (e.g. Ying et al. [2018]). This representation is then further processed by common machine learning techniques like a multilayer perceptron for the final output. We will present a more formal definition of this architecture in the following part in Section 3.6; however, important to note is that the information exchange in the graph across nodes is limited to a one-hop neighbor per layer.

With this general framework and the empirical success of some models using this message-passing architecture, the question of how expressive models based on this architecture can be gained a lot of attention in the scientific community. Many papers immediately established connections to the 1-WL algorithm, among the most prominent being Morris et al. [2019] and Xu et al. [2019]. These connections seem natural, as both methods share similar properties in terms of how they process graph data. Most strikingly, both methods never change the graph structurally since they only compute new node features in each iteration. Moreover, both methods use a one-hop neighborhood aggregation as the basis for computing the new node feature. Following this intuition, Morris et al. [2019], as well as Xu et al. [2019], showed that the expressiveness of GNNs is upper-bounded by the 1-WL in terms of distinguishing non-isomorphic graphs. Moreover, Morris et al. [2019] proposed a new k-GNN architecture that operates over the set of subgraphs of size k. Interestingly, Geerts [2020] has shown that this architecture imposes a hierarchy over $k \in \mathbb{N}$ that is equivalent to the k-WL hierarchy in terms of its ability to distinguish non-isomorphic graphs, i.e., if there is a k-GNN that can distinguish

two non-isomorphic graphs, it is equivalent to say that the k-WL algorithm can also distinguish these graphs.

Although there are other modifications of the message-passing architecture besides the theoretical concept of k-GNN to increase the expressiveness of GNNs in terms of distinguishing non-isomorphism, e.g., using node identifiers Vignac et al. [2020], adding random node features Sato et al. [2021], Abboud et al. [2020], adding directed flows Beaini et al. [2021] and many more. Relatively few works have been published that attempt to understand the representation learned from a standard GNN.

Notable works include Nikolentzos et al. [2023b], where the authors, in addition to the normal learning process, optimized GNNs to preserve a notion of distance in their representation and examined the effectiveness of GNNs in utilizing such representations. However, their insights can only be applied to these specially trained GNN models and not be generalized. In another publication, Nikolentzos et al. [2023a] presented mathematical proof and empirical confirmation showing how much structural information is encoded by modern GNN models. Their research highlights that GNN models like DGCNN (Zhang et al. [2018]) and GAT (Veličković et al. [2017]) encode all nodes with the same feature vector, while in contrast, models like GCN (Kipf and Welling [2017]) and GIN (Xu et al. [2019]) encode nodes after k layers of message-passing with features that relate with the number of walks of length k over the input graph form each node, disregarding the local structure within the nodes are contained.

Part I.

Theoretical Equivalence

This part of the thesis focuses on the equivalence between 1-WL+NN and GNN. We will begin by providing a preliminary section that formalizes all the concepts used in the proof and introduces a general notation. Afterward, we will dedicate a separate section to present and prove two theorems, which combined conclude the equivalence.

3. Preliminaries

This section will introduce and formalizes all concepts used throughout the proof and the rest of the thesis. We start with general notations, introduce a general definition of graphs and multilayer perceptrons, and familiarize the reader with the Weisfeiler-Leman algorithm. We will introduce each framework independently, first the 1-WL+NN and then GNN. In the end, we will briefly introduce important properties of collections of functions computed by both methods.

3.1. General Notation

Let $\mathbb{N}$ denote the set of natural numbers such that $\mathbb{N} := \{0, 1, 2, \ldots\}$. By $[n]$, we denote the set $\{0, \ldots, n\} \subset \mathbb{N}$ for each $n \in \mathbb{N}$. Further, with $\{\!\{\ldots\}\!\}$, we denote a multiset formally defined as a 2-tuple (X, m), where X is a set of all unique elements and $m : X \to \mathbb{N}_{\geq 1}$ a mapping that maps each element in X to the number of its occurrences in the multiset.

3.2. Graphs

We will briefly introduce a formal definition for graphs and coloring on graphs. Starting with the definition of a graph.

Definition 1 (Graph)**.** A graph G is defined as a 3-tuple denoted by $G := (V, E, l)$. This tuple consists of a set of nodes $V \subset \mathbb{N}$, a set of edges $E \subseteq V \times V$, and a labeling function $l : M \to \Sigma$. The domain M of the labeling function can be either V, $V \cup E$, or E, and the codomain Σ is an alphabet with $\Sigma \subseteq \mathbb{N}^k$, where $k \in \mathbb{N}_{\geq 1}$ is arbitrary. In the context of this thesis, the assigned values by the labeling function are referred to as either labels or features, depending on the dimension of Σ. In detail, if $k = 1$, we usually refer to the values as labels, otherwise as features. Additionally, the set of all graphs is denoted by $\mathcal{G}$.

Furthermore, a graph G can be either directed or undirected based on the definition of its set of edges E. If $E \subseteq \{(v, u) \mid v, u \in V\}$, it represents a directed graph, whereas if $E \subseteq \{(v, u) \mid v, u \in V, v \neq u\}$ such that for every $(v, u) \in E$ there exists $(u, v) \in E$, it defines an undirected graph. Additionally, for ease of notation, we will use $V(G)$ and $E(G)$ to denote the set of nodes and the set of edges of G, respectively, as well as l_G to denote the label function of G. Further, with $\mathcal{N}(v)$ for $v \in V(G)$ we denote the set of neighbors of v defined as $\mathcal{N}(v) := \{u \mid (u, v) \in E(G)\}$, and with $d(v)$ for $v \in V(G)$ the degree of node v, defined as $d(v) := |\mathcal{N}(v)|$.

We continue with the definition of a graph coloring.

Definition 2 (Graph Coloring)**.** A coloring of a Graph G is a function $C : V(G) \to \mathbb{N}$ that assigns each node in the graph a color (here, a positive integer). Further, a coloring C induces a partition $\mathcal{P}$ on the set of nodes, for which we define C^{-1} being the function that maps each color $c \in \mathbb{N}$ to its class of nodes with $C^{-1}(c) = \{v \in V(G) \mid C(v) = c\}$. In addition, we define $\text{hist}_{G,C}$ as the histogram of graph G with coloring C that maps every color in the image of C under $V(G)$ to the number of occurrences. In detail, $\forall c \in \mathbb{N} : \text{hist}_{G,C}(c) \coloneqq |\{v \in V(G) \mid C(v) = c\}| = |C^{-1}(c)|$.

Permutation-invariance and -equivariance

We use S_n to denote the symmetric group over the elements $[n]$ for any $n \in \mathbb{N}$. S_n consists of all permutations over these elements. Let G be a graph with $V(G) = [n]$, applying a permutation $\pi \in S_n$ on G, is defined as $G_\pi \coloneqq \pi \cdot G$ where $V(G_\pi) = \{\pi(0), \ldots, \pi(n)\}$ and $E(G_\pi) = \{(\pi(v), \pi(u)) \mid (v, u) \in E(G)\}$. We will now introduce two key concepts for classifying functions on graphs.

Definition 3 (Permutation Invariant)**.** Let $f : \mathcal{G} \to \mathcal{Y}$ be an arbitrary function, then f is *permutation-invariant* if and only if for all $G \in \mathcal{G}$, where $n_G \coloneqq |V(G)|$ and for every $\pi \in S_{n_G}$: $f(G) = f(\pi \cdot G)$.

Definition 4 (Permuation Equivariant)**.** Let $f : \mathcal{G} \to \mathcal{Y}$ be an arbitrary function, then f is *permuation-equivariant* if and only if for all $G \in \mathcal{G}$, where $n_G \coloneqq |V(G)|$ and for every $\pi \in S_{n_G}$: $f(G) = \pi^{-1} \cdot f(\pi \cdot G)$.

3.3. Multilayer Perceptrons

In the following, we give a formal definition of multilayer perceptrons. These functions are also known as feedforward neural networks in the literature. However, for the remainder of this thesis, we will refer to them as multilayer perceptrons.

Definition 5 (Multilayer Perceptron)**.** Multilayer perceptrons are a class of functions from $\mathbb{R}^n$ to $\mathbb{R}^m$, where $n, m \in \mathbb{N}_{\geq 1}$ are free to choose. In this thesis, we define a multilayer perceptron as a finite sequence, such that a multilayer perceptron MLP is defined as $\mathsf{MLP} \coloneqq (\mathsf{MLP})_{t \in [T]}$ where T is the number of layers. For every $t \in [T]$, the t.th layer of the MLP is the t.th item in the finite sequence $(\mathsf{MLP})_t$. Further, all layers are recursively defined on any input v as:

$$
\begin{aligned}
(\mathsf{MLP})_0(v) &\coloneqq v \\
(\mathsf{MLP})_{t+1}(v) &\coloneqq \sigma_t(W_t \cdot (\mathsf{MLP})_t(v) + b_t), \quad \forall t \in [T-1]
\end{aligned}
$$

where σ_t is an element wise activation function, W_t is the weight matrix and b_t the bias vector of layer t. Note, that for each W_t, the succeeding W_{t+1} must have the same number of columns as W_t has rows, in order to be well-defined. Similarly, for every layer t, W_t and b_t have to have the same number of rows. Following this definition, when applying a MLP on an input $v \in \mathbb{R}^n$ it is defined as $\mathsf{MLP}(v) \coloneqq (\mathsf{MLP})_T(v)$.

3.4. Weisfeiler and Leman Algorithm

The Weisfeiler-Leman algorithm consists of two main parts: the coloring algorithm and the graph isomorphism test. We will introduce each part individually and present some implications afterward.

The Weisfeiler-Leman Graph Coloring Algorithm

The 1-WL algorithm computes a node coloring of its input graph in each iteration. In detail, a color is assigned to each node based on the colors of its neighbors and its own current color. The algorithm continues until convergence is reached, resulting in the final coloring of the graph. We will now formally define this procedure and provide an illustrative example in Figure 3.1.

Definition 6 (1-WL Algorithm)**.** Let $G = (V, E, l)$ be a labeled graph. In each iteration i, the 1-WL algorithm computes a node coloring $C_i : V(G) \to \mathbb{N}$. In the initial iteration $i = 0$, the coloring is set to $C_0 = l$ if l exists. Otherwise, for all $v \in V(G) : C_0(v) = c$ with $c \in \mathbb{N}$ being an arbitrary but fixed constant. For $i > 0$, the algorithm assigns a color to $v \in V(G)$ as follows:

$$C_i(v) = \mathsf{RELABEL}(C_{i-1}(v),\ \{\!\{C_{i-1}(u) \mid u \in \mathcal{N}(v)\}\!\}),$$

where RELABEL injectively maps the above pair to a unique, previously not used, color. The algorithm terminates when the number of colors between two iterations does not change, meaning the algorithm terminates after iteration i if the following condition is satisfied:

$$\forall v, w \in V(G) : C_i(v) = C_i(w) \iff C_{i+1}(v) = C_{i+1}(w).$$

Upon terminating we define $C_\infty \coloneqq C_i$ as the stable coloring, such that $\text{1-WL}(G) \coloneqq C_\infty$.

The colorings computed in each iteration always converge to the final one, such that the algorithm always terminates. In more detail, Grohe [2017] showed that it always holds after at most $|V(G)|$ iterations. For an illustration of this algorithm, see Figure 3.1. Moreover, based on the work of Paige and Tarjan [1987] about efficient refinement strategies, Cardon and Crochemore [1982] proved that the stable coloring C_∞ can be computed in time $\mathcal{O}(|V(G)| + |E(G)| \cdot \log |V(G)|)$.

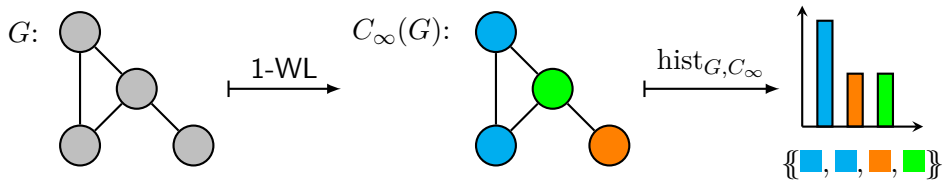

Figure 3.1.: An example of the final coloring computed by applying the 1-WL algorithm on the graph G. The graph G consists of 4 nodes with all their labels being set to the same color.

It is important to understand that since the algorithm was originally developed as a simple heuristic for the *graph isomorphism problem*, which is an inherently discrete problem, the 1-WL algorithm in its simplest form, as we presented it here, does only work on graphs with discrete, one-dimensional node labels. Although it is quite easy to adapt the algorithm to respect discrete edge labels of a graph by using them as weights in the neighborhood aggregation (Shervashidze et al. [2011]), modifying its definition to work with continuous graph features is more complex. Numerous proposed modifications have been put forward to address this integration in the literature, such as those discussed by Morris et al. [2016]. However, note that this particular topic will not be further investigated in this thesis, although its mention holds value for Part II.

The Weisfeiler-Leman Graph Isomorphism Test

The isomorphism test uses the 1-WL coloring algorithm and is defined as follows.

Definition 7 (1-WL Isomorphism Test)**.** To determine if two graphs $G, H \in \mathcal{G}$ are non-isomorphic ($G \ncong H$), one applies the 1-WL coloring algorithm on both graphs "in parallel" and checks after each iteration if the occurrences of each color are equal, else the algorithm would terminate and conclude non-isomorphic. Formally, the algorithm concludes non-isomorphic in iteration i if there exists a color c such that:

$$|\{v \in V(G) \mid C_i(v) = c\}| \neq |\{w \in V(H) \mid C_i(w) = c\}|.$$

Note that this test is only sound and not complete for the *graph isomorphism problem*. Counterexamples can be easily constructed where the algorithm fails to distinguish non-isomorphic graphs. See Figure 3.2 for a straightforward example of where this test fails that was discovered and proven by Cai et al. [1992].

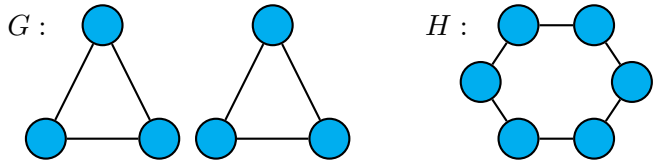

Figure 3.2.: This is an example of two graphs G and H that are non-isomorphic but cannot be distinguished by the 1-WL isomorphism test.

Implications of the 1-WL Algorithm

One implication of the 1-WL algorithm and its isomorphism test is that, due to it not being complete for solving the *graph isomorphism problem*, it gives rise to a related but weaker relation than the isomorphism relation ($\simeq$). We define this relation as follows.

Definition 8 (1-WL Relation)**.** Let $\mathcal{X} \subseteq \mathcal{G}$. For any graphs $G, H \in \mathcal{X}$ we will denote $G \simeq_{1\mathrm{WL}} H$ if the 1-WL isomorphism test can not distinguish both graphs. Note that due to the soundness of this algorithm, if $G \not\simeq_{1\mathrm{WL}} H$, we always can conclude that $G \not\simeq H$.

The $\simeq_{1\mathrm{WL}}$ relation can further be classified as an equivalence relation, as it is reflexive, symmetric and transitive. With this, we introduce a notation of its equivalence classes. Let $\mathcal{X} \subseteq \mathcal{G}$ and $G \in \mathcal{X}$, then we denote with $\mathcal{X}/\simeq_{1\mathrm{WL}}(G) := \{G' \in \mathcal{X} \mid G \simeq_{1\mathrm{WL}} G'\}$ its equivalence class.

Similarly, we define the notion 1-WL-Discriminating for collections of permutation invariant functions.

Definition 9 (1-WL-Discriminating)**.** Let $\mathcal{X} \subseteq \mathcal{G}$. Further, let $\mathcal{C}$ be a collection of permutation invariant functions from $\mathcal{X}$ to $\mathbb{R}$. We say $\mathcal{C}$ is 1-WL-Discriminating if for all graphs $G_1, G_2 \in \mathcal{X}$ for which the 1-WL isomorphism test concludes non-isomorphic ($G_1 \not\simeq_{1\mathrm{WL}} G_2$), there exists a function $h_{G_1,G_2} \in \mathcal{C}$ such that $h_{G_1,G_2}(G_1) \neq h_{G_1,G_2}(G_2)$.

3.5. 1-WL+NN

As the Section 2.1 shows, the 1-WL algorithm is quite powerful in identifying a graph's substructures and distinguishing non-isomorphic graph pairs. With the 1-WL+NN framework, we define functions that utilize this structural information to derive application-specific insights.

Definition 10 (1-WL+NN)**.** A 1-WL+NN model consists of three components that are applied sequentially to its input: 1) The 1-WL algorithm, 2) An encoding function f_{enc} operating on graph colorings, and 3) An arbitrary multilayer perceptron MLP that further processes the output of f_{enc}. In detail, a 1-WL+NN model computes the function $\mathcal{B}$, that is defined as follows:

$$\mathcal{B} : \mathcal{G} \to \mathbb{R}^k,\ G \mapsto \text{MLP} \circ f_{\text{enc}}(\{\!\{\text{1-WL}(G)(v) \mid v \in V(G)\}\!\}),$$

where 1-WL(G) is the coloring computed by the 1-WL algorithm when applied on G, and $k \in \mathbb{N}_{\geq 1}$ is a freely selectable hyperparameter. For a better understanding and an illustrative explanation, see Figure 3.3.

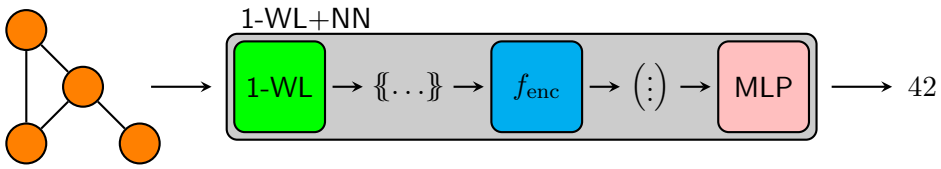

Figure 3.3.: This simplified illustration explains the components that make up a 1-WL+NN model and how each one processes the input further. In detail, the model takes the graph on the left as input and first applies the 1-WL algorithm, thereby obtaining a multiset of the colors assigned by the algorithm. Then the encoding function f_{enc} is applied, resulting in a fixed-sized vector that is further processed by the multilayer perceptron MLP. The output of the MLP is then propagated as the 1-WL+NN models output, here the number 42.

It is worth noting that this definition can be easily adjusted to accommodate node- or edge-level tasks by applying the encoding function f_{enc} and the multilayer perceptron MLP elementwise to the colors of the multiset. However, for the purposes of this thesis, we will not delve into these variations, as our main focus will be on graph-level tasks such as graph classification or regression, which possess greater theoretical interest and are more prevalent in most datasets. Furthermore, all the theoretical findings presented in this thesis can be straightforwardly adapted to 1-WL+NN models designed for node- or edge-level tasks.

3.6. Graph Neural Networks (Message-Passing)

A Graph Neural Network (GNN) is a composition of multiple layers, where each layer computes a new feature for each node and edge. Each GNN layer thus technically obtains a new graph structurally identical to the previous one but with new feature information. After an input graph has been passed through all layers, a final readout function is applied that pools all graph features and derives a task-related output. With this, it is possible to apply a GNN to every graph, regardless of its size, as the "computation" will only take place on the nodes and edges of the graph.

Note that in the following, we will restrict the definition to consider only node features; however, one can easily extend it to include edge features as well.

Definition 11 (Graph Neural Network)**.** Let $G = (V, E, l)$ be an arbitrary graph. A GNN is a composition of multiple layers and a final readout function where each layer t is represented by a function $f^{(t)}$. The initial layer at $t = 0$ is a function of the format $f^{(0)} : V(G) \to \mathbb{R}^{1\times d}$ that is consistent with l and translates all labels into a vector representation. In contrast, for every $t > 0$, $f^{(t)}$ is recursively defined as:

$$f^{(t)}(v) = f^{(t)}_{\text{merge}}(f^{(t-1)}(v),\ f^{(t)}_{\text{agg}}(\{\!\{f^{(t-1)}(w) \mid w \in \mathcal{N}(v)\}\!\})),$$

where $f^{(t)}_{\text{merge}}$ is an arbitrary function that maps the aforementioned tuple to a vector, effectively "merging" them, while $f^{(t)}_{\text{agg}}$ is an arbitrary function that maps the multiset to a vector, effectively "aggregating" it.

The readout function, referred to as Readout, is applied after the input graph has been passed subsequently through all layers and is defined as follows:

$$\text{Readout}(\{\!\{f^{(t)}(v) \mid v \in V(G)\}\!\}).$$

This function pools the information from every node feature, processes it, and calculates a fixed-sized output vector for the entire graph.

In summary, a GNN model will compute the function $\mathcal{A}$ defined as follows:

$$\mathcal{A} : \mathcal{G} \to \mathbb{R}^k,\ G \mapsto \text{Readout}(\{\!\{f^{(T)}(v) \mid v \in V(G)\}\!\}),$$

where T is the number of layer of the GNN, and $k \in \mathbb{N}$ an arbitrary constant. To enable end-to-end training of a GNN, it is essential that all its components are differentiable. Therefore, we require all $f^{(t)}_{\text{merge}}$ and $f^{(t)}_{\text{agg}}$ functions for all $t \in [T]$, along with the final Readout function, to be differentiable.

Note that, due to our definition of the $f^{(t)}_{\text{agg}}$ and the Readout function to operate over multisets, both functions are permutation invariant by definition. With this, we can conclude that the total composition $\mathcal{A}$ is permutation invariant, and with similar reasoning, it is also differentiable. This property enables us to train $\mathcal{A}$ like any other machine learning method in an end-to-end fashion, regardless of the underlying encoding used for graphs.

Furthermore, GNNs following this definition are regarded as Message-Passing-Neural-Network (MPNN). This designation stems from each node exchanging information with its direct neighbors in each layer. As a result, information during the processing of a graph is propagated by passing many messages across the graph; thus, these layers are also referred to as *message-passing* layers. As outlined in the introduction to this thesis, we will solely focus on GNNs utilizing the *message-passing* architecture. Therefore we will use the term GNN and MPNN interchangeably throughout this thesis. The definition and notation used here are inspired by Morris et al. [2019] and Xu et al. [2019].

To bridge the gap from the theoretical definition to practical instances of the definition, we will introduce in the following three distinct GNN architectures, as well as commonly deployed Readout. Specifically, we will explore the Graph Attention Network (GAT) developed by Veličković et al. [2017], Graph Convolutional Network (GCN) proposed by Kipf and Welling [2017], and the Graph Isomorphism Network (GIN) introduced by Xu et al. [2019]. These architectures will

serve as empirical baselines in Part II. Additionally, we will also elaborate on the reasons for this choice of models in Part II in Section 5.2. We listed the definitions of the *message-passing* layers of each model in Table 3.1.

Table 3.1.: Overview of the construction of the *message-passing* layers and their respective learnable parameters by popular GNN architectures. A complete definition of the GAT architecture including the attention coefficient α_{vu} can be found in Definition 25 in the Appendix.

Model	**Merge Function**	**Aggregation Function**	**Learnable Parameters**
GAT	$f_{\text{merge}}^{(t)} = \sigma(\alpha_{vv} \cdot f^{(t)}(v) + f_{\text{agg}}^{(t)})$	$f_{\text{agg}}^{(t)} = \sum_{u \in \mathcal{N}(v)} \alpha_{vu} \cdot W^{(t)} \cdot f^{(t-1)}(u)$	$\alpha_{vu}, W^{(t)}$
GCN	$f_{\text{merge}}^{(t)} = \text{ReLU}\left(\frac{W^{(t)}}{1+d(v)} f^{(t-1)}(v) + f_{\text{agg}}^{(t)}\right)$	$f_{\text{agg}}^{(t)} = \sum_{u \in \mathcal{N}(v)} \frac{W^{(t)}}{\sqrt{(1+d(v))\cdot(1+d(u))}} f^{(t-1)}(u)$	$W^{(t)}$
GIN	$f_{\text{merge}}^{(t)} = \text{MLP}^{(t)}\left((1+\epsilon^{(t)}) \cdot f^{(t-1)}(v) + f_{\text{agg}}^{(t)}\right)$	$f_{\text{agg}}^{(t)} = \sum_{u \in \mathcal{N}(v)} f^{(t-1)}(u)$	$\epsilon^{(t)}, \text{MLP}^{(t)}$

Commonly employed Readout functions in this context often involve straightforward pooling techniques like elementwise summation, mean calculation, or maximum extraction. These pooling operations are typically followed by a multilayer perceptron, which performs additional processing on the aggregated information. Although more sophisticated pooling operations exist, such as Set2Set developed by Vinyals et al. [2015], Xu et al. [2019] showed that given the correct configuration, the elementwise summation pooling function combined with a following multilayer perceptron suffices to create a GNN that is as expressive as the 1-WL algorithm in distinguishing non-isomorphism.

4. Theoretical Connection

This chapter forms the core of our theoretical investigation, where we explore the equivalence between two frameworks: 1-WL+NN and GNN. We present two theorems to establish this equivalence, each showing a separate equivalence direction. By combining these theorems, we conclusively establish the equivalence. To maintain clarity and rigor, we will prove each theorem separately afterward in a corresponding section.

In particular, the theorem will establish a theoretical connection between the frameworks when applied to a finite collection of graphs, which we denote by $\mathcal{X}$ with $\mathcal{X} \subset \mathcal{G}$.

Theorem 12 ("GNN $\subseteq$ 1-WL+NN")**.** Let $\mathcal{A}$ be a function from $\mathcal{X}$ to $\mathbb{R}$ computable by a GNN, then $\mathcal{A}$ is also computable by 1-WL+NN.

Theorem 13 ("1-WL+NN $\subseteq$ GNN")**.** Let $\mathcal{B}$ be a function from $\mathcal{X}$ to $\mathbb{R}$ computable by 1-WL+NN, then $\mathcal{B}$ is also computable by a GNN.

With these two theorems, the equivalence between both frameworks follows. Specifically, every function computed by 1-WL+NN working over any arbitrary but finite $\mathcal{X} \subset \mathcal{G}$ is also computable by a GNN, and vice versa. Consequently, we can draw the following corollary:

Corollary 14. For an arbitrary function f working over $\mathcal{X}$ to $\mathbb{R}$: The function f is computable by a 1-WL+NN model, if and only if, the function f is computable by a GNN model.

As we move towards the empirical evaluation in Part II, it is evident that if we test a 1-WL+NN model on any of the benchmark datasets, it can theoretically achieve the same level of performance as a GNN model. Notice that we did not leverage any constraints on the encoding of graphs throughout the two theorems and their corresponding proofs.

4.1. Proof of Theorem 12: "GNN $\subseteq$ 1-WL+NN"

We will prove Theorem 13 by first introducing a set of lemmas, which will be leveraged in the proof of the theorem at the end of this section. The Lemmas 19 and 20, and the proof of Theorem 12 extend the results by Chen et al. [2019].

To begin, we prove an essential insight that for any pair of graphs indistinguishable by the 1-WL isomorphism test, the output of any 1-WL+NN model applied to both graphs is identical.

Lemma 15 (1-WL+NN Equivalence)**.** Let $\mathcal{B}$ be a function over $\mathcal{X}$ computable by 1-WL+NN, then for every pair of graphs $G_1, G_2 \in \mathcal{X}$: if $G_1 \simeq_{1\text{WL}} G_2$ then $\mathcal{B}(G_1) = \mathcal{B}(G_2)$.

Proof of Lemma 15. Assume the above. Let $\mathcal{B}$ be an arbitrary function over $\mathcal{X}$ computable by 1-WL+NN, then $\mathcal{B}$ is composed as follows: $\mathcal{B}(\cdot) = \mathsf{MLP} \circ f_{\text{enc}}\{\!\{\text{1-WL}(\cdot)(v) \mid v \in V(\cdot)\}\!\}$. Further, let $G_1, G_2 \in \mathcal{X}$ be arbitrary graphs with $G_1 \simeq_{1\text{WL}} G_2$, then by definition of the $\simeq_{1\text{WL}}$ relation we know that $\text{1-WL}(G_1) = \text{1-WL}(G_2)$. With this, the equivalence follows, since it implies the equivalence of the multiset of colors for both graphs. □

As a consequence of this lemma, we establish that every function computable by 1-WL+NN is also permutation invariant.

Lemma 16 (1-WL+NN Permuation Invariance)**.** Let $\mathcal{B}$ be a function over $\mathcal{X}$ computable by 1-WL+NN, then $\mathcal{B}$ is permutation invariant.

Proof of Lemma 16. Assume the above. Let $G \in \mathcal{X}$ be an arbitrary graph, and π be a permutation of the set of nodes, $V(G)$. By the definition of isomorphism, we know that G is isomorph to $\pi \cdot G$. Further, since the 1-WL isomorphism test is sound, we know that $G \simeq \pi \cdot G$ implies $G \simeq_{1\text{WL}} \pi \cdot G$. Using Lemma 15, we can therefore conclude that: $\mathcal{B}(G) = \mathcal{B}(\pi \cdot G)$. □

With this property of 1-WL+NN functions, we can show the existence of a 1-WL-Discriminating collection of functions computable by 1-WL+NN with Lemma 17. It is necessary to prove this lemma as it forms the basis of Lemma 19.

Lemma 17. There exists a collection $\mathcal{C}$ of functions from $\mathcal{X}$ to $\mathbb{R}$ computable by 1-WL+NN that is 1-WL-Discriminating.

Proof of Lemma 17. We will prove the lemma by giving a construction of such a collection. In particular, we define the collection $\mathcal{C}$ as follows:

$$\mathcal{C} := \{\mathcal{B}_c : \mathcal{X} \to \mathbb{R},\ G \mapsto \mathsf{MLP}_{\text{id}} \circ f_c(\{\!\{\text{1-WL}(G)(v) \mid v \in V(G)\}\!\}) \mid c \in \mathbb{N}\},$$

where MLP_{id} is the identity function encoded as a multilayer perceptron that returns its input and f_c is an encoding function that returns the number of nodes colored as c. Since every function $\mathcal{B}_c \in \mathcal{C}$ is composed of the 1-WL algorithm, an encoding function f_c, and a multilayer perceptron MLP_{id}, each function is computable by 1-WL+NN, and consequently, also the whole collection.

To prove that this collection is 1-WL-Discriminating, we need to show two properties: 1) Each function in the collection is permutation invariant, and 2) For each pair of graphs in $\mathcal{X}$ distinguishable by the 1-WL isomorphism test, there must exist a function in the collection that also distinguishes the pair.

For the first property, we already established in Lemma 16 that all 1-WL+NN functions are permutation invariant. For the second property, let $G_1, G_2 \in \mathcal{X}$ with $G_1 \not\simeq_{1\text{WL}} G_2$. Further, let C_1, C_2 be the final colorings computed by the 1-WL algorithm when applied on G_1, G_2 respectively. Due to $G_1 \not\simeq_{1\text{WL}} G_2$, there exists a color $c \in \mathbb{N}$ such that $\text{hist}_{G_1,C_1}(c) \neq \text{hist}_{G_2,C_2}(c)$, such that $\mathcal{B}_c \in \mathcal{C}$ exists with $\mathcal{B}_c(G_1) \neq \mathcal{B}_c(G_2)$, satisfying the second property. □

The following Lemma 18 forms the basis in constructing 1-WL+NN computable functions in the subsequent proofs of the Lemmas 19 and 20, as well as in the proof of Theorem 12. Specifically, it shows that combining the output of multiple 1-WL+NN computable functions and processing them further with a multilayer perceptron is also 1-WL+NN computable.

Lemma 18 (1-WL+NN Composition)**.** Let $\mathcal{C}$ be a collection of functions computable by 1-WL+NN. Further, let $\mathcal{B}_1, \ldots \mathcal{B}_n \in \mathcal{C}$ and $\mathsf{MLP}^\bullet$ be a multilayer perceptron operating from $\mathbb{R}^n$ to $\mathbb{R}$, then the function $\hat{\mathcal{B}}$ composed as follows:

$$\hat{\mathcal{B}} : \mathcal{X} \to \mathbb{R},\ G \mapsto \mathsf{MLP}^\bullet\left(\begin{bmatrix}\mathcal{B}_1(G)\\ \vdots \\ \mathcal{B}_n(G)\end{bmatrix}\right),$$

is also computable by 1-WL+NN.

Proof of Lemma 18. Assume the above. Let $f_1, \ldots, f_n$ be the encoding functions, and $\mathsf{MLP}_1, \ldots, \mathsf{MLP}_n$ be the multilayer perceptrons used by $\mathcal{B}_1, \ldots, \mathcal{B}_n$, respectively. The key idea of this proof is to construct an encoding function f^* that "duplicates" its input and applies each encoding function f_i followed by each multilayer perceptron MLP_i individually. Afterward, we apply $\mathsf{MLP}^\bullet$ to the resulting concatenated vector. Thus, we can represent $\hat{\mathcal{B}}$ as follows:

$$\hat{\mathcal{B}}(\cdot) = \mathsf{MLP}^\bullet \circ f^*(\{\!\{\text{1-WL}(\cdot)(v) \mid v \in V(\cdot)\}\!\}).$$

In detail, we define the encoding function f^* as follows:

$$f^*(\cdot) := \mathsf{concat}\left(\begin{bmatrix} \mathsf{MLP}_1 \circ f_1(\cdot) \\ \vdots \\ \mathsf{MLP}_n \circ f_n(\cdot) \end{bmatrix}\right),$$

where concat is the concatenation function that combines all encoding vectors into a single vector. By doing so, we have shown that $\hat{\mathcal{B}}$ can be decomposed into three components of a 1-WL+NN model, allowing us to conclude that it is 1-WL+NN computable. □

In the following two Lemmas 19 and 20, we will show that the indicator function $\mathbb{1}$ for the $\simeq_{1\text{WL}}$ relation on $\mathcal{X}$ is 1-WL+NN computable. We formally define this function for any pair of graphs $G_1, G_2 \in \mathcal{X}$ as follows:

$$\mathbb{1}_{G_1 \simeq_{1\text{WL}} G_2} = \begin{cases} 1, & \text{if } G_1 \simeq_{1\text{WL}} G_2 \\ 0, & \text{else} \end{cases}.$$

This function plays a crucial role in the proof of Theorem 12. We will first introduce an approximation of the negated version of $\mathbb{1}_{G_1 \simeq_{1\text{WL}} G_2}$ in Lemma 19, where the output is switched. Subsequently, we will use this approximation for the proof of Lemma 20 to construct a function $\varphi_{G_1}(G_2)$ that is equivalent to the indicator function $\mathbb{1}_{G_1 \simeq_{1\text{WL}} G_2}$.

Lemma 19. Let $\mathcal{C}$ be a collection of functions from $\mathcal{X}$ to $\mathbb{R}$ computable by 1-WL+NN that is 1-WL-Discriminating. Then for all $G^* \in \mathcal{X}$, there exists a function h_{G^*} from $\mathcal{X}$ to $\mathbb{R}$ computable by 1-WL+NN, such that on any input $G \in \mathcal{X} : h_{G^*}(G) = 0$, if and only if, $G \simeq_{1\text{WL}} G^*$.

Proof of Lemma 19. Assume the above. Since $\mathcal{C}$ is 1-WL-Discriminating, we know that for any pair of graphs $G_1, G_2 \in \mathcal{X}$ with $G_1 \not\simeq_{1\text{WL}} G_2$, the function $h_{G_1,G_2} \in \mathcal{C}$ exists, that distinguishes the pair, such that $h_{G_1,G_2}(G_1) \neq h_{G_1,G_2}(G_2)$. We define the function $\overline{h}_{G_1,G_2}$ working over $\mathcal{X}$ for every such pair as follows:

$$\begin{aligned} \overline{h}_{G_1,G_2}(\cdot) &= |h_{G_1,G_2}(\cdot) - h_{G_1,G_2}(G_1)| \\ &= \max(h_{G_1,G_2}(\cdot) - h_{G_1,G_2}(G_1),\ 0) + \max(h_{G_1,G_2}(G_1) - h_{G_1,G_2}(\cdot),\ 0) \\ &= \text{ReLU}(h_{G_1,G_2}(\cdot) - h_{G_1,G_2}(G_1)) + \text{ReLU}(h_{G_1,G_2}(G_1) - h_{G_1,G_2}(\cdot)) \end{aligned} \tag{4.1.1}$$

Note, that in the equations above $h_{G_1,G_2}(G_1)$ is independent of the input of $\overline{h}_{G_1,G_2}(\cdot)$ and hence, a fixed constant. Furhter, the resulting function $\overline{h}_{G_1,G_2}$ is non-negative. Let $G^* \in \mathcal{X}$ now be fixed, then we will construct the function h_{G^*} with the desired properties as follows:

$$h_{G^*}(\cdot) = \sum_{\substack{G_2 \in \mathcal{X} \\ G^* \not\simeq_{1\text{WL}} G_2}} \overline{h}_{G^*,G_2}(\cdot). \tag{4.1.2}$$

Since $\mathcal{X}$ is finite, the sum is finite and therefore well-defined. Next, we will show that this construction fulfills the desired properties, by proving that for any input $G \in \mathcal{X} : h_{G^*}(G) = 0$, if and only if, $G \simeq_{1\text{WL}} G^*$. Note that G^* is arbitrary but fixed. Let $G \in \mathcal{X}$ be an arbitrary input graph:

1. If $G^* \simeq_{1\text{WL}} G$, then every summand $\overline{h}_{G^*,G_2}$ with $G^* \not\simeq_{1\text{WL}} G_2$, we know, using Lemma 15, that $\overline{h}_{G^*,G_2}(G)$ is equal to $\overline{h}_{G^*,G_2}(G^*)$ which is by definition 0, such that $h_{G^*}(G) = 0$.
2. If $G^* \not\simeq_{1\text{WL}} G$, then $\overline{h}_{G^*,G}(G)$ is a summand of $h_{G^*}(\cdot)$, and since $\overline{h}_{G^*,G}(G) > 0$, we can conclude $h_{G^*}(G) > 0$ due to the non-negativity of each $\overline{h}_{G^*,G_2}$ function.

Using Lemma 18, we can conclude that for any $G^* \in \mathcal{X}$, h_{G^*} is computable by 1-WL+NN, as we can encode Equation (4.1.2) via a multilayer perceptron MLP where the constant $h_{G^*,G_2}(G^*)$ of Equation (4.1.1) will be the bias of the corresponding channel, such that the MLP exists.

It is crucial to note that in the special case where no pair of graphs within $\mathcal{X}$ is indistinguishable by the 1-WL isomorphism test from another, the function h_{G^*} is still defined. However, the function sums over zero summands, resulting in $h_{G^*}(\cdot) = 0$. □

Thus, we proved that the function h_{G^*} is 1-WL+NN computable for any graph $G^* \in \mathcal{X}$. The function h_{G^*} approximates the negated indicator function for the fixed graph G^* by mapping graphs indistinguishable from G^* by the 1-WL algorithm to 0 while mapping every other graph to something strictly larger than 0. The following proof will use this property to construct the indicator function.

Lemma 20. Let $\mathcal{C}$ be a collection of functions from $\mathcal{X}$ to $\mathbb{R}$ computable by 1-WL+NN such that for all $G^* \in \mathcal{X}$, there exists $h_{G^*} \in \mathcal{C}$ satisfying $h_{G^*}(G) = 0$, if and only if, $G \simeq_{1\text{WL}} G^*$, for all $G \in \mathcal{X}$. Then for every $G^* \in \mathcal{X}$, there exists a function φ_{G^*} computable by 1-WL+NN such that for all $G \in \mathcal{X}$: $\varphi_{G^*}(G) = \mathbb{1}_{G \simeq_{1\text{WL}} G^*}$.

Proof of Lemma 20. Assume the above. Due to $\mathcal{X}$ being finite, we can define for every graph G^* the constant:

$$\delta_{G^*} \coloneqq \frac{1}{2} \min_{\substack{G \in \mathcal{X} \\ G \not\simeq_{1\text{WL}} G^*}} |h_{G^*}(G)|.$$

The constant δ_{G^*} represents the minimum value to which the corresponding function $h_{G^*}(\cdot)$ maps a graph G that is distinguishable from G^* by the 1-WL isomorphism test, multiplied by the factor $\frac{1}{2}$. The specific value of this factor is arbitrary; the crucial aspect is that it remains less than 1, ensuring that the constant δ_{G^*} remains strictly smaller than the minimum value of $h_{G^*}(\cdot)$ for any graph G where $G \not\simeq_{1\text{WL}} G^*$.

It is important to note that in the special case where no pair of graphs within $\mathcal{X}$ is indistinguishable by the 1-WL isomorphism test, the constant δ_{G^*} is not well-defined. For these cases, we set $\delta_{G^*} \coloneqq 1$ for all $G^* \in \mathcal{X}$.

We further introduce a so-called "bump" function $\psi_a(x)$ working from $\mathbb{R}$ to $\mathbb{R}$, parametrized by $a \in \mathbb{R}$ with $a > 0$ and defined as follows:

$$\begin{aligned} \psi_a(x) &\coloneqq \max(\frac{x}{a} - 1,\ 0) + \max(\frac{x}{a} + 1,\ 0) - 2 \cdot \max(\frac{x}{a},\ 0) \\ &= \text{ReLU}(\frac{x}{a} - 1) + \text{ReLU}(\frac{x}{a} + 1) - 2 \cdot \text{ReLU}(\frac{x}{a}) \end{aligned} \tag{4.1.3}$$

The interesting property of ψ_a is that it maps every value x to 0, except when x is being drawn from the interval $(-a, a)$. In particular, it maps x to 1, if and only if, x is equal to 0. See Figure 4.1 for a plot of the relevant part of this function with exemplary values for a.

We use these properties and the constant δ_{G^*} to define for every graph $G^* \in \mathcal{X}$ the function φ_{G^*} that is equivalent to the indicator function for all graphs in $\mathcal{X}$ as follows:

$$\varphi_{G^*}(\cdot) \coloneqq \psi_{\delta_{G^*}}(h_{G^*}(\cdot)).$$

We will prove the correctness of this construction by showing that for a fixed graph G^* the following condition holds: $\forall G \in \mathcal{X} : \varphi_{G^*}(G) = \mathbb{1}_{G \simeq_{1\text{WL}} G^*}$. For this, consider two cases:

1. If $G \simeq_{1\text{WL}} G^*$, then $h_{G^*}(G) = 0$ resulting in $\varphi_{G^*}(G) = \psi_{\delta_{G^*}}(0) = 1$.
2. If $G \not\simeq_{1\text{WL}} G^*$ then $h_{G^*}(G) \neq 0$, such that $|h_{G^*}(G)| > \delta_{G^*}$ so that $h_{G^*}(G) \notin (-\delta_{G^*}, \delta_{G^*})$ resulting in $\varphi_{G^*}(G) = 0$.

Note that we can encode φ_{G^*} using Equation (4.1.3) via a multilayer perceptron MLP, where δ_{G^*} is a constant, such that the MLP exists. With Lemma 18 we can therefore conclude that φ_{G^*} is computable by 1-WL+NN for every graph $G^* \in \mathcal{X}$. □

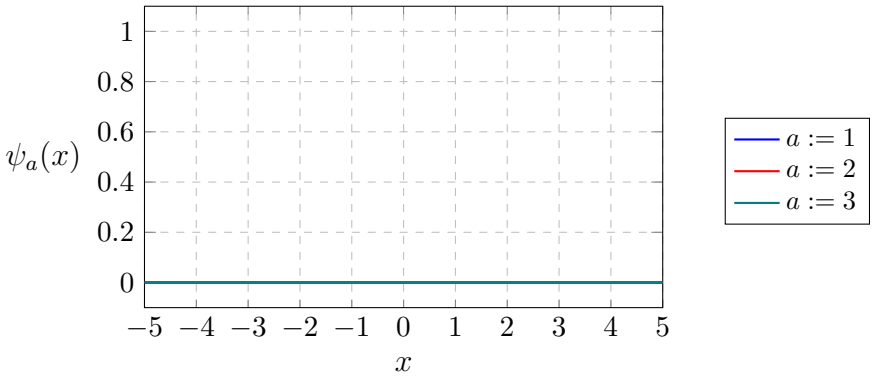

Figure 4.1.: Illustration of the so-called "bump" function $\psi_a(x)$ used in the proof of Lemma 20 with different exemplary values for a.

In conclusion, with Lemma 17, the Lemmas 19 and 20 establish the computability of the indicator function $\mathbb{1}_{G_1 \simeq_{1\text{WL}} G_2}$ over the set $\mathcal{X}$ by a 1-WL+NN model. Building upon these results, we can prove Theorem 12, which states:

"Let $\mathcal{A}$ be a function from $\mathcal{X}$ to $\mathbb{R}$ computable by a GNN, then $\mathcal{A}$ is computable by 1-WL+NN."

Proof of Theorem 12. Let $\mathcal{A}$ be a function that works over $\mathcal{X}$ to $\mathbb{R}$ computed by a GNN model. We will prove that $\mathcal{A}$ is 1-WL+NN computable by decomposing the function and then argue that the decomposition is computable by a 1-WL+NN model. For this let $G \in \mathcal{X}$ be an arbitrary input graph, we can decompose $\mathcal{A}(G)$ as follows:

$$\mathcal{A}(G) = \Big(\frac{1}{|\mathcal{X}/\simeq_{1\text{WL}}(G)|} \sum_{G^* \in \mathcal{X}} \mathbb{1}_{G \simeq_{1\text{WL}} G^*} \Big) \cdot \mathcal{A}(G) \tag{4.1.4}$$

$$= \sum_{G^* \in \mathcal{X}} \frac{1}{|\mathcal{X}/\simeq_{1\text{WL}}(G)|} \cdot \mathcal{A}(G) \cdot \mathbb{1}_{G \simeq_{1\text{WL}} G^*} \tag{4.1.5}$$

$$= \sum_{G^* \in \mathcal{X}} \frac{1}{|\mathcal{X}/\simeq_{1\text{WL}}(G^*)|} \cdot \mathcal{A}(G^*) \cdot \mathbb{1}_{G \simeq_{1\text{WL}} G^*} \tag{4.1.6}$$

$$= \sum_{G^* \in \mathcal{X}} \frac{\mathcal{A}(G^*)}{|\mathcal{X}/\simeq_{1\text{WL}}(G^*)|} \cdot \varphi_{G^*}(G) \tag{4.1.7}$$

where $\mathcal{X}/\simeq_{1\text{WL}}(G)$ denotes the set of all graphs that are equivalent to G according to the $\simeq_{1\text{WL}}$ relation. We explain each equation step by step:

Equation (4.1.4): Multiplying $\mathcal{A}(G)$ by the factor in the parentheses maintains the equation because it equals 1. This is because the sum "counts" the number of graphs $G^* \in \mathcal{X}$ that are indistinguishable from the input graph G by the 1-WL isomorphism test, and then the count is divided by the number of graphs in the equivalence class of G, which equals the count.

Equation (4.1.5): We can move both the factor $\mathcal{A}(G)$ and $\frac{1}{|\mathcal{X}/\simeq_{1\text{WL}}(G)|}$ into the sum by using the distributive property of the space $\mathbb{R}$.

Equation (4.1.6): Due to the output of the indicator function $\mathbb{1}$ being either 0 or 1, we can infer that the product of each summand can only be nonzero if G^* is indistinguishable by the 1-WL isomorphism test from G. This implies that both are in the same equivalence class in these cases, such that $|\mathcal{X}/\simeq_{1\text{WL}}(G)|$ is equal to $|\mathcal{X}/\simeq_{1\text{WL}}(G^*)|$.
Additionally, since GNNs are, at most, as good as the 1-WL algorithm in distinguishing pairs of non-isomorphic graphs (Morris et al. [2019], Xu et al. [2019]), we can use the fact that for every graph $G^* \in \mathcal{X}$: if $G^* \simeq_{1\text{WL}} G$, then $\mathcal{A}(G^*) = \mathcal{A}(G)$. Using the same reasoning as above with the indicator function, we can replace the term $\mathcal{A}(G)$ by $\mathcal{A}(G^*)$.

Equation (4.1.7): Utilizing Lemma 20, we can replace the indicator function with $\varphi_{G^*}(G)$.

In conclusion, we have decomposed the GNN function $\mathcal{A}(G)$ such that the only factors that depend on the input graph G are the functions φ_{G^*}, which take G as input. This observation implies that all other factors are constants. Consequently, the entire decomposition can be computed by a multilayer perceptron with a single layer, which takes the output of all φ_{G^*} for all $G^* \in \mathcal{X}$, applied to the input graph G. The multilayer perceptron then multiplies each of these values with the constant $\frac{\mathcal{A}(G^*)}{|\mathcal{X}/\simeq_{1\text{WL}}(G^*)|}$ and takes the sum. The existence of such a multilayer perceptron is evident, and when combined with Lemma 18, we can assert that this composition is 1-WL+NN computable.

Important, we can only do this since $\mathcal{X}$ is finite, making the overall sum finite and the cardinality of $\mathcal{X}/\simeq_{1\text{WL}}(G^*)$ well-defined for all graphs. □

4.2. Proof of Theorem 13: "1-WL+NN $\subseteq$ GNN"

In this section, we will prove the converse direction of Theorem 12. Similar to the previous section, we will begin by introducing a set of lemmas that will play a crucial role in proving Theorem 13.

We start by showing the existence of a collection of functions computable by GNNs that is 1-WL-Discriminating. For the proof, we will devise message-passing layers for a GNN that effectively compute a single iteration of the 1-WL algorithm per layer. Afterward, we show that with a proper choice of the Readout function, we construct a collection of GNN functions that is 1-WL-Discriminating. Although prior works by Morris et al. [2019] and Xu et al. [2019] have already demonstrated how to construct message-passing layers to compute a single iteration of the 1-WL algorithm per layer, we include our own construction with our notation in the proof for two crucial reasons. First, it ensures the completeness of our proof without assuming major

parts from other works. Second, and most importantly, the construction effectively highlights the remarkable similarities and key distinctions between the 1-WL algorithm and GNNs in general.

Lemma 21 (GNN 1-WL-Discriminating)**.** There exists a collection $\mathcal{C}$ of functions from $\mathcal{X}$ to $\mathbb{R}$ computable by GNNs that is 1-WL-Discriminating.

Proof of Lemma 21. Due to $\mathcal{X}$ being finite, we define the constants n, m, k as follows:

$$n := \max_{G \in \mathcal{X}} |V(G)|, \quad m := \sum_{G \in \mathcal{X}} |V(G)|, \quad \text{and} \quad k := 1 + \max_{\substack{G \in \mathcal{X} \\ v \in V(G)}} |l_G(v)|,$$

such that n is the maximum number of nodes of any graph in $\mathcal{X}$, m is the total number of nodes of the set $\mathcal{X}$, and k is the largest label of any node of a graph in $\mathcal{X}$ plus 1.

We will utilize these constants to construct the collection of functions $\mathcal{C} := \{\mathcal{A}_c \mid c \in \mathbb{N}\}$ that is 1-WL-Discriminating. For the remainder of this proof, we first describe the construction of an arbitrary $\mathcal{A}_c \in \mathcal{C}$ and afterward, prove that the collection $\mathcal{C}$ is 1-WL-Discriminating.

Each $\mathcal{A}_c$ consists of n message-passing layers. For the input layer of each input graph $G \in \mathcal{X}$, we define $f^{(0)}(v) := l_G(v)$ as the identity function, where no preprocessing of the node labels occurs. Further, we define every other layer t with $1 \leq t \leq n$ as follows:

$$f^{(t)}(v) \coloneqq f^{(t)}_{\text{merge}}(f^{(t-1)}(v),\ \{\!\{f^{(t-1)}(u) \mid u \in \mathcal{N}(v)\}\!\}).$$

Here $f^{(t)}_{\text{merge}}$ is an injective function that maps its input into its codomain:

$$\{i \in \mathbb{N} \mid k + (t-1) \cdot m \ \leq \ i \ \leq \ k + t \cdot m\}$$

This function exists due to the finiteness of $\mathcal{X}$. We can upper bound the cardinality of its domain, the number of unique tuples, by the total number of nodes in $\mathcal{X}$, which is m, and since the cardinality of its codomain is exactly m, we can conclude the existence of the function.

Next, we will define the Readout function of $\mathcal{A}_c$ to be the function that returns the number of nodes colored as c in the coloring of $f^{(n)}$.

By leveraging the results of *Theorem 3* from the work of Xu et al. [2019], we can infer that each layer of each $\mathcal{A}_c$ computes a single iteration of the 1-WL algorithm. This observation is reasonable since the update equation for each layer injectively maps each tuple to a previously unused color, similar to how the RELABEL function of the 1-WL algorithm operates. Moreover, since the 1-WL algorithm terminates on any graph $G \in \mathcal{X}$ after at most $|V(G)| \leq n$ iterations, the coloring computed by the layers of each $\mathcal{A}_c$ effectively perform n iterations of the 1-WL algorithm when applied to any graph $G \in \mathcal{X}$. Due to the convergence behavior of the 1-WL algorithm, these additional iterations do not increase the expressiveness of the colorings computed by each $\mathcal{A}_c$, such that we can conclude for any graph $G \in \mathcal{X}$:

$$\forall c \in \mathbb{N}: \quad |\{v \in V(G) \mid f^{(n)}(v) = c\}| = |\{v \in V(G) \mid \text{1-WL}(G)(v) = c\}|,$$

which states that the colorings are equal for a bijection $\phi : \mathbb{N} \to \mathbb{N}$, such that we can infer that the colorings are equally expressive for distinguishing non-isomorphism.

To prove that the collection $\mathcal{C}$ is 1-WL-Discriminating, we need to show two properties: 1) Each function in the collection is permutation invariant, and 2) For each pair of graphs in $\mathcal{X}$ distinguishable by the 1-WL isomorphism test, there must exist a function in the collection that also distinguishes the pair.

For the first property, by Definition 11 of GNNs, all functions computed by GNNs are permutation-invariant. Regarding the second property, consider $G_1, G_2 \in \mathcal{X}$ with $G_1 \not\simeq_{1\text{WL}} G_2$. Let C_1 and C_2 represent the final colorings computed by the 1-WL algorithm when applied to G_1 and G_2, respectively. Since $G_1 \not\simeq_{1\text{WL}} G_2$, there exists a color $c \in \mathbb{N}$ such that $\text{hist}_{G_1,C_1}(c) \neq \text{hist}_{G_2,C_2}(c)$. Since, we know that each $\mathcal{A}_c$ computes equally expressive colorings of G_1 and G_2, we know that there exists a $c' \in \mathbb{N}$, such that $\mathcal{A}_{c'}(G_1) \neq \mathcal{A}_{c'}(G_2)$. □

Similar to the proof in the previous section, we will use Lemma 22 to introduce the ability to construct GNNs that take in as input multiple GNNs and then apply a multilayer perceptron to the combined output. This insight is leveraged in the following two corollaries in the proof, as well as in the final proof.

Lemma 22 (GNN Composition)**.** Let $\mathcal{C}$ be a collection of functions computable by GNNs. Further, let $\mathcal{A}_1, \ldots, \mathcal{A}_n \in \mathcal{C}$ and $\mathsf{MLP}^\bullet$ be a multilayer perceptron operating from $\mathbb{R}^n$ to $\mathbb{R}$, then the function $\hat{\mathcal{A}}$ composed as follows:

$$\hat{\mathcal{A}} : \mathcal{X} \to \mathbb{R},\ G \mapsto \mathsf{MLP}^\bullet\left(\begin{bmatrix} \mathcal{A}_1(G) \\ \vdots \\ \mathcal{A}_n(G) \end{bmatrix}\right),$$

is also computable by GNN.

Proof of Lemma 22. Before we begin the proof, we briefly introduce two notations. For any $x \in \mathbb{R}^d$, we will use the notation $x[i]$ to indicate the i.th element of the vector x. Additionally, we indicate the merge and aggregation function used in layer t by $\mathcal{A}_i$ as $f^{(t)}_{\text{merge},i}$ and $f^{(t)}_{\text{agg},i}$. Similarly, we denote the Readout function as $\mathsf{Readout}_i$ and the input function of $\mathcal{A}_i$ as $f^{(0)}_i$.

We will prove the lemma by giving a construction of a GNN model computing $\hat{\mathcal{A}}$. For the ease of readability and to reduce the complexity of the subsequent construction, we assume that for all $\mathcal{A}_i$ its functions $f^{(t)}_{\text{merge},i}, f^{(t)}_{\text{agg},i}$ and $\mathsf{Readout}_i$ map into the one-dimensional space $\mathbb{R}$ for all layers t. With this assumption, we avoid the need for a formal notation of the number of dimensions each of these functions map to.

Assume the above. Let T be the maximum number of layers of all $\mathcal{A}_1, \ldots, \mathcal{A}_n$. We construct the GNN $\hat{\mathcal{A}}$ with T layers, with the input layer defined as follows on an input graph G:

$$\forall v \in V(G) :\ \hat{f}^{(0)}(v) \coloneqq \begin{bmatrix} f^{(0)}_1(v) \\ \vdots \\ f^{(0)}_n(v) \end{bmatrix},$$

and each other layer $0 < t \leq T$ utilizing the merge $\hat{f}^{(t)}_{\text{merge}}$ and aggregation $\hat{f}^{(t)}_{\text{agg}}$ functions as constructed in the following:

$$\hat{f}^{(t)}_{\text{merge}}(\hat{f}^{(t-1)}(v),\ Agg) \coloneqq \begin{bmatrix} f^{(t)}_{\text{merge},1}(\hat{f}^{(t-1)}(v)[1],\ Agg[1]) \\ \vdots \\ f^{(t)}_{\text{merge},n}(\hat{f}^{(t-1)}(v)[n],\ Agg[n]) \end{bmatrix}, \quad \text{and}$$

$$\hat{f}^{(t)}_{\text{agg}}(\{\!\{\hat{f}^{(t-1)}(w) \mid w \in \mathcal{N}(v)\}\!\}) \coloneqq \begin{bmatrix} f^{(t)}_{\text{agg},1}(\{\!\{\hat{f}^{(t-1)}(w)[1] \mid w \in \mathcal{N}(v)\}\!\}) \\ \vdots \\ f^{(t)}_{\text{agg},n}(\{\!\{\hat{f}^{(t-1)}(w)[n] \mid w \in \mathcal{N}(v)\}\!\}) \end{bmatrix}.$$

Note that, not all $\mathcal{A}_i$ will be comprised of T layers, such that for these cases the functions $f^{(t)}_{\text{merge},i}$ and $f^{(t)}_{\text{agg},i}$ will not be defined for all $t \in [T]$. In these cases, we define the functions as follows:

$$f^{(t)}_{\text{merge},i}(\hat{f}^{(t-1)}(v),\ Agg) \coloneqq \hat{f}^{(t-1)}(v), \quad \text{and}$$
$$f^{(t)}_{\text{agg},i}(\{\!\{\hat{f}^{(t-1)}(w) \mid w \in \mathcal{N}(v)\}\!\}) \coloneqq 0.$$

This definition of $f^{(t)}_{\text{merge},i}$ and $f^{(t)}_{\text{agg},i}$ results in the fact that the representation computed in the last layer of $\mathcal{A}_i$ is forwarded to the last layer T of $\hat{\mathcal{A}}$. Finally, we construct the $\mathsf{Readout}$ function of $\hat{\mathcal{A}}$ as follows:

$$\mathsf{Readout}(\{\!\{\hat{f}^{(T)}(v) \mid v \in V(G)\}\!\}) \coloneqq \mathsf{MLP}^{\bullet} \circ \begin{bmatrix} \mathsf{Readout}_1(\{\!\{\hat{f}^{(T)}(v)[1] \mid v \in V(G)\}\!\}) \\ \vdots \\ \mathsf{Readout}_n(\{\!\{\hat{f}^{(T)}(v)[n] \mid v \in V(G)\}\!\}) \end{bmatrix}.$$

With this, the proof concludes. Note that this proof can easily be extended to work without the assumption of each function mapping into a one-dimensional space. □

As a consequence of the previous two lemmas, we find ourselves in a similar position as at the beginning of the proof in Section 4.1. Specifically, we have established, through Lemma 21, the existence of a collection C of functions that can be computed by GNNs and can effectively distinguish any pair of graphs that are also distinguishable by the 1-WL algorithm. Furthermore, with Lemma 22, we have demonstrated that the composition of multiple GNNs and a multilayer perceptron remains computable by a single GNN. Consequently, we can utilize the same proofs of Lemmas 19 and 20 to derive Corollaries 23 and 24, as the proofs are independent of the concrete structure of 1-WL+NN functions, allowing us to apply them seamlessly to establish the GNN computability of the indicator function.

Corollary 23. Let $\mathcal{C}$ be a collection of functions from $\mathcal{X}$ to $\mathbb{R}$ computable by GNNs that is 1-WL-Discriminating. Then for all $G^* \in \mathcal{X}$, there exists a function h_{G^*} from $\mathcal{X}$ to $\mathbb{R}$ computable by GNN, such that on any input $G \in \mathcal{X} : h_{G^*}(G) = 0$, if and only if, $G \simeq_{1\text{WL}} G^*$.

Corollary 24. Let $\mathcal{C}$ be a collection of functions from $\mathcal{X}$ to $\mathbb{R}$ computable by GNNs such that for all $G^* \in \mathcal{X}$, there exists $h_{G^*} \in \mathcal{C}$ satisfying $h_{G^*}(G) = 0$, if and only if, $G \simeq_{1\text{WL}} G^*$, for all $G \in \mathcal{X}$. Then for every $G^* \in \mathcal{X}$, there exists a function φ_{G^*} computable by GNNs such that for all $G \in \mathcal{X}$: $\varphi_{G^*}(G) = \mathbb{1}_{G \simeq_{1\text{WL}} G^*}$.

In conclusion, with Lemma 21, the corollaries establish the computability of the indicator function $\mathbb{1}_{G_1 \simeq_{1\text{WL}} G_2}$ over the set $\mathcal{X}$ by a GNN. Building upon these results, we can prove Theorem 13, which states:

"Let $\mathcal{B}$ be a function from $\mathcal{X}$ to $\mathbb{R}$ computable by 1-WL+NN, then $\mathcal{B}$ is computable by a GNN."

Proof of Theorem 13. Let $\mathcal{B}$ be a function that works over $\mathcal{X}$ to $\mathbb{R}$ computed by a 1-WL+NN model. We will prove that $\mathcal{B}$ is GNN computable by decomposing the function and then argue that the decomposition is computable by a GNN model. For this let $G \in \mathcal{X}$ be an arbitrary

input graph, we can decompose $\mathcal{B}(G)$ as follows:

$$\begin{aligned}
\mathcal{B}(G) &= \Big(\frac{1}{|\mathcal{X}/\!\simeq_{1\mathrm{WL}}(G)|} \sum_{G^* \in \mathcal{X}} \mathbb{1}_{G \simeq_{1\mathrm{WL}} G^*} \Big) \cdot \mathcal{B}(G) \\
&= \sum_{G^* \in \mathcal{X}} \frac{1}{|\mathcal{X}/\!\simeq_{1\mathrm{WL}}(G)|} \cdot \mathcal{B}(G) \cdot \mathbb{1}_{G \simeq_{1\mathrm{WL}} G^*} \\
&= \sum_{G^* \in \mathcal{X}} \frac{1}{|\mathcal{X}/\!\simeq_{1\mathrm{WL}}(G^*)|} \cdot \mathcal{B}(G^*) \cdot \mathbb{1}_{G \simeq_{1\mathrm{WL}} G^*} \qquad (4.2.1) \\
&= \sum_{G^* \in \mathcal{X}} \frac{\mathcal{B}(G^*)}{|\mathcal{X}/\!\simeq_{1\mathrm{WL}}(G^*)|} \cdot \varphi_{G^*}(G) \qquad (4.2.2)
\end{aligned}$$

where $\mathcal{X}/\!\simeq_{1\mathrm{WL}}(G)$ denotes the set of all graphs that are equivalent to G according to the $\simeq_{1\mathrm{WL}}$ relation. Since the decomposition is very similar to the one present in the proof of Theorem 12, we will only provide reasoning for the correctness of Equations (4.2.1) and (4.2.2):

Equation (4.2.1): Due to the output of the indicator function $\mathbb{1}$ being either 0 or 1, we can infer that the product of each summand can only be nonzero if G^* is indistinguishable by the 1-WL isomorphism test from G. Using Lemma 15, we know that for every graph $G^* \in \mathcal{X}$: if $G^* \simeq_{1\mathrm{WL}} G$, then $\mathcal{B}(G^*) = \mathcal{B}(G)$.

Equation (4.2.2): Utilizing Corollary 24, we can replace the indicator function with $\varphi_{G^*}(G)$.

For all other equations, refer to the explanation provided in the proof of Theorem 12.

In conclusion, we have decomposed the GNN function $\mathcal{B}(G)$ such that the only factors that depend on the input graph G are the functions φ_{G^*}, which take G as input. This observation implies that all other factors are constants. Consequently, we can reason that the entire decomposition can be computed by a multilayer perceptron with a single layer, which takes the output of all φ_{G^*} for all $G^* \in \mathcal{X}$, applied to the input graph G. The multilayer perceptron then multiplies each of these values with the constant $\frac{\mathcal{B}(G^*)}{|\mathcal{X}/\!\simeq_{1\mathrm{WL}}(G^*)|}$ and takes the sum. The existence of such a multilayer perceptron is evident, and when combined with Lemma 22, we can assert that this composition is GNN computable.

Important to note, we can only do this since $\mathcal{X}$ is finite, making the overall sum finite and the cardinality of $\mathcal{X}/\!\simeq_{1\mathrm{WL}}(G^*)$ well-defined for all graphs. □

Part II.

Empirical Testing

The empirical part of this thesis is organized into three chapters. Firstly, we cover the methodology used for conducting our experiments. Afterward, in Chapter 6, we explore the results of the experiments and analyze various properties of both model types in detail. Finally, Chapter 7 concludes the thesis with a discussion, highlighting insights, identifying issues, and suggesting future research directions.

5. Experimental Setup

This part aims to compare the empirical performance of the 1-WL+NN framework to the GNN framework. In particular, we aim to answer the following research questions:

Q1 Can 1-WL+NN models achieve comparable performance to GNN models empirically?

Q2 Are there observable differences in the learning behavior between 1-WL+NN and GNN models?

Q3 To what extent does the expressiveness of 1-WL+NN models in terms of distinguishing non-isomorphic graphs contribute to their empirical performance, and do GNN models leverage their theoretical ability to be equally expressive?

Q4 Is there a substantial difference in the graph representations computed by each model type?

To address these questions, this chapter delves into the configuration and setup of our empirical testing. We begin by presenting our carefully selected datasets, which serve as the foundation for our evaluation. We highlight specific insights and characteristics of these datasets that make them compelling choices for our study. Afterward, we focus on the models we employ for testing and subsequent result comparison. We provide an overview of the selected models, outlining their key features and motivations behind their inclusion in our evaluation. Subsequently, we provide a description of the training pipeline and explain specific hyperparameters for which we will optimize these models.

5.1. Datasets

We will begin by discussing our dataset selection and providing an individual introduction to each dataset. Subsequently, we will assess the dataset balance and investigate the maximum achievable accuracy of all our models on these datasets.

Choice of Datasets

In selecting the datasets for our thesis, we adhered to two fundamental principles to ensure the robustness and diversity of our evaluation for GNN and 1-WL+NN models. The first principle focuses on using widely recognized benchmark datasets that have been extensively employed in previous studies. This principle enables us and readers to make meaningful comparisons with existing results. The second principle focuses on choosing datasets that are distinct from one another in terms of both their application domains and the way they encode information in graphs.

To fulfill the first principle, we opted for datasets from the TUDataset library. This library, curated by Morris et al. [2020], serves as a widely recognized standard for evaluating graph-related methods.

Regarding the second principle, we incorporated the insights from Liu et al. [2022], who developed a comprehensive taxonomy for common graph benchmark datasets. Their work examined the degree to which information is encoded in graph structures compared to node features with respect to solving the task of the datasets. Based on their taxonomy, they categorized datasets into three distinct classes:

Category 1: Datasets in which the most crucial information for solving the task is contained in the node features.

Category 2: Datasets similar to the first category, but with the significant exception that the node degree strongly correlates with the node features. In these datasets, utilizing simple structural information, such as computing the node degree, is as beneficial for solving the task as using the original node features.

Category 3: Datasets where the most crucial information is encoded within the graph structure itself.

These categories help us understand how information is encoded in various datasets, such that we aim to choose datasets from all three categories.

As a result of considering these two principles, we selected the following datasets for our thesis: Enzymes, Imdb-Binary, Mutag, Nci1, Proteins, and Reddit-Binary for classification tasks, and Alchemy and Zinc for regression tasks. For an overview of the elemental properties of each dataset, see Table 5.1. We will now shortly introduce each dataset individually:

Enzymes, provided by Borgwardt et al. [2005], contains proteins in their tertiary structure. Each node represents a secondary structure and has an edge to its three spatially closest nodes. Furthermore, each node feature encodes the type of secondary structure (*helix*, *sheet* or *turn*), as well as physical and chemical information. The task involves classifying each graph into one of six distinct enzyme classes.

Imdb-Binary, provided by Yanardag and Vishwanathan [2015], contains ego networks. Each node in the network represents an actor/actress, and a unidirectional edge exists between two nodes if and only if the corresponding actors played together in a movie. The task involves determining whether each ego network's genre is *action* or *romance*.

Mutag, provided by Debnath et al. [1991], contains Nitroaromatic compounds. Each compound is represented by a graph in which nodes represent atoms, with their types encoded as node features, and edges represent atomic bonds. The task involves determining whether a given compound has a mutagenic effect on Salmonella typhimurium bacteria.

Nci1, provided by Wale et al. [2008], contains chemical compounds. Each compound is represented using a graph, in which nodes represent atoms, and edges represent atomic bonds. Moreover, the atom types are encoded in the node features. The overall task involves determining whether a given compound is active or inactive in inhibiting non-small cell lung cancer.

Proteins, provided by Borgwardt et al. [2005], contains proteins encoded similarly to Enzymes. The task here is to determine whether each graph represents an enzyme.

Reddit-Binary, provided by Yanardag and Vishwanathan [2015], contains graphs that are derived from popular Reddit communities. The nodes in these graphs represent users who are

active in the community, while the edges represent interactions between the users. The task is to identify whether a graph belongs to a community that is focused on questions and answers, or one that is focused on discussions.

Alchemy, provided by Chen et al. [2019], consists of organic molecules, with each node representing an atom and each edge representing an atomic bond. Additionally, each node feature encodes various properties for each atom, while each edge encodes the bond type and distance between atoms. The overall task is to compute 12 different continuous quantum mechanical properties for each graph.

Zinc, provided by Bresson and Laurent [2019] and Irwin et al. [2012], consists of molecular graphs where each node represents a heavy atom, and the corresponding node feature specifies its type. The edges in the graph encode the bonds between atoms, and their features further describe the type of bond. The task is to calculate a molecular property known as constrained solubility ($\log P - \mathrm{SA} - \mathrm{cycle}$).

Table 5.1.: Dataset statistics and properties for graph-level prediction tasks. This table has been adapted from Morris et al. [2022].

	Dataset	Properties						
		Number of graphs	Number of classes/targets	∅ Number of nodes	∅ Number of edges	Node labels	Edge labels	Taxonomy Category[6]
Classification	Enzymes	600	6	32.6	62.1	✓	✗	1
	Imdb-Binary	1 000	2	19.8	96.5	✗	✗	3
	Mutag	188	2	17.9	19.8	✓	✗	2
	Nci1	4 110	2	29.9	32.3	✓	✗	3
	Proteins	1 113	2	39.1	72.8	✓	✗	2
	Reddit-Binary	2 000	2	429.6	497.8	✗	✗	3
Reg.	Alchemy	202 579	12	10.1	10.4	✓	✓	-
	Zinc	249 456	1	23.1	24.9	✓	✓	-

Analysis of the Datasets

To ensure the reliability and fairness of our evaluation, we assess the balance of our selected datasets for classification. To do this, we employ the Normalized Shannon-Index to evaluate the balance of a dataset, where a value close to 0 indicates maximum imbalance, while a value close to 1 signifies perfect balance. See Definition 26 in the Appendix for a formal definition of this metric.

Table 5.2.: An overview of the Normalized Shannon-Index calculated for each dataset.

	Dataset					
	Enzymes	Imdb-Multi	Mutag	Nci1	Proteins	Reddit-Binary
Normalized Shannon-Index	1	1	0.920	1	0.973	1

[6]Taxonomy of common graph benchmark datasets developed by Liu et al. [2022]

Table 5.2 provides an overview of the Normalized Shannon-Index computed for each selected classification dataset. Upon analyzing the data, we observe that all the datasets exhibit high balance, as all their values are close to 1, assuring that the datasets do not suffer significant class imbalances, which will remain important in the following section.

In addition to the balance of all datasets, another important aspect is understanding the upper bound of performance achievable by both GNN and 1-WL+NN models on these datasets. Unlike in other areas of machine learning where multilayer perceptrons can achieve near-perfect performance due to their universal approximation capabilities (Hornik [1991]), GNN and 1-WL+NN models have inherent limitations on their expressiveness. This restriction stems from the connection of both frameworks to the 1-WL algorithm, which as outlined in Section 3.4 is restricted in its expressiveness. Therefore, assuming that GNN or 1-WL+NN models exist that can achieve almost perfect accuracy on all classification datasets is not reasonable. Thus, we calculate the theoretical maximum accuracy achievable by a perfect model for each dataset. In detail, we investigate how many iterations of the 1-WL algorithm it takes to achieve this accuracy. For a comprehensive overview of the accuracies achievable on all datasets, please refer to Table 5.3. In this table, we have included the accuracy achievable when running the 1-WL algorithm for 0 iterations, which means taking the initial node features as a coloring and assessing the expressiveness of this initial coloring.

Table 5.3.: An overview of the maximum theoretical classification accuracy achievable for each dataset based on the number of 1-WL iterations in percent. A hyphen "-" indicates that the maximum accuracy has converged with fewer iterations, implying that further iterations do not improve the accuracy.

1-WL	**Dataset**					
	Enzymes	Imdb-Binary	Mutag	Nci1	Proteins	Reddit-Binary
Iterations: 0	81.4	60.6	93.1	91.3	91.9	83.9
Iterations: 1	100.0	88.6	95.7	99.5	99.7	100.0
Iterations: 2	-	-	99.5	99.8	-	-
Iterations: 3	-	-	100.0	99.8	-	-
Iterations: 4	-	-	-	-	-	-
Max Accuracy	100.0	88.6	100.0	99.8	99.7	100.0

Upon examining the results, we observe that all datasets exhibit perfect or near-perfect theoretical classification accuracies. This result makes interpreting results obtained from actual 1-WL+NN or GNN models later on more straightforward. Additionally, the accuracy achievable after each number of iterations provides a theoretical lower limit on the number of message-passing layers a GNN must be composed of to be even capable of achieving this accuracy.

We have conducted the same analyses on additional datasets, as their results might be valuable to the reader. For these, see Table B.1 in the Appendix.

5.2. Choice of Models

In selecting our models, we aimed to use techniques that are generic and not highly specialized for any of the datasets, such that insights we gain upon analyzing the model's performance can

be generalized better. Consequently, we opted for a basic set of models to maintain simplicity and versatility.

1-WL+NN Models

Our primary consideration for the 1-WL+NN models revolves around choosing an encoding function, as all other components are fixed. We opt for encoding functions with two main components: an optional preprocessing step of the color computed by the 1-WL algorithm and a basic pooling function to convert the color histogram into a fixed-size vector.

In more detail, the optional preprocessing step involves a simple look-up table. If utilized, this step maps each color injectively to a vector in the range of $[-1, 1]^n$, where the value of n is a hyperparameter. By encoding the color information into higher dimensions, this approach aims to enhance efficiency during subsequent processing steps. For the second step, the pooling component, we selected elementary functions such as elementwise Max, Mean, and summation (Sum). In summary, each of the 1-WL+NN models can be uniquely identified by their encoding functions; therefore, we will refer to each model by their encoding function as follows:

$$\mathsf{Embedding} - \{\mathsf{Max}, \mathsf{Mean}, \mathsf{Sum}\} \quad \text{or} \quad \{\mathsf{Max}, \mathsf{Mean}, \mathsf{Sum}\},$$

where "Embedding" indicates the use of the optional preprocessing step.

GNN Models

As mentioned in the introduction to this section, our focus is on keeping the models basic. Hence, we opt for GIN by Xu et al. [2019], GCN by Kipf and Welling [2017], and GAT by Veličković et al. [2017] as the base architecture for the message-passing layers. Each of these architectures was chosen for specific reasons. Additionally, we formally defined each of these architectures in Table 3.1 in Part I.

Firstly, we included GIN as an obvious candidate because it has been proven to be as expressive as the 1-WL algorithm (Xu et al. [2019], Morris et al. [2019]). This characteristic makes it interesting when comparing it to 1-WL+NN models. Next, we also included GCN based on its good empirical success in recent years. Furthermore, the insights provided by Nikolentzos et al. [2023a] demonstrated that the node features computed by GCN and GIN are similar as elaborated in Section 2.2, making GCN a reasonable alternative to GIN in cases where the advantage of GIN's expressiveness is not needed. Lastly, we added GAT as an alternative approach to the other two architectures. In detail, Nikolentzos et al. [2023a] also showed that the node features computed by GAT are entirely different from those computed by GIN or GCN.

Regarding the choice of Readout functions, we decided to utilize functions that are composed of two components. The first component is one of the elementwise pooling functions, such as Max, Mean, and Sum, to aggregate the information from a graph representation into a fixed-sized vector. Secondly, we incorporate a multilayer perceptron to process the aggregated information further, similarly to the 1-WL+NN models.

In summary, each of the GNN models can be uniquely identified by their GNN architecture and the pooling function utilized; therefore, we will refer to each model by these two properties as follows:

$$\{\mathsf{GAT}, \mathsf{GCN}, \mathsf{GIN}\} - \{\mathsf{Max}, \mathsf{Mean}, \mathsf{Sum}\}.$$

Note that the selection of the Readout function creates similarities between the GNN and 1-WL+NN models since the encoding functions of the 1-WL+NN model use the same pooling

functions, and the in both frameworks, a multilayer perceptron further processes the output of the pooling. These similarities play a crucial role in ensuring that any empirical differences observed between the two frameworks are not attributed to the utilization of more powerful techniques.

5.3. Experiments

For the empirical testing, we took measures to ensure the reliability of our results in terms of hyperparameter configuration. Additionally, we aimed to ensure the reproducibility of the training pipeline for each model.

5.3.1. Testing Procedure

We started by conducting experiments on the classification datasets, which serve as the basis for our evaluation as these datasets allow for better scalability due to their smaller size than the regression datasets. Therefore, the thesis will mainly investigate these datasets.

In our testing code, we employ a 10-fold cross-validation approach. Within this framework, we further partition the training data randomly, allocating 10 % of it for validation purposes. Consequently, each training iteration consisted of 81 % of the original dataset as the training set, 9 % as the validation set, and 10 % as the test set. We repeat this testing procedure five times to mitigate the influence of randomness on the model's performance. Ultimately, we record the mean accuracy on the test set along with its standard deviation as the performance metric of the model. Note that the use of standard cross-validation for generating the splits and the choice of mean accuracy as our metric is reasonable and justified as the datasets are highly balanced, as demonstrated in Section 2.

For the regression datasets, we adopted a slightly different testing procedure. Due to their larger scale compared to the classification datasets, we opted for a more time-efficient approach. To achieve this, we utilized pre-existing training pipelines developed by Morris et al. [2020] and Morris et al. [2022]. These pipelines utilize a fixed training, validation, and test splits, accelerating the testing process. Similar to the classification datasets, we performed five runs for each model configuration. We record the mean absolute error and its standard deviation, as well as the mean logarithmic absolute error and its standard deviation of the test set across all runs. Furthermore, we test two different fixed splits for each regression dataset: one utilizing only 10 000 samples for training, while the other split uses the entire training set.

5.3.2. Hyperparameter Optimization

To ensure the trustworthiness of our empirical results and gain valuable insights into the optimal configuration of 1-WL+NN models, we conducted a thorough hyperparameter optimization for each type of model, both GNN and 1-WL+NN, and performed this optimization individually for each dataset.

In order to ensure the comparability of our results with other works and limit the number of hyperparameters requiring optimization, we followed standard practices when configuring our models. Detailed information on all hyperparameters, including the ones we optimized for, can be found in the Appendix. In particular, the hyperparameters for 1-WL+NN models that are applied on the classification datasets can be found in Table B.2, for GNN models on

the classification datasets in Table B.3, for 1-WL+NN models on the regression datasets in Table B.4, and for GNN models on the regression datasets in Table B.5.

We also provide visualizations that attempt to illustrate the effect each hyperparameter has on the performance of the resulting model when employed on a specific dataset. These visualizations can be found for the hyperparameter optimization of 1-WL+NN models in Figures Figures B.1 to B.6 and for GNN models in Figures B.7 to B.12 in the Appendix.

In the beginning, the first hyperparameter configurations we tested for 1-WL+NN models showed considerable performance discrepancies when comparing them to the results achieved by GNN models. We hypothesize that this difference can be attributed to the expressiveness of the 1-WL algorithm, such that most graphs in a dataset get mapped to a unique coloring very dissimilar to the colorings of graphs of the same class.

Consequently, we investigated the possibility of parametrizing the 1-WL algorithm to enhance control over the expressiveness of the colorings it computes. Specifically, we focused on two crucial parameters: 1) the number of iterations and 2) the usage of the convergence behavior as an early termination criterion.

The advantage of this more granular parametrization is that it enables us to apply the same number of 1-WL iterations to each graph processed by a 1-WL+NN model by deactivating the convergence behavior and fixing the number of iterations. By doing so, the number of colors used by the 1-WL algorithm remains contained, both in terms of the number of total unique colors as well as the distance to another. Therefore, one of the most crucial hyperparameters we optimized for all 1-WL+NN models was the number of 1-WL iterations. Additionally, if employed, the size of the dimension of the look-up table was another significant parameter to optimize. We will explore this hypothesis and the effect of the number of iterations on performance in detail in Section 6.1.

In contrast, the hyperparameter selection for the GNN models was relatively less intricate. The key parameters of interest here are the GNN architecture and the size of the hidden dimensions used in each layer. The reason for this is that the different architectures offer certain advantages over one another, while the size of the hidden dimensions enables easier learning by allowing the model to store more information during graph processing.

5.3.3. Implementation Details and Result Reproducibility

The implementation of our models and training procedures was carried out using Python 3.10 along with the open-source library PyTorch[7] and its extension PyTorch Geometric[8]. Moreover, we leveraged Weights&Biases[9] as our tool for coordinating and recording the results of the hyperparameter optimization. The code for our experiments is publicly available on GitHub at `https://github.com/ericbill21/BachelorThesis`, and the corresponding results can be accessed via Weights&Biases at `https://wandb.ai/eric-bill/BachelorThesisExperiments`. We conducted our experiments on the RWTH High Performance Computing cluster by the RWTH Aachen University as well as on private hardware, a MacBook Air M1 2020. In detail, a total of 6 754 runs were conducted, with each run testing a specific model configuration on a designated dataset. These runs required a substantial amount of

[7] A free and open-source machine learning framework that was originally developed by Meta AI and is now part of the Linux Foundation umbrella. https://pytorch.org

[8] An open-source library that extends PyTorch and allows for easy development and training of graph neural networks. https://pytorch-geometric.readthedocs.io

[9] A platform for experiment tracking, hyperparameter tuning, and sharing of results. https://wandb.ai/

computation time, totaling 2 114 hours (over 88 days).

6. Empirical Results

In this section, we present the empirical findings of our study. To examine the classification accuracy achieved by the best-performing configuration of each model on each classification dataset, please refer to Table 6.1. For regression datasets, Table 6.2 provides an overview of the mean absolute error (MAE) for the best-performing configurations.

Due to the usage of existing training pipelines for experiments on the regression datasets, we include the results of the GINE-ε model proposed by Morris et al. [2020] in Table 6.2. The GINE-ε model utilizes the GIN architecture for message-passing layers, Mean as its pooling function, and a two-layer MLP for the final processing of its input graph. This design closely resembles our GIN:Mean model, with the crucial distinction being that GINE-ε incorporates edge features in its computations.

The decision to exclude edge features from all our models, including all 1-WL+NN models, was driven by two key factors. Firstly, our focus primarily revolved around the classification datasets, all of which do not encode any information in their edge features (refer to Table 5.1). Secondly, the regression datasets we utilized in our evaluation include continuous edge features, making the application of the 1-WL algorithm more complex. Although some work exists on modifying the 1-WL algorithm to incorporate continuous features, we opted for a more straightforward and more scalable approach by not considering edge features in the computations of all our

Table 6.1.: Overview of the mean classification accuracies achieved by the best configuration of each model for each dataset in percent and standard deviation. We highlighted the best accuracy for the 1-WL+NN and GNN models for each dataset.

	Method	Dataset					
		Enzymes	Imdb-Binary	Mutag	Nci1	Proteins	Reddit-Binary
1-WL+NN	Max	16.7 ±4.2	52.0 ±5.3	73.8 ±12.4	58.6 ±3.3	62.9 ±4.9	69.2 ±4.0
	Mean	18.2 ±4.8	59.4 ±5.8	77.1 ±11.5	64.0 ±3.3	60.9 ±4.5	66.1 ±3.2
	Sum	18.0 ±6.2	57.5 ±5.1	66.8 ±13.9	56.9 ±3.8	65.6 ±4.8	73.0 ±5.1
	Embedding-Max	41.9 ±7.5	69.4 ±4.9	81.1 ±11.2	82.7 ±2.0	**75.2** ±3.9	71.8 ±3.2
	Embedding-Mean	45.8 ±6.8	**72.4** ±4.1	84.1 ±9.1	83.1 ±1.9	72.7 ±4.6	75.4 ±2.8
	Embedding-Sum	**48.3** ±8.1	72.0 ±3.8	**85.1** ±8.6	**83.6** ±2.2	75.2 ±4.5	**78.4** ±2.7
Graph Neural Networks	GAT:Max	31.2 ±6.0	70.7 ±4.8	71.1 ±12.2	58.0 ±4.2	72.5 ±5.1	77.7 ±5.0
	GAT:Mean	28.9 ±5.9	70.9 ±3.7	74.8 ±9.1	66.1 ±2.8	64.9 ±6.4	70.0 ±6.9
	GAT:Sum	**34.4** ±7.0	72.2 ±4.5	82.1 ±11.2	69.8 ±2.6	73.4 ±3.9	78.1 ±4.2
	GCN:Max	33.1 ±7.5	73.5 ±4.1	74.5 ±11.3	61.1 ±3.6	69.8 ±5.9	74.3 ±4.5
	GCN:Mean	29.9 ±5.7	**74.7** ±3.8	75.0 ±10.4	68.9 ±2.4	70.9 ±5.2	82.3 ±3.3
	GCN:Sum	31.7 ±7.2	73.0 ±4.4	81.5 ±10.3	70.4 ±2.1	73.9 ±4.0	**86.9** ±3.2
	GIN:Max	29.2 ±6.2	70.8 ±4.7	77.3 ±10.7	**79.9** ±2.2	**74.3** ±5.1	76.1 ±3.6
	GIN:Mean	31.7 ±6.7	71.1 ±5.4	82.4 ±9.8	71.3 ±2.2	72.0 ±4.0	73.5 ±3.8
	GIN:Sum	28.9 ±8.7	69.5 ±4.8	**84.6** ±8.7	70.8 ±2.3	73.2 ±4.3	74.0 ±4.3

Table 6.2.: Overview of the mean absolute error and the standard deviation (logMAE) on large-scale (multi-target) molecular regression tasks. We highlighted the lowest error for the 1-WL+NN and GNN models for each dataset.

	Method	Dataset			
		Alchemy	Alchemy (10k)	Zinc	Zinc (10k)
	GINE-ε	0.103 ±0.001 -2.956 ±0.029[8]	0.180 ±0.006 -1.958 ±0.047[9]	0.084 ±0.004[8]	-
GNN	GIN:Max	0.604 ±0.004 -0.578 ±0.009	0.353 ±0.003 -1.228 ±0.006	0.124 ±0.004	0.427 ±0.009
GNN	GIN:Mean	0.643 ±0.014 -0.505 ±0.021	0.314 ±0.004 -1.469 ±0.044	0.110 ±0.005	0.339 ±0.032
GNN	GIN:Sum	**0.523** ±0.016 -0.705 ±0.035	**0.282** ±0.002 -1.890 ±0.031	**0.104** ±0.005	**0.298** ±0.034
1-WL+NN	Embedding-Max	0.648 ±0.003 -0.511 ±0.009	0.409 ±0.003 -1.023 ±0.009	0.382 ±0.005	0.659 ±0.007
1-WL+NN	Embedding-Mean	0.617 ±0.003 -0.564 ±0.005	0.355 ±0.004 -1.269 ±0.020	**0.229** ±0.003	0.484 ±0.009
1-WL+NN	Embedding-Sum	**0.600** ±0.004 -0.625 ±0.032	**0.305** ±0.001 -1.740 ±0.042	0.326 ±0.014	**0.465** ±0.009

models. Nonetheless, this limitation does not compromise the integrity of our results, as our main objective is to compare similar GNN and 1-WL+NN models. The inclusion of GINE-ε showcases the potential and highlights the significance of edge feature information for solving the dataset tasks of Alchemy and Zinc.

A notable finding when analyzing the presented results is that the performance of 1-WL+NN models is comparable to that of GNN models. In fact, the best 1-WL+NN models even outperform the GNN models in all classification datasets, with the exception of Imdb-Binary and Reddit-Binary. These two datasets stand out among the classification datasets as they lack node features. We will investigate this insight later on in more detail. Moreover, our results align with the empirical findings of other GNN models in various studies. The accuracy reported here falls within a similar range as observed in works by Xu et al. [2019], Morris et al. [2022, 2020] and Zhang et al. [2018].

In the subsequent section, we will further analyze these results. Specifically, we will investigate the tradeoff between generality and expressiveness in 1-WL+NN models, the differences in their learning behaviors, the ability of GNN models to approximate 1-WL+NN models, the learned pooled graph representations of each model type, the impact of GNN models performance by preprocessing the data using the 1-WL algorithm, and finally the effect of large datasets on the performance of 1-WL+NN models.

6.1. Fixed 1-WL Iterations: Tradeoff between Expressiveness and Generality

As discussed in Section 5.3.2, we explored constraining the expressiveness of the 1-WL algorithm by fixing the number of iterations it is applied to each graph in a 1-WL+NN model. The intention behind this was to ensure that the resulting colorings of graphs computed using a fixed number of iterations of the 1-WL algorithm would fall within a similar color range, thereby limiting the total number of colors and the overall distance between each used color.

From a theoretical perspective, fixing the number of 1-WL iterations in a 1-WL+NN model only limits its expressiveness. For instance, let $k \in \mathbb{N}$ now be fixed. If the standard 1-WL

[8]The results of GINE-ε on Alchemy and Zinc are adopted from Morris et al. [2020].
[9]The results of GINE-ε on Alchemy(10k) is adopted from Morris et al. [2022].

algorithm converges on an input graph G after $k' < k$ iterations, the coloring computed after k iterations is as expressive as the one obtained from the standard 1-WL algorithm since the coloring converges after k' iterations. On the contrary, if the standard 1-WL algorithm converges after $k' > k$ iterations on an input graph G, the coloring obtained after k iterations is less expressive and contains less information than the coloring derived from the standard 1-WL algorithm.

Comparing the performance of 1-WL+NN models utilizing the standard 1-WL algorithm to those utilizing the parametrized version with a fixed number of 1-WL iteration reveals a significant difference across all classification datasets, which we demonstrate in Table 6.3. This data confirms our belief that the standard 1-WL algorithm can be overly expressive for specific tasks, as evidenced by the considerable performance gap between the two algorithm types. As a consequence of these results, for the remainder of this thesis, we will only investigate 1-WL+NN models utilizing the parametrized version of the 1-WL algorithm with a fixed number of iterations.

Table 6.3.: Comparison between the best performing 1-WL+NN models using the standard or the paraemetrized 1-WL algorithm in percent and standard deviation. Additionally, we included the average number of iterations for the standard version and the optimal fixed number of iterations for the parametrized version of the 1-WL algorithm.

1-WL+NN Models		**Dataset**					
		Enzymes	Imdb-Binary	Mutag	Nci1	Proteins	Reddit-Binary
Standard	Test Accuracy:	34.2 ±6.7	67.0 ±4.3	76.3 ±9.4	78.9 ±2.1	71.4 ±4.9	70.9 ±3.8
	∅ 1-WL Iterations:	3.0 ±1.7	1.1 ±0.7	4.2 ±1.6	3.9 ±1.7	3.0 ±1.7	4.1 ±0.9
Parametrized	Test Accuracy:	48.3 ±8.1	72.4 ±4.1	85.1 ±8.6	83.6 ±2.2	75.2 ±3.9	78.4 ±2.7
	# 1-WL Iterations:	1	1	1	3	1	1

Building on this insight, we will investigate the optimal number of 1-WL iterations that lead to the best-performing models. Interestingly, the outcomes of the optimal number will indicate how essential the expressiveness of the 1-WL algorithm is to solve the task. Therefore, a small optimal number of iterations would suggest that tasks require minimal structural information, while a higher number would indicate the importance of structural information.

To illustrate its effect, in Figure 6.1, we showcase the performance achieved by all models and configurations grouped by the number of 1-WL iterations for each dataset in a violin graph. Note that both classification and regression datasets are included in this figure. Depending on the dataset type, the y-axis represents either classification accuracy or test error, where higher accuracies imply better performance for classification tasks, and higher test errors imply poorer performance for regression tasks (and vice versa).

In general, the results indicate that the performance of 1-WL+NN models tends to improve as the number of 1-WL iterations decreases, except for the Nci1 and Zinc datasets.

Notably, for Nci1, the optimal number of iterations coincides with the number of 1-WL iterations needed for the maximum achievable accuracy (refer to Table 5.3). This correlation holds for all other classification datasets, except for Mutag. However, the behavior observed in Mutag can potentially be attributed to the fact that according to the introduced taxonomy (Liu et al. [2022]) in Section 5.1, Mutag can be effectively solved by simply replacing its node features with an encoding of the node degree. Since the first iteration of the 1-WL algorithm is efficiently an encoding of the node degree, this might explain the observed pattern.

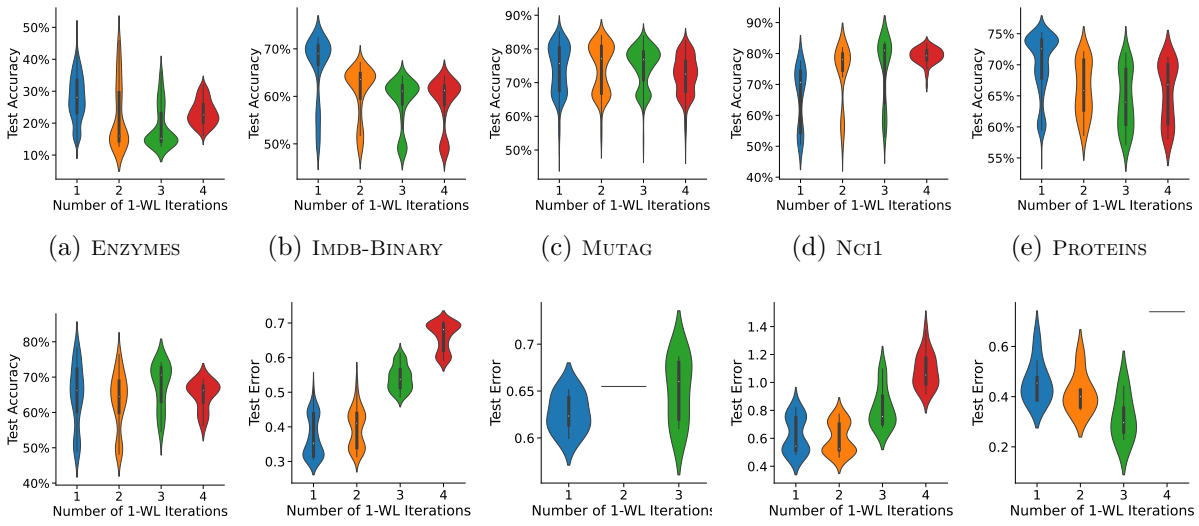

(a) Enzymes (b) Imdb-Binary (c) Mutag (d) Nci1 (e) Proteins

(f) Reddit-Binary (g) Alchemy (10k) (h) Alchemy (i) Zinc (10k) (j) Zinc

Figure 6.1.: Overview of the performance achieved by all tested 1-WL+NN configurations grouped by the fixed number of 1-WL iterations for each dataset. The y-axis uses different metrics based on dataset type: accuracy in percent for classification datasets and mean absolute error for regression datasets.

Interpreting the results of the Zinc dataset is more complex. While the results on the smaller subset of the dataset, Zinc10K, clearly indicate that fewer 1-WL iterations yield better results, the results for the full Zinc dataset suggest the opposite. This discrepancy could be attributed to the limited number of runs conducted on the entire dataset, which were restricted due to time constraints. Therefore, these results should be interpreted with caution.

In conclusion, reducing the number of 1-WL iterations leads to improved generability and overall better performance of the models, with the clear exception of Nci1. However, as our results indicate, most 1-WL+NN models achieve optimal performance when employing only a single iteration of the 1-WL algorithm, which is essentially equivalent to encoding the node degree. This observation demonstrates that 1-WL+NN models do not require the full expressiveness of the 1-WL algorithm to achieve comparable performance to GNN models, which raises the question of whether GNN models, despite their theoretical ability to be highly expressive, also tend to rely primarily on node degree information for computation. To explore this question fully, we will first investigate the difference in the learning behavior, in which we will give reasons as to why 1-WL+NN models achieve their best performance with a small number of 1-WL iterations.

6.2. Difference in Learning Behavior between GNN and 1-WL+NN Models

This section investigates the differences in learning behavior between 1-WL+NN and GNN models. In particular, we will investigate the ability to generalize by assessing the degree of overfit for each type of model.

Figure 6.2 represents the difference in performance between the training and testing performance

for both 1-WL+NN and GNN models across all classification datasets. Different quantiles from the best-performing models were considered, ranging from the top 1 % to the top 100 %. Each bar in the graph represents the mean difference between training accuracy and test accuracy for the respective quantile of runs. 1-WL+NN models are depicted in blue, while GNN models are represented in orange. In comparison, shorter or negative bars indicate better generalization where the performance on the training set aligns more closely with the testing set. The black line in each bar represents the standard error.

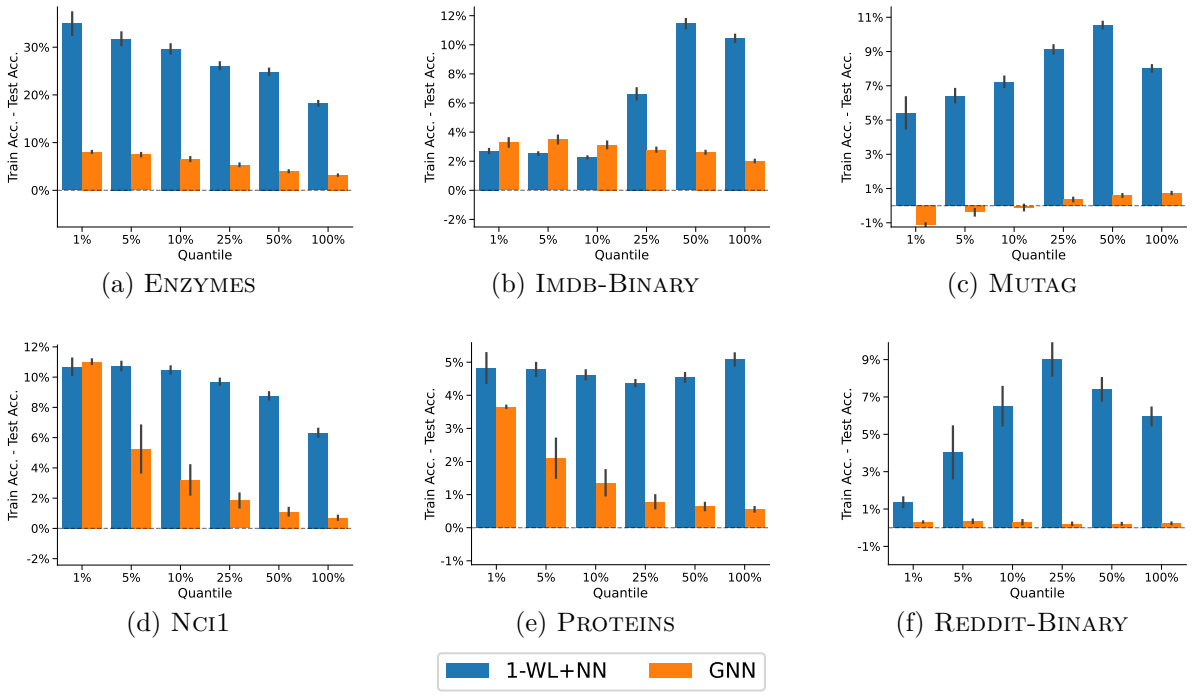

(a) Enzymes (b) Imdb-Binary (c) Mutag

(d) Nci1 (e) Proteins (f) Reddit-Binary

Figure 6.2.: Mean difference of the classification accuracies of the training and testing set for each dataset. In detail, we grouped by different quantiles of the best-performing models and the type of the model.

The learning behavior of 1-WL+NN models presents a unique challenge due to the expressiveness of the 1-WL algorithm, which directly impacts their performance. Compared to GNN models, 1-WL+NN models exhibit a significant discrepancy between their training and test performance. While it is common to observe higher training performance than testing performance in various machine learning applications, this discrepancy is particularly pronounced in our evaluation of the 1-WL+NN models.

Analyzing Figure 6.2 reveals that 1-WL+NN models exhibit more significant overfitting than GNN models, especially on datasets such as Enzymes, Mutag, Proteins, and Reddit-Binary. For instance, in the case of Enzymes, the top 1 % of best-performing 1-WL+NN models display, on average, a 27 % higher training accuracy than their test accuracy, highlighting the extreme extent of overfitting in 1-WL+NN models.

While GNN models also experience some overfitting, primarily observed for the Nci1 dataset, it is not as prevalent across all datasets and not as drastic as for 1-WL+NN models. Moreover, in datasets like Mutag or Reddit-Binary, GNN models demonstrate superior generalization capability. In these cases, the mean difference in performance is close to 0 %, and in the case

of Mutag, it is even negative, which indicates that the tested GNN models were able to learn general patterns in these datasets rather than simply memorizing the data.

However, this raises the question as to why 1-WL+NN models exhibit such drastic overfitting. We hypothesize that the expressiveness of the 1-WL algorithm leads to the computation of highly detailed colorings of the 1-WL+NN's input graphs, such that the models simply memorizes these.

To gain insight into the algorithm's expressiveness, we calculated the ratio of unique colors to the total number of possible colors for each classification dataset. For example, the ENZYMES dataset consists of 600 graphs with a total of 19 580 nodes. After a single iteration of the 1-WL algorithm, all colorings consist of only 231 unique colors, accounting for less than 0.01 % of the total number of possible unique colors (the total number of nodes). However, after two iterations, this number has already increased to 10 416, comprising 53.2 % of the total available colors. This example demonstrates the significant expressiveness of the colorings after just a few iterations.

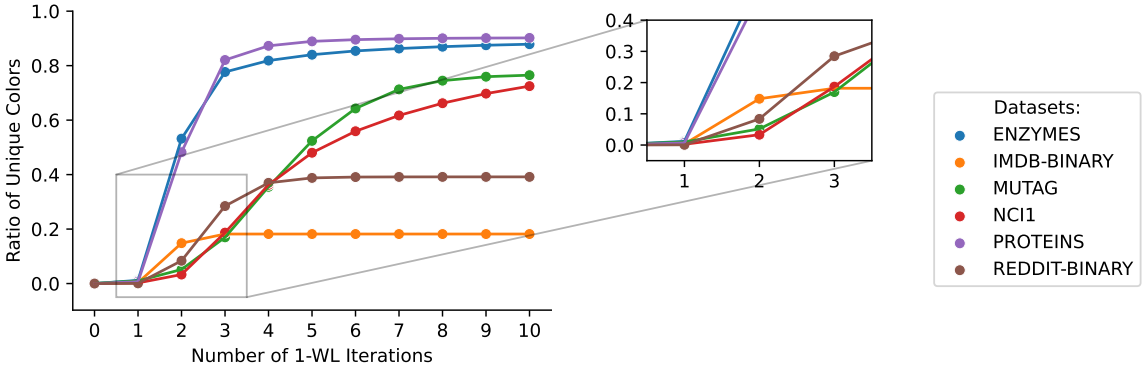

Figure 6.3.: Overview of the ratio of unique colors used by the 1-WL algorithm when applied for a specified number of iterations for each dataset relative to the total number of possible unique colors (the total number of nodes in the dataset). We provided an enlargement of the number of 1-WL iterations commonly used to showcase the values for these numbers better.

Figure 6.3 illustrates the ratio of unique colors used compared to the total possible number of unique colors (total number of nodes in each dataset). As expected, due to the convergence behavior of the 1-WL algorithm, each ratio converges at some point. However, the ratios rise rapidly and drastically for all datasets initially, indicating the strong expressiveness of the algorithm for already small numbers of iterations. Even a relatively small ratio, such as approximately 10 %, signifies a significant number of unique colors in the colorings computed by the 1-WL algorithm. It is important to consider the scale of the datasets when interpreting these ratios. For example, the MUTAG dataset consists of approximately 3 000 nodes, while the ENZYMES and IMDB-BINARY datasets contain around 20 000 nodes each. The PROTEINS dataset reaches 43 000 nodes, followed by the NCI1 dataset with 122 000 nodes, and finally, the REDDIT-BINARY dataset with 859 000 nodes. For a comprehensive overview of the datasets and their sizes, please refer to Table 5.1, and for detailed information on the unique color count, also including the regression datasets and their different splits, consult Table B.7 in the Appendix.

Furthermore, it is important to note that the colors assigned by the 1-WL algorithm have no inherent structural connection between them. Even if two nodes are colored with two distinct

integers with a small numerical distance, this does not imply any similarity between them. While our experiments use an implementation of the 1-WL algorithm that assigns each node the smallest unused color, a meaningful connection about the numerical distance of colors is still absent due to shuffling the dataset and applying the 1-WL algorithm for a fixed number of iterations.

To investigate the impact of the number of 1-WL iterations on overfitting, we plotted Figure 6.4, which focuses solely on 1-WL+NN models and compares the different numbers of 1-WL iterations. Across all classification datasets, it is evident that the overfitting behavior becomes more substantial when increasing the number of 1-WL iterations. This finding supports our belief that the explosive increase in the number of unique colors is the primary reason for the observed overfitting behavior. In the case of Enzymes, with an increased number of 1-WL iterations, the average training accuracy is over 60 % higher than the test accuracy, demonstrating the worsening of the overfitting behavior.

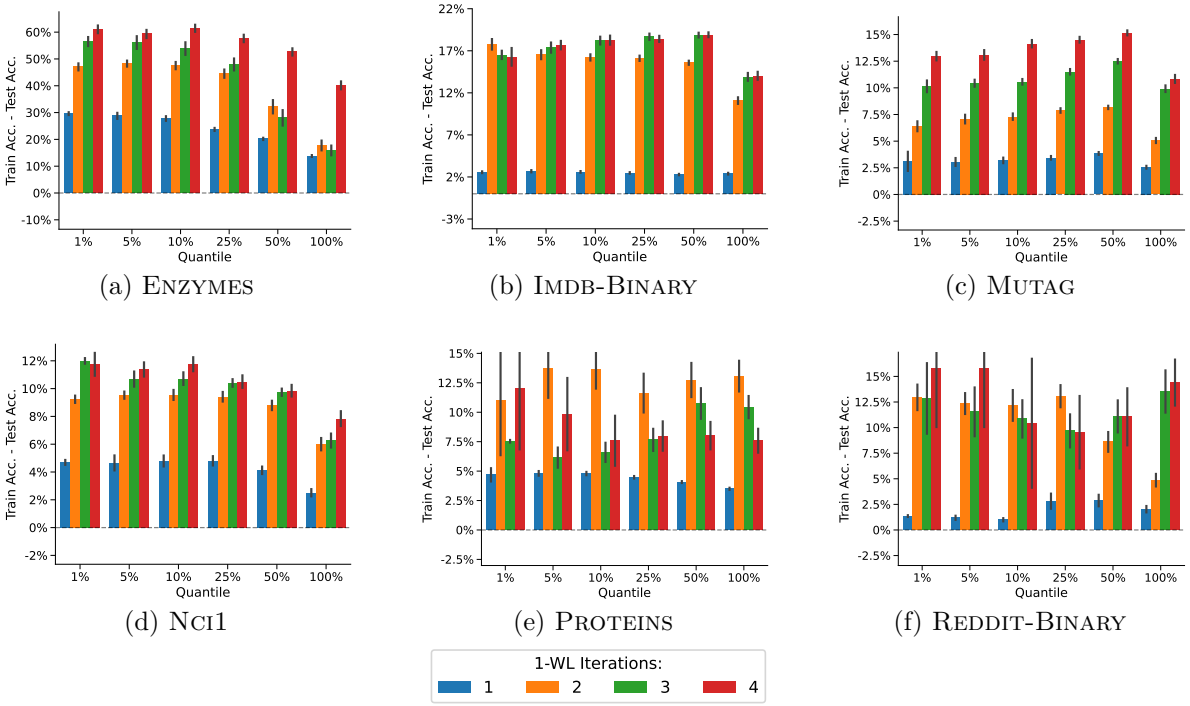

(a) Enzymes (b) Imdb-Binary (c) Mutag

(d) Nci1 (e) Proteins (f) Reddit-Binary

Figure 6.4.: Mean difference in the classification accuracy of the training and test sets achieved by all 1-WL+NN models for each dataset. In detail, we grouped the best models according to different quantiles and the number of iterations of the 1-WL algorithm used by each model.

In conclusion, our analysis reveals that 1-WL+NN models exhibit optimal generalization when limited to one iteration of the 1-WL algorithm. Increasing the number of iterations leads to a significant overfitting behavior. This insight indicates that the expressiveness of the 1-WL algorithm surpasses the requirements for effective learning. In comparison, GNN models excel in learning and representing graph structures in a more generalized manner. The observation that a single iteration of the 1-WL algorithm leads to the best generalization also aligns with the results from the previous section, where the models achieving the highest accuracy on the test set also utilized only a single iteration of the 1-WL algorithm (except for the Nci1 dataset).

This observation raises an intriguing question: Do GNNs also attempt to compute a similarly expressive representation of all graphs, akin to a single iteration of the 1-WL algorithm? We will explore this question in the following section.

6.3. GNNs approximating 1-WL Coloring

This section will explore the node features computed by a GNN. Specifically, we will analyze the ability of GNNs to approximate the coloring computed by a single iteration of the 1-WL algorithm.

To visualize the approximation capabilities of the best-performing GNN models on the classification datasets, refer to Figure 6.5. The visualization consists of a pair of color-coded matrices for each dataset, where each pair corresponds to a single randomly drawn graph from the test set of the respective GNN model. The left matrix illustrates the distance matrix of the node representations computed by the GNN model for each pair of nodes i and j. Similarly, the right matrix represents the distances of the colorings generated by a single iteration of the 1-WL algorithm between each pair of nodes i and j. The distances are measured using the Euclidean distance and then normalized between 0 and 1 for the GNN matrix. While the distances between the 1-WL coloring are either 0 (for nodes with the same color) or 1 (for nodes with different colors) since the colorings produced by the 1-WL algorithm are discrete and do not encode any information in their distances. Furthermore, we computed the Mean Absolute Error (MAE) as a single value by averaging the absolute differences between both matrices, such that the value indicates the similarity between both matrices. The MAE, along with its standard deviation and the index of the graph in the datasets, is included on the right side of the 1-WL distance matrix.

The visualization shows that the GNN representations already provide convincing approximations of the patterns observed in the 1-WL algorithm's matrix. However, it is important to note that these results are based on a single randomly selected graph from each model's test set. To obtain a more comprehensive understanding of the approximation capabilities, we repeated this process for each dataset using ten randomly selected graphs from the test set of the respective GNN model, refer to Figures B.13 to B.19 in the Appendix.

Before diving deeper into analyzing the approximation capabilities, it is crucial to highlight the significant difference between the node representations computed by a GNN and the colors computed by the 1-WL algorithm. Unlike the discrete colors with no order relation calculated by the 1-WL algorithm, the representations computed by each GNN model are multidimensional and continuous. This difference makes a perfect approximation of the 1-WL colorings challenging, as determining when two node representations are similar is not as straightforward as in the discrete 1-WL case. In the visualization, we avoided making this decision by uniformly normalizing the distances between 0 and 1 and using a continuous color bar for color coding similar nodes.

To evaluate the approximation of the 1-WL coloring of the best-performing GNN on the entire dataset, we employed two approaches that dynamically determine the significance of a distance: 1) Continues Approximation: evaluating the approximation using a threshold value for determining similarity and 2) Binary Approximation: translating distances into binary distances and using the F1 score for assessing similarity.

In the first procedure, Continous Approximation, two node representations are considered similar if their Euclidean distance is less than a threshold value, ϵ. Additionally, we consider

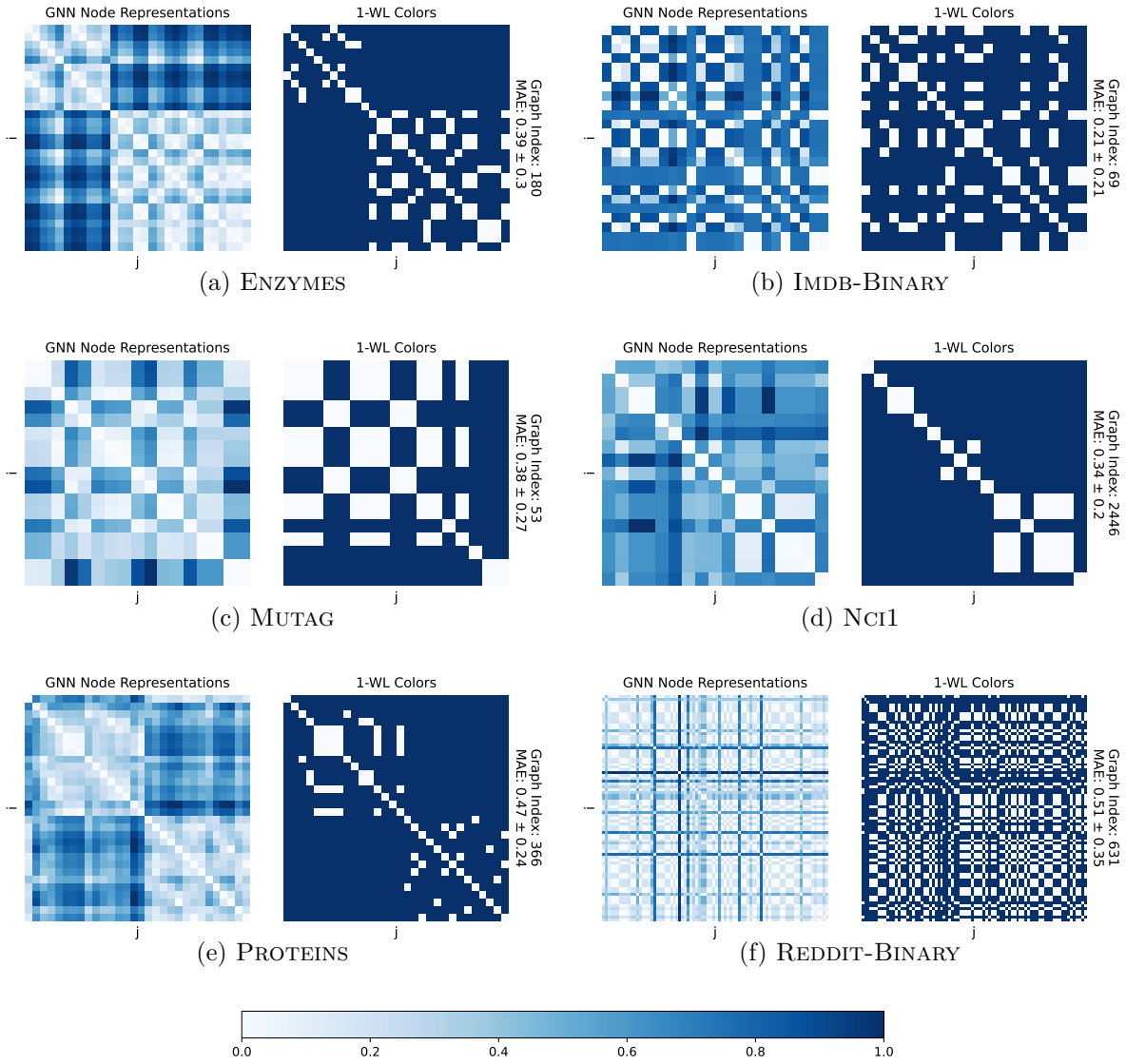

Figure 6.5.: Visualizing the performance of the best-performing GNN models of each dataset in approximating node colors computed by the 1-WL algorithm after running for one iteration. Here we randomly sampled a single graph for each dataset and visualized the approximation performance.

the distances perfectly separable if their distance is greater or equal to $1 - \epsilon$. In detail, we modify the GNN distance matrix for every graph such that all distances less than ϵ are set to 0, all distances greater or equal to $1 - \epsilon$ to 1, otherwise the original distance is preserved. Afterward, we compute, as before, the MAE between each GNN matrix and the 1-WL color matrix and average all values for the entire dataset in a single MAE value in the end. We tested this procedure with various threshold values $\epsilon \in [0, 0.5)$. See Figure 6.6a for a visualization of the MAE for all classification datasets. Since the distances are normalized, a higher ϵ value indicates classifying the majority of distances as negligible. As a result, the values of interest are small, which is why a logarithmic scale is used for the x-axis.

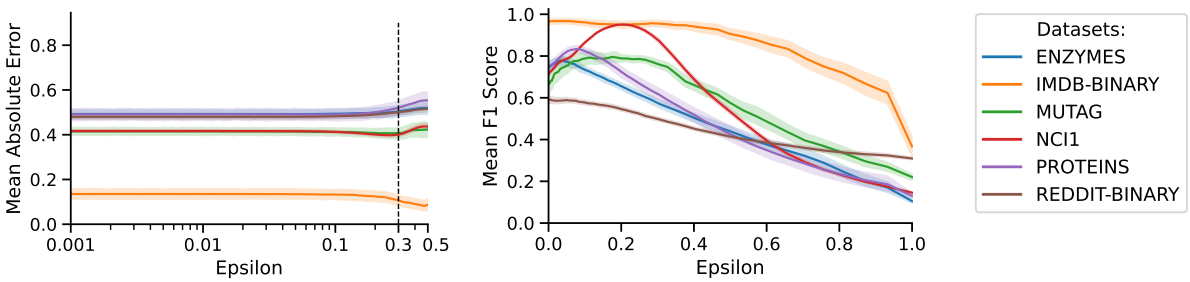

(a) Continous Approximation (b) Binary Approximation

Figure 6.6.: Results obtained by using the proposed evaluation procedures to assess the ability of GNNs to approximate 1-WL colorings.

The second procedure, Binary Approximation, aims to transform the regression-like values into a classification task by introducing a threshold value, ϵ, which maps distances between two node representations to a binary value. Distances less than ϵ are classified as 0, while distances greater than or equal to ϵ are classified as 1. This process generates a distance matrix with binary values, and the F1 score is used to evaluate the approximation capability of this newly devised matrix to the 1-WL coloring distance matrix. The process is repeated for each graph in a dataset, and the average F1 score is calculated as the final evaluation metric. Since the number of node pairs distinguished by the 1-WL algorithm differs from the number of nodes assigned the same color, an imbalance between the two distances, 0 and 1, exists. To counter any biases due to this imbalance, where the F1 score is calculated independently for each distance and then averaged. Figure 6.6b provides a visualization of the results for each classification dataset.

Analyzing the figures, it becomes apparent that the approximation of the 1-WL coloring is imprecise, as indicated by the relatively high MAE and the varying F1 scores for different datasets, with the clear exception of the IMDB-BINARY dataset.

The performance of the IMDB-BINARY dataset can be attributed to the fact that the IMDB-BINARY and REDDIT-BINARY datasets lack node features, such that we initialize their features using the common procedure of one-hot encoding their node degrees. Since the coloring computed by a single iteration of the 1-WL algorithm is an encoding of the node degree, this explains the good performance of the IMDB-BINARY dataset. However, due to the large size of the REDDIT-BINARY dataset and its graphs, a one-hot encoding of the node degree is not practical. Instead, a continuous, one-dimensional node degree encoding is employed that uniformly maps a node degree into the range $[-1, 1]$. This difference in encoding explains the significant performance gap observed between the two datasets in both approximation evaluations, see Figure 6.6.

Interestingly, the MAE remains constant for ϵ values up to 0.3, as depicted in Figure 6.6a, suggesting that the GNN models tend to map nodes with different values far away from each other and vice versa for small values. This observation aligns with the low standard deviation values, indicating consistent behavior across all graphs. Since $\epsilon = 0.3$ is already a considerable threshold for removing distances as the maximum is 0.5, we infer that the GNNs compute a coloring that incorporates essential information from the 1-WL coloring while leaving out less important information. The visual representations show that the distances between nodes exhibit similar patterns as the coloring produced by the 1-WL algorithm, although not as

perfect. Since the GNN models perform nearly as well as most of the 1-WL+NN models in terms of their accuracy performance, we conclude that GNNs are able to learn a more efficient encoding of the graph structure that holds the most important structural information of the 1-WL coloring.

Analyzing Figure 6.6b, where we mapped each distance matrix to discrete distances based on the ϵ value, we observe that each dataset has its own optimal threshold value ϵ for the F1 score. Interestingly, these optima consistently fall within a narrow range between 0.0 and 0.2. Moreover, most datasets achieve a high F1 score, providing further evidence for our hypothesis regarding the encoding of essential structural information. With the exception of REDDIT-BINARY, almost all datasets achieve a score higher than 0.77. Notably, the NCI1 dataset stands out with an exceptional Mean F1 score of 0.95 for $\epsilon = 0.2$. This result indicates that the node representations computed by the best GNN model for NCI1 effectively encode the structural information captured by a single iteration of the 1-WL algorithm. Furthermore, considering the dataset taxonomy introduced in Section 5.1, NCI1 belongs to the dataset category that encodes a substantial amount of information in their graph structures, which aligns with our findings.

It is also worth noting that NCI1 is the only dataset that demonstrates improved performance, in terms of accuracy, with an increased number of 1-WL iterations in the testing of the 1-WL+NN models (refer to Figure 6.1). Therefore we also, explored the capability of the best performing GNN model on NCI1 to approximate the colorings computed after applying the 1-WL iteration for three iterations. The results are visualized in Figure B.17 in the Appendix. However, as explained in the previous section, the number of unique colors increases significantly with an increased number of 1-WL iterations, which leads to the fact that the majority of nodes are colored uniquely (refer to Figure 6.3). Consequently, almost all nodes in a graph need to be mapped to separable node representation by a GNN. To investigate whether this holds for any of the datasets, we visualized the frequency of distances by creating ten uniformly non-overlapping intervals between 0 and 1 and counted the number of distances that fall in each interval in Figure 6.7. Analyzing the figure reveals no concentration in the frequency of large distances for any of the datasets. Therefore, we conclude that GNNs cannot effectively approximate a higher number of 1-WL iterations.

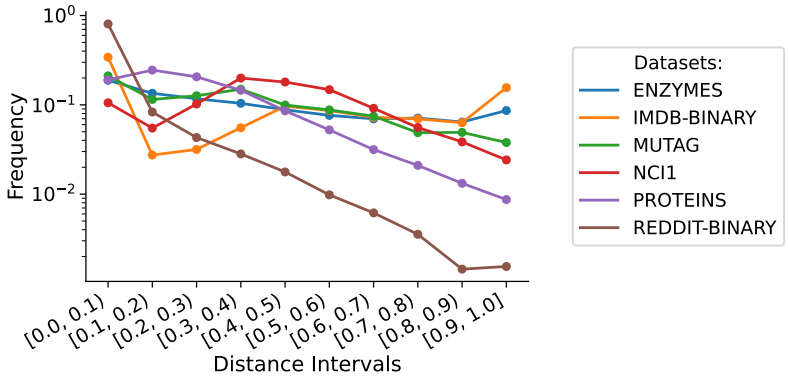

Figure 6.7.: Visualization of the frequency of the distance between node pairs in the representation computed by the best-performing GNN mode, using a logarithmic scale on the y-axis. In detail, we divided the distance space into ten non-overlapping intervals and counted the number of occurrences that fall into this interval for each dataset.

In conclusion, considering the similar accuracy performance of GNN and 1-WL+NN models and the relatively robust approximation capabilities of GNNs compared to the 1-WL coloring after a single iteration, we argue that GNNs learn to efficiently encode the essential information in a graph for solving the task by striking the right balance between incorporating structural and label information. Further, given that both frameworks achieve comparable performance on all datasets in terms of accuracy, combined with the fact that most models utilize only a single iteration of the 1-WL algorithm or an approximation of the coloring, the question arises as to whether this difference remains when pooling this information using the same pooling function. We will investigate this question in the following section.

6.4. Comparing Pooled Graph Representations: GNN vs. 1-WL+NN Models

After the previous section, we observed that GNNs do not perfectly approximate the coloring calculated by the 1-WL algorithm. However, we hypothesized that GNNs might employ a more efficient encoding containing only essential information. To investigate further, we will examine the graph representations derived after pooling the node representations analyzed in the previous section. We aim to establish if these graph representations hold the same amount of information and share similarities. If they do, this will strengthen our hypothesis that the GNN models learn a more efficient encoding, and it suggests that the full expressiveness of the 1-WL algorithm may not be necessary for these tasks.

To achieve this, we selected the best-performing GNN and 1-WL+NN models in terms of classification accuracy for each dataset and replaced the final multilayer perceptron with various algorithms. Specifically, we used two different configurations of Support Vector Machines (SVM): one with a linear kernel (SVM Linear) and another with a radial basis function (SVM RBF). Additionally, we employed the k-Nearest-Neighbor (k-NN) classifier for different values of k. Each algorithm was trained exclusively on the fixed output of the pooling function. To ensure fair comparisons, we froze the weights of the GNN models and the Look-Up Table of the 1-WL+NN models during this process to ensure no optimization of underlying parameters before pooling. This approach guarantees more comparable results across algorithms. Moreover, we maintained the same training, validation, and test split used for training and evaluating the MLP. For a comprehensive evaluation, we summarized the accuracies and standard deviations achieved by each method, comparing them to the MLP's performance in Table 6.4. Furthermore, in the case of the k-NN algorithm, we provided the achieved accuracy for the optimal k value, including the k value in the parentheses. This analysis will allow us to make statements about the linear separability of the graph representations as well as how well these cluster with respect to their class labels.

Evaluating Linear Separability

Starting with the investigation of linear separability, we used the performance of SVM Linear as our basis of evaluation since this method learns a linear high-dimensional hyperplane to separate the graph representations optimally. The results of the SVM RBF serve as a baseline that shows how effectively the data will be linear separable after applying the RBF kernel. Therefore, if both SVM methods achieve similar performance, we can conclude that the graph representations are already relatively linearly separable, and there is no need for applying an

Table 6.4.: Overview of accuracy and standard deviation in percent achieved by various methods, trained and tested on graph representations computed by the best 1-WL+NN and GNN models.

	Method	Dataset					
		ENZYMES	IMDB-BINARY	MUTAG	NCI1	PROTEINS	REDDIT-BINARY
1-WL+NN	MLP	48.3 ±8.1	**72.4** ±4.1	85.1 ±8.6	83.6 ±4.1	**75.2** ±3.9	78.4 ±2.7
	SVM Linear	34.4 ±5.5	71.2 ±3.9	86.4 ±8.9	83.4 ±2.1	73.9 ±4.1	77.8 ±2.7
	SVM RBF	45.0 ±7.0	72.8 ±4.3	83.2 ±7.5	83.6 ±1.9	75.2 ±4.0	78.3 ±2.4
	k-NN	**56.3** ±5.8 (k=1)	72.3 ±4.1 (k=11)	**86.7** ±7.7 (k=10)	**83.9** ±1.8 (k=5)	73.9 ±4.1 (k=19)	**83.2** ±2.5 (k=13)
GNN	MLP	34.4 ±7.0	**74.7** ±3.8	84.6 ±8.7	**79.9** ±2.2	74.3 ±5.1	86.9 ±3.2
	SVM Linear	33.2 ±5.9	73.9 ±4.2	**87.4** ±6.8	67.4 ±2.2	74.7 ±4.2	84.2 ±2.8
	SVM RBF	35.9 ±6.0	74.1 ±3.9	86.0 ±7.4	73.0 ±1.9	74.6 ±4.6	88.7 ±2.4
	k-NN	**51.6** ±7.0 (k=1)	74.3 ±4.0 (k=132)	88.3 ±6.5 (k=38)	77.5 ±1.7 (k=2)	**74.9** ±4.3 (k=27)	**90.8** ±1.8 (k=15)

additional kernel function.

Interestingly, for both GNN and 1-WL+NN models, the linear SVM performed comparably to the MLP, with the exceptions of ENZYMES for the 1-WL+NN model and NCI1 for the GNN model. In fact, SVM Linear even outperformed the MLP of the GNN model on MUTAG, indicating strong linear separability of the graph representations. Furthermore, since the insights were similar for both GNN and 1-WL+NN models, we concluded that both methods map their graph representations in such a way as to facilitate easy linear separation. Additionally, we observed that the accuracy achieved by SVM RBF is higher than the one of SVM Linear; however, this difference is negligible and insignificant (except for the ENZYMES dataset). This insight, again, demonstrates how well the graph representations are linear separability.

For a visualization of the decision boundary calculated by SVM Linear, see Figure 6.8. We used the t-distributed stochastic neighbor embedding (t-SNE) to reduce the dimensions of the graph representation for visualization purposes. However, note that the t-SNE method distorts the actual distances between data points, such that these visualizations only aid the imagination of the actual relation between graph representations.

The insight that the GNN and the 1-WL+NN model compute node representations that, when pooled into a single graph representation, allow for good linear separability further support our hypothesis that the extra expressiveness contained in the 1-WL colorings is unnecessary, and GNNs indeed employ a more efficient encoding, as suggested in the previous section.

Evaluating Clustering Performance

Another interesting property we also want to investigate is how well these graph representations cluster in their high dimensional space with respect to their class label. To do so, we utilized the k-NN classifier for different values of k with k ranging from 1 to 200 (except for the MUTAG dataset, which only contains 188 graphs, k was limited to a range of 1 to 150). Our primary interest was to observe if any range of k values exists where the accuracy consistently remained high. The existence of such a range indicates the presence of meaningful clusters among all graph representations. In order to observe such patterns, we plotted the accuracy achieved on each dataset against the corresponding k values, as illustrated in Figure 6.10.

Before analyzing Figure 6.10, we explain why the existence of such a range indicates good clustering. Consider the two artificial scenarios depicted in Figure 6.9, where we construct two balanced datasets with 1000 two-dimensional data points for a binary classification task. The

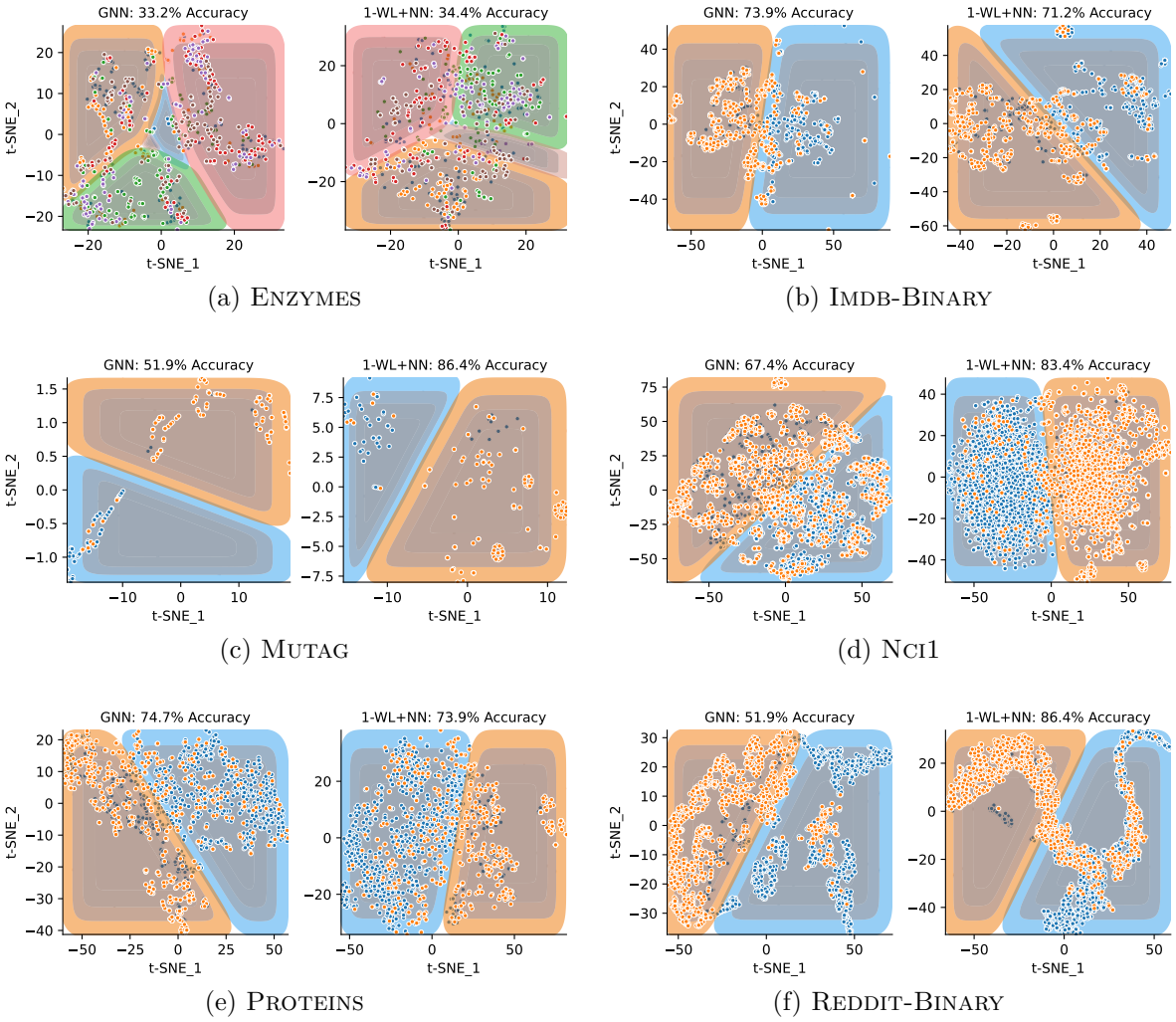

(a) Enzymes (b) Imdb-Binary

(c) Mutag (d) Nci1

(e) Proteins (f) Reddit-Binary

Figure 6.8.: Visualization of the decision boundary of each SVM Linear using t-SNE for the reduction of the dimensionality to two dimensions.

dataset in Figure 6.9a clusters well, meaning it is easy to determine which region in the feature space corresponds to each class, while the other dataset in Figure 6.9b clusters poorly. By training a k-NN classifier on both datasets individually for various k, we observe the following: If the data clusters well, the accuracy achieved by the k-NN classifier will be consistently high and not fluctuate significantly for different values of k. Conversely, accuracies around 50 % with strong fluctuations indicate poor clustering.

Upon analyzing Figure 6.10, we can see for all datasets that for some range of k values, there exists a plateau of the accuracy curve, except for the Enzymes and Nci1 datasets. These plateaus correspond to the highest accuracy achieved among all k values, indicating that both graph representations computed by 1-WL+NN and GNN models indeed form meaningful clusters with respect to their class labels. Furthermore, as the GNN model outperformed the 1-WL+NN model for most k values, we can conclude that the higher expressiveness of the node representation computed by the 1-WL algorithm is obsolete and the GNN models indeed compute a more efficient encoding of its nodes, which leads to pooled graph representations

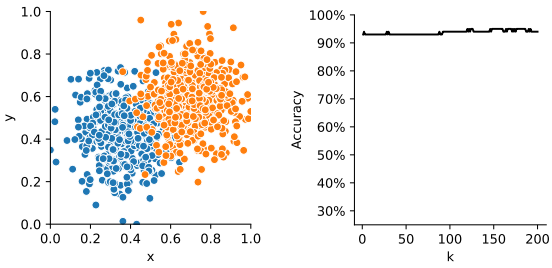

(a) Example for good clustering Performance

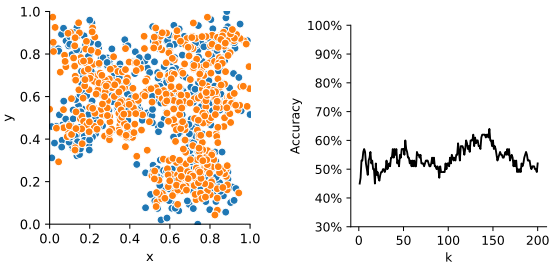

(b) Example for bad clustering Performance

Figure 6.9.: Impact of clustered data on the performance of the k-NN classifier. Two artificial, balanced binary classification datasets with 1000 two-dimensional data points are used. One dataset exhibits good clustering, while the other does not. The k-NN classifier accuracy, trained on both datasets, is plotted for various k values.

that achieved the same or even better results in terms of clustering. This insight is even more pronounced in the example of the REDDIT-BINARY dataset, as here, a significant difference exists in its clustering behavior compared to the 1-WL+NN models.

In the case of the ENZYMES dataset, although there is no such range of values of k observable, the accuracy curve is very similar for both types of models, indicating that the lack of a distinct clustering indication may be attributed to the characteristics of the dataset.

The real exception, however, lies in the behavior of the k-NN when applied to the NCI1 dataset. Here, only the graph representations computed by the 1-WL+NN model exhibit strong clustering performance that remains consistently high across all values of k. In contrast, the graph representations of the GNN model do not seem to cluster at all, and the maximum achievable accuracy is significantly lower than the average accuracy achieved by the 1-WL+NN model representations. We attribute this effect to the 1-WL+NN model's use of three iterations of the 1-WL algorithm, compared to just one iteration used by all other models of the other datasets. Since the NCI1 dataset encodes essential information for solving its respective task mainly in the structure of its graphs (Liu et al. [2022]), this pattern might only be specific to this dataset. Moreover, we observed that no other dataset showed better performance of its 1-WL+NN models with an increased number of 1-WL iterations, as evident in Figure 6.1.

In conclusion, our findings indicate that the pooled graph representations computed by both 1-WL+NN and GNN models are highly linearly separable in their high-dimensional space while also forming meaningful clusters with respect to their class labels. Notably, the GNN models demonstrated superior clustering performance, providing further support for our hypothesis that the message-passing layers of a GNN encode essential information without overly emphasizing expressiveness. This suggests that the GNN models strike a balance between efficient encoding and required expressiveness depending on their application.

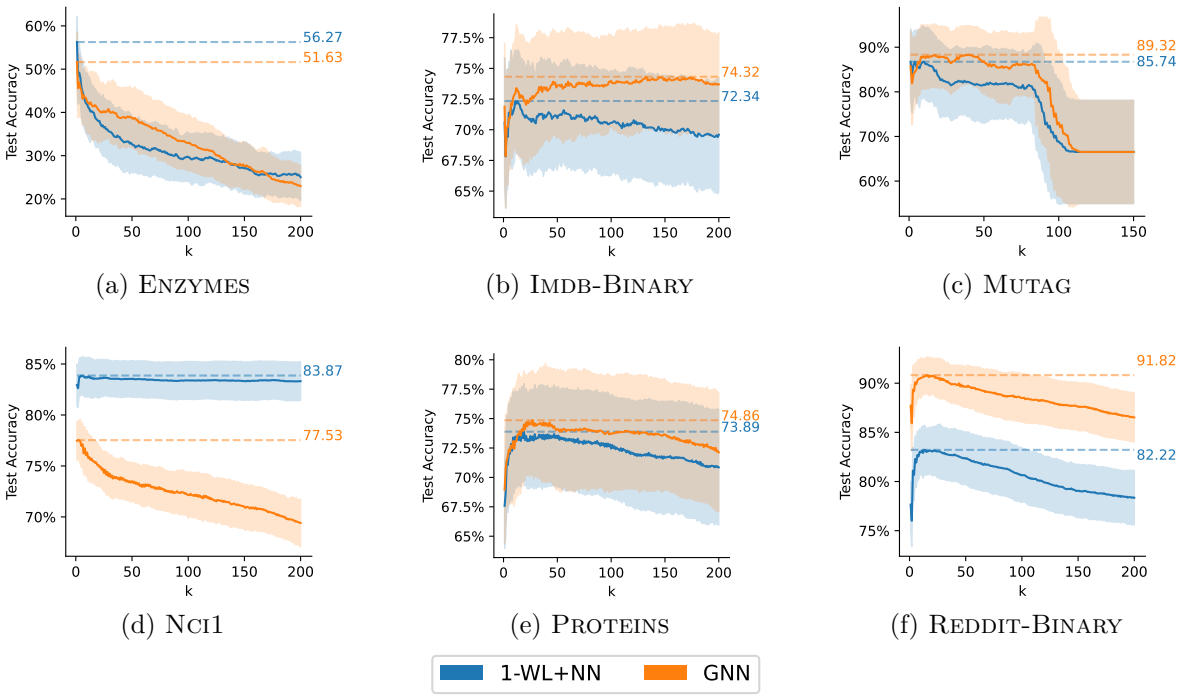

(a) Enzymes (b) Imdb-Binary (c) Mutag

(d) Nci1 (e) Proteins (f) Reddit-Binary

Figure 6.10.: Average classification accuracy achieved on each dataset by replacing the multilayer perceptron of the best-performing 1-WL+NN and GNN model with a classifier based on the k-nearest neighbors algorithm. We tested for different values of k.

6.5. Combining the 1-WL algorithm with GNNs

As already outlined at the beginning of this chapter, in comparison to all configurations we tested for 1-WL+NN and GNN models, the best accuracy on all classification datasets was achieved by a 1-WL+NN model, except for the Imdb-Binary and Reddit-Binary dataset. What makes this observation so interesting is that both datasets are the only ones lacking node features, such that we initialize the features of the dataset with an encoding of their node degree for GNN models tested on these datasets.

This difference raises the question of whether GNN models generally perform better when their input graphs undergo preprocessing. Specifically, we aim to explore if GNN models achieve improved performance when their graphs are preprocessed using the 1-WL algorithm for a single iteration. We will refer to such GNN models as 1-WL:GNN.

This idea seems promising as most of the best-performing 1-WL+NN models also utilize a single iteration of the 1-WL algorithm as their basis for computation. Further, we know that a 1-WL:GNN model can already achieve the same accuracy as each 1-WL+NN model by simply forwarding the preprocessed input graph to the pooling function. However, we hope that 1-WL:GNN models leverage their message-passing layers to generate an improved node representation, ultimately leading to enhanced performance in the end.

We conducted the same hyperparameter optimization routines as for the normal GNN models and listed the classification accuracy achieved by the best-performing configuration of a 1-WL:GNN model for each dataset in Table 8. We also included the best performances of each 1-WL+NN and GNN models for comparison. However, it is essential to note that due to the

time constraints of this work and the prioritization of hyperparameter optimization for GNN and 1-WL+NN models, we tested fewer configurations for 1-WL:GNN models. Consequently, these results should be interpreted with caution.

Table 6.5.: Accuracy and standard deviation in percent achieved by the best-performing 1-WL+NN, 1-WL:GNN, and GNN model on each classification dataset.

Model	Dataset					
	Enzymes	Imdb-Binary	Mutag	Nci1	Proteins	Reddit-Binary
1-WL+NN	48.3 ±8.1	72.4 ±4.1	85.1 ±8.6	83.6 ±2.2	75.2 ±3.9	78.4 ±2.7
1-WL:GNN	35.9 ±6.9	72.0 ±4.1	83.9 ±11.0	78.2 ±2.4	74.5 ±4.1	84.3 ±2.8
GNN	34.4 ±7.0	74.7 ±3.8	84.6 ±8.7	79.9 ±2.2	74.3 ±5.1	86.9 ±3.2

Upon analyzing the best accuracies achieved by each 1-WL:GNN model in comparison to the other model types, we observed that its performance is not significantly better than any of the GNN or 1-WL+NN models. While it does show minor improvements compared to the GNN models, such as in the Enzymes and Proteins datasets, these improvements are not significant.

This observation leads to the conclusion that artificially incorporating the expressiveness of the 1-WL algorithm into the node representations computed by a GNN does not necessarily improve the performance of GNNs. Moreover, it reinforces our finding that the representations learned by a GNN tend to emphasize essential aspects rather than computing a fully expressive representation.

6.6. Impact of the Size of Datasets on the Performance of 1-WL+NN

After learning about the expressiveness of the 1-WL algorithm in terms of the number of unique colors its uses in Figure 6.3, compared with the fact that this number is increasingly larger for larger datasets as outlined in Table B.7 in the Appendix, the question arises: Do 1-WL+NN models scale as effectively as GNN models in terms of performance as the dataset size increases? To investigate this hypothesis, we selected two regression datasets, Alchemy and Zinc, and utilized two fixed splits of different sizes for each dataset. These splits allowed us to test 1-WL+NN models on both the entire dataset and a smaller subset representing less than 5 % of the total data, enabling us to explore potential performance differences. An overview of the results is provided in Table 6.2 at the beginning of this section.

Similar to the classification datasets, we conducted a hyperparameter optimization for both 1-WL+NN and GNN models. The primary question of interest here was whether we would observe performance differences between the various splits for each dataset and if there would be discrepancies between the two types of models.

Upon analyzing these results, the first notable observation is that the best performances were achieved entirely by GNN models, specifically the GIN:Sum model. However, in comparison to the GINE-ε model by Morris et al. [2020], which we included as a reference to showcase the performance achieved by a different GNN model than ours, both our GNN and 1-WL+NN models demonstrated inferior performance. We conjecture that this discrepancy can be attributed to

GINE-ε utilizing the edge features of its input graph in its computation, while our models do not.

Regarding the differences in performance between the various splits for each dataset, the evidence is not straightforward. While 1-WL+NN models performed better on the smaller split ALCHEMY(10K) than the full split, GNN models demonstrated a similar margin of improvement. Moreover, we observed the opposite phenomenon on ZINC, with 1-WL+NN and GNN models achieving better performance on the larger ZINC split than the smaller ZINC(10K) split.

One reason such differences are not evident for 1-WL+NN models may be because the best-performing 1-WL+NN configurations still utilized only a limited number of 1-WL iterations. For instance, the models for ALCHEMY employed only a single iteration of the 1-WL algorithm for both splits, resulting in a constant number of 70 unique colors. Similarly, the best model for ZINC(10K) used two iterations, leading to 9,818 unique colors, while the best model on ZINC utilized three iterations and encountered 290,473 unique colors. Both numbers are significantly smaller than the number of unique colors used by a higher number of iterations. See Table B.7 for a summary of the number of unique colors for different numbers of 1-WL iterations.

Furthermore, the variations in the splits might also have contributed to the observed differences between the datasets. In particular, the number of unique colors after a single 1-WL iteration differs for ZINC and ZINC(10K), whereas it remains the same for both splits of ALCHEMY.

Further, it is important to note that due to time constraints and the immense time required, especially for training models on the entire ALCHEMY or ZINC dataset, the number of configurations we tested is relatively low compared to ZINC(10K) and ALCHEMY(10K). For a complete overview of the number of runs for each dataset and each model, refer to Table B.6 in the Appendix.

Another aspect to consider is that, unlike all other results, the ALCHEMY and ZINC datasets are regression tasks, which might not be as suitable for 1-WL+NN models due to the discrete nature of the 1-WL algorithm and the resulting discrete node representations. In this context, the ability of GNN models to compute continuous node representations may be better suited for regression tasks. However, it is important to note that the difference between GNN and 1-WL+NN models in Table 6.2 is not as substantial as this aspect might initially indicate.

In conclusion, the impact of the size of a dataset on the performance of 1-WL+NN models must be investigated further. In detail, future research needs to investigate datasets not only of large size but also datasets that consist of large graphs, such that the number of unique colors is already relatively high even after a single iteration of the 1-WL algorithm. A good example of such a dataset is the REDDIT-BINARY dataset, where the number of unique colors after a single iteration of the 1-WL algorithm is 566 due to the high number of nodes on average per graph. For this dataset, a performance gap between 1-WL+NN and GNN models can be observed, with the best GNN model achieving up to an 8 % higher accuracy than the best 1-WL+NN model (refer to Table 6.2). However, it is also essential to acknowledge that the reasons for this performance gap are not solely attributable to the dataset's size, as other factors are at play, as discussed in the preceding sections.

7. Discusssion

This concluding chapter discusses and summarizes the key findings and conclusions from our empirical investigation by addressing our initial research questions. Moreover, it examines the use case of the 1-WL+NN framework beyond the scope of this work and outlines potential areas for future research. Finally, the thesis concludes with some final remarks.

7.1. Insights into the Representations learned by GNNs

In the following, we answer our research questions **Q1** to **Q4**.

Q1 Can 1-WL+NN models achieve comparable performance to GNN models empirically?
A1 Yes, the results on the classification datasets indicate that 1-WL+NN models achieved comparable performance and even outperformed GNN models on 4 out of 6 datasets. However, the experiments on the regression datasets show a performance discrepancy between GNN and 1-WL+NN models, suggesting that 1-WL+NN models might be more suitable for classification tasks than regression tasks due to the discrete nature of the 1-WL algorithm.

Q2 Are there observable differences in the learning behavior between 1-WL+NN and GNN models?
A2 Yes, 1-WL+NN models tend to exhibit more pronounced overfitting than GNN models. This behavior is primarily due to the highly expressive nature of the 1-WL algorithm and the intricate colorings it computes, which can lead to memorizing specific patterns in the data. To ensure good generality of 1-WL+NN models, it is often necessary to limit the expressiveness of the 1-WL algorithm in most applications. In contrast, GNN models do not demonstrate severe overfitting issues, primarily because they map their node representations into a continuous, contained space. To put this into perspective, the colorings computed by a 1-WL+NN model utilize many distinct integers whose numerical distances to one another are huge compared to the colorings produced by GNN models. This difference in representation spaces contributes to the contrasting overfitting behavior observed between the two model types.

Q3 To what extent does the expressiveness of 1-WL+NN models contribute to their empirical performance, and do GNN models leverage their theoretical ability to be equally expressive?
A3 In the majority of cases, 1-WL+NN models do not fully utilize the expressiveness of the 1-WL algorithm to achieve comparable performance. Most best-performing 1-WL+NN models use only a single iteration of the 1-WL algorithm, effectively equivalent to a node degree encoding. Interestingly, GNN models also mainly rely on this information, computing node representations similar to those produced by a single iteration of the 1-WL algorithm. However, there are exceptions where utilizing an increased number of 1-WL iterations for a 1-WL+NN model improves its performance, demonstrating the potential of the expressiveness of 1-WL+NN models. In these exceptional cases, GNN models also show better approximation capability of

the coloring computed by the 1-WL algorithm Additionally, we noticed that this approximation is very robust, meaning modifying the distance between node representations artificially yields the same approximation performance. These observations lead us to conclude that GNN models strike a balance between efficient encoding and required expressiveness depending on the application. They are able to capture the essential information needed for the task without fully leveraging the complete expressiveness of the 1-WL algorithm in most cases.

Q4 Is there a substantial difference in the graph representations computed by each model type?

A4 The graph representations derived from pooling the node representations of 1-WL+NN and GNN models share many similarities. Both graph representations demonstrate good linear separability and clustering in their high-dimensional space, indicating that the full expressiveness of the 1-WL algorithm is not always necessary, as GNNs achieve similar results with more efficient encoding. Moreover, GNN models even perform better on most datasets regarding linear separability and clustering, indicating that the information encoded in their node representations is more efficiently captured, even though it may not be as expressive as the 1-WL coloring.

7.2. The 1-WL+NN Framework beyond the Scope of this Work

Throughout this work, we have extensively explored the similarities between the 1-WL+NN and GNN frameworks, establishing their theoretical equivalence in terms of computability and uncovering various shared characteristics. As a result, the 1-WL+NN framework emerges as a valuable tool for investigating GNN models and datasets and even offers certain advantages over GNNs.

One significant advantage lies in the ease of deployment. Configuring a 1-WL+NN model involves only selecting a suitable encoding function and configuring the size of its multilayer perceptron. Additionally, the colors computed by the 1-WL algorithm remain fixed and only need to be calculated once during the initialization of the model. Consequently, the training process of a 1-WL+NN model mainly revolves around optimizing the multilayer perceptron, making it notably faster than training GNN models. For instance, in our experiments training a GIN:Sum model on the ZINC dataset took nearly 13 hours, while our best 1-WL+NN model completed training in under 3 hours.

However, despite these advantages, it is crucial to acknowledge that 1-WL+NN models are restricted in their real-world applicability. The requirement to initialize the 1-WL algorithm with unique colors for all local substructures the model will encounter before training makes the 1-WL+NN framework more suitable for research purposes and tasks with a known set of input graphs. In contrast, GNNs exhibit greater versatility, proving effective on any input graph and thus better suited for real-world applications.

In conclusion, the 1-WL+NN framework can be utilized as a research tool, offering valuable insights into GNN behavior and performance evaluation for datasets. Their advantages make them well-suited for research and understanding the theoretical underpinnings of GNNs.

7.3. Recommendations for Future Research

This section highlights potential areas for further investigation that emerged during our study, offering valuable opportunities for future research.

The impact of the 1-WL algorithm as a tool for preprocessing data for GNN models, as discussed and investigated in Section 6.5, needs further research. While initial results did not show significant improvements, they at least demonstrated comparable performance to GNNs. Investigating the reasons behind this phenomenon and conducting additional hyperparameter optimization runs for 1-WL:GNN models will shed light on the potential advantages and limitations of incorporating 1-WL as a tool for preprocessing data of GNN models.

The observed discrepancies in performance on the regression datasets, as discussed in Section 6.6, prompt us to investigate whether these differences are inherent to the nature of the regression task or influenced by the dataset size. To address this, conducting further experiments on smaller-scale regression datasets and larger-scale classification datasets would yield valuable insights into the scalability and generalizability of both 1-WL+NN and GNN models.

One such large-scale classification dataset that can be considered is the MalNet dataset curated by Freitas et al. [2022]. It offers two fixed splits: one utilizes the entire dataset, consisting of 1.2 million samples, while the smaller split, called MalNet(tiny), consists of only 5 000 samples. Utilizing this dataset would enable us to explore the impact of dataset size on the performance of both 1-WL+NN and GNN models, providing a deeper understanding of their behavior and capabilities across different data scales.

7.4. Conclusion

In conclusion, this thesis has introduced the novel 1-WL+NN framework, establishing its theoretical equivalence to GNNs in terms of computability. The extensive investigation using the 1-WL+NN framework has provided valuable insights into the behavior of GNN models.

By leveraging the 1-WL+NN framework as a tool for understanding GNNs, we have discovered that GNN models exhibit greater efficiency in generalization and encoding. In detail, GNNs effectively capture the essential structural information required to solve specific tasks without fully leveraging the complete expressiveness of the 1-WL algorithm.

These findings not only enhance our understanding of graph neural networks but also open new possibilities for further advancements. The 1-WL+NN framework offers researchers a valuable tool for gaining deeper insights into GNN behavior and performance, leading to novel approaches and improvements in graph-based machine learning.

Bibliography

[1] R. Abboud, I. I. Ceylan, M. Grohe, and T. Lukasiewicz. The surprising power of graph neural networks with random node initialization. *arXiv preprint arXiv:2010.01179*, 2020.

[2] J. Atwood and D. Towsley. Diffusion-convolutional neural networks. *Advances in neural information processing systems*, 29, 2016.

[3] L. Babai. Lectures on graph isomorphism. University of Toronto, Department of Computer Science. Mimeographed lecture notes, October 1979, 1979.

[4] L. Babai. Graph isomorphism in quasipolynomial time. In *Proceedings of the forty-eighth annual ACM symposium on Theory of Computing*, pages 684–697, 2016.

[5] L. Babai and L. Kucera. Canonical labelling of graphs in linear average time. In *20th annual symposium on foundations of computer science (sfcs 1979)*, pages 39–46. IEEE, 1979.

[6] D. Bahdanau, K. Cho, and Y. Bengio. Neural machine translation by jointly learning to align and translate. *arXiv preprint arXiv:1409.0473*, 2014.

[7] D. Beaini, S. Passaro, V. Létourneau, W. Hamilton, G. Corso, and P. Liò. Directional graph networks. In *International Conference on Machine Learning*, pages 748–758. PMLR, 2021.

[8] K. M. Borgwardt, C. S. Ong, S. Schönauer, S. Vishwanathan, A. J. Smola, and H.-P. Kriegel. Protein function prediction via graph kernels. *Bioinformatics*, 21(suppl_1):i47–i56, 2005.

[9] X. Bresson and T. Laurent. A two-step graph convolutional decoder for molecule generation. *arXiv preprint arXiv:1906.03412*, 2019.

[10] T. Brown, B. Mann, N. Ryder, M. Subbiah, J. D. Kaplan, P. Dhariwal, A. Neelakantan, P. Shyam, G. Sastry, A. Askell, et al. Language models are few-shot learners. *Advances in neural information processing systems*, 33:1877–1901, 2020.

[11] J. Bruna, W. Zaremba, A. Szlam, and Y. LeCun. Spectral networks and locally connected networks on graphs. *arXiv preprint arXiv:1312.6203*, 2013.

[12] J. Cai, M. Fürer, and N. Immerman. An optimal lower bound on the number of variables for graph identifications. *Combinatorica*, 12(4):389–410, 1992.

[13] A. Cardon and M. Crochemore. Partitioning a graph in o (¦ a¦ log2¦ v¦). *Theoretical Computer Science*, 19(1):85–98, 1982.

[14] G. Chen, P. Chen, C.-Y. Hsieh, C.-K. Lee, B. Liao, R. Liao, W. Liu, J. Qiu, Q. Sun, J. Tang, et al. Alchemy: A quantum chemistry dataset for benchmarking ai models. *arXiv preprint arXiv:1906.09427*, 2019.

[15] Z. Chen, S. Villar, L. Chen, and J. Bruna. On the equivalence between graph isomorphism testing and function approximation with gnns. *Advances in neural information processing systems*, 32, 2019.

[16] A. K. Debnath, R. L. Lopez de Compadre, G. Debnath, A. J. Shusterman, and C. Hansch. Structure-activity relationship of mutagenic aromatic and heteroaromatic nitro compounds. correlation with molecular orbital energies and hydrophobicity. *Journal of medicinal chemistry*, 34(2):786–797, 1991.

[17] M. Defferrard, X. Bresson, and P. Vandergheynst. Convolutional neural networks on graphs with fast localized spectral filtering. *Advances in neural information processing systems*, 29, 2016.

[18] D. K. Duvenaud, D. Maclaurin, J. Iparraguirre, R. Bombarell, T. Hirzel, A. Aspuru-Guzik, and R. P. Adams. Convolutional networks on graphs for learning molecular fingerprints. *Advances in neural information processing systems*, 28, 2015.

[19] S. Freitas, R. Duggal, and D. H. Chau. Malnet: A large-scale image database of malicious software. In *Proceedings of the 31st ACM International Conference on Information & Knowledge Management*, pages 3948–3952, 2022.

[20] F. Geerts. The expressive power of kth-order invariant graph networks, 2020.

[21] J. Gilmer, S. S. Schoenholz, P. F. Riley, O. Vinyals, and G. E. Dahl. Neural message passing for quantum chemistry. In *International conference on machine learning*, pages 1263–1272. PMLR, 2017.

[22] M. Grohe. *Descriptive Complexity, Canonisation, and Definable Graph Structure Theory*. Lecture Notes in Logic. Cambridge University Press, 2017.

[23] W. Hamilton, Z. Ying, and J. Leskovec. Inductive representation learning on large graphs. *Advances in neural information processing systems*, 30, 2017.

[24] K. He, X. Zhang, S. Ren, and J. Sun. Deep residual learning for image recognition. In *Proceedings of the IEEE conference on computer vision and pattern recognition*, pages 770–778, 2016.

[25] K. Hornik. Approximation capabilities of multilayer feedforward networks. *Neural networks*, 4(2):251–257, 1991.

[26] N. Immerman and E. Lander. *Describing Graphs: A First-Order Approach to Graph Canonization*, pages 59–81. Springer, 1990.

[27] J. J. Irwin, T. Sterling, M. M. Mysinger, E. S. Bolstad, and R. G. Coleman. Zinc: a free tool to discover chemistry for biology. *Journal of chemical information and modeling*, 52 (7):1757–1768, 2012.

[28] T. N. Kipf and M. Welling. Semi-supervised classification with graph convolutional networks. In *International Conference on Learning Representations*, 2017.

[29] A. Krizhevsky, G. Hinton, et al. Learning multiple layers of features from tiny images. 2009.

[30] Y. Li, D. Tarlow, M. Brockschmidt, and R. Zemel. Gated graph sequence neural networks. *arXiv preprint arXiv:1511.05493*, 2015.

[31] R. Liu, S. Cantürk, F. Wenkel, S. McGuire, X. Wang, A. Little, L. O'Bray, M. Perlmutter, B. Rieck, M. Hirn, et al. Taxonomy of benchmarks in graph representation learning. In *Learning on Graphs Conference*, pages 6–1. PMLR, 2022.

[32] A. Micheli. Neural network for graphs: A contextual constructive approach. *IEEE Transactions on Neural Networks*, 20(3):498–511, 2009.

[33] C. Morris, N. M. Kriege, K. Kersting, and P. Mutzel. Faster kernel for graphs with continuous attributes via hashing. In *IEEE International Conference on Data Mining*, pages 1095–1100, 2016.

[34] C. Morris, M. Ritzert, M. Fey, W. L. Hamilton, J. E. Lenssen, G. Rattan, and M. Grohe. Weisfeiler and leman go neural: Higher-order graph neural networks. In *Proceedings of the AAAI conference on artificial intelligence*, volume 33, pages 4602–4609, 2019.

[35] C. Morris, N. M. Kriege, F. Bause, K. Kersting, P. Mutzel, and M. Neumann. Tudataset: A collection of benchmark datasets for learning with graphs. In *ICML 2020 Workshop on Graph Representation Learning and Beyond (GRL+ 2020)*, 2020. URL `www.graphlearning.io`.

[36] C. Morris, G. Rattan, S. Kiefer, and S. Ravanbakhsh. Speqnets: Sparsity-aware permutation-equivariant graph networks. In *International Conference on Machine Learning*, pages 16017–16042. PMLR, 2022.

[37] G. Nikolentzos, M. Chatzianastasis, and M. Vazirgiannis. What do gnns actually learn? towards understanding their representations. *arXiv preprint arXiv:2304.10851*, 2023a.

[38] G. Nikolentzos, M. Chatzianastasis, and M. Vazirgiannis. Weisfeiler and leman go hyperbolic: Learning distance preserving node representations. In *International Conference on Artificial Intelligence and Statistics*, pages 1037–1054. PMLR, 2023b.

[39] R. Paige and R. E. Tarjan. Three partition refinement algorithms. *SIAM Journal on computing*, 16(6):973–989, 1987.

[40] A. Radford, J. Wu, R. Child, D. Luan, D. Amodei, I. Sutskever, et al. Language models are unsupervised multitask learners. *OpenAI blog*, 1(8):9, 2019.

[41] R. Sato, M. Yamada, and H. Kashima. Random features strengthen graph neural networks. In *Proceedings of the 2021 SIAM International Conference on Data Mining (SDM)*, pages 333–341. SIAM, 2021.

[42] F. Scarselli, M. Gori, A. C. Tsoi, M. Hagenbuchner, and G. Monfardini. The graph neural network model. *IEEE transactions on neural networks*, 20(1):61–80, 2008.

[43] F. Scarselli, M. Gori, A. C. Tsoi, M. Hagenbuchner, and G. Monfardini. The graph neural network model. *IEEE Transactions on Neural Networks*, 20(1):61–80, 2009.

[44] N. Shervashidze, P. Schweitzer, E. J. Van Leeuwen, K. Mehlhorn, and K. M. Borgwardt. Weisfeiler-lehman graph kernels. *Journal of Machine Learning Research*, 12(9), 2011.

[45] A. Sperduti and A. Starita. Supervised neural networks for the classification of structures. *IEEE Transactions on Neural Networks*, 8(3):714–735, 1997.

[46] P. Veličković, G. Cucurull, A. Casanova, A. Romero, P. Lio, and Y. Bengio. Graph attention networks. *arXiv preprint arXiv:1710.10903*, 2017.

[47] C. Vignac, A. Loukas, and P. Frossard. Building powerful and equivariant graph neural networks with structural message-passing. *Advances in neural information processing systems*, 33:14143–14155, 2020.

[48] O. Vinyals, S. Bengio, and M. Kudlur. Order matters: Sequence to sequence for sets. *arXiv preprint arXiv:1511.06391*, 2015.

[49] N. Wale, I. A. Watson, and G. Karypis. Comparison of descriptor spaces for chemical compound retrieval and classification. *Knowledge and Information Systems*, 14:347–375, 2008.

[50] B. Weisfeiler and A. Leman. The reduction of a graph to canonical form and the algebra which appears therein. *Nauchno-Technicheskaya Informatsia*, 2(9):12–16, 1968.

[51] K. Xu, W. Hu, J. Leskovec, and S. Jegelka. How powerful are graph neural networks? In *International Conference on Learning Representations*, 2019.

[52] P. Yanardag and S. Vishwanathan. Deep graph kernels. In *Proceedings of the 21th ACM SIGKDD international conference on knowledge discovery and data mining*, pages 1365–1374, 2015.

[53] Z. Ying, J. You, C. Morris, X. Ren, W. Hamilton, and J. Leskovec. Hierarchical graph representation learning with differentiable pooling. *Advances in neural information processing systems*, 31, 2018.

[54] M. Zhang, Z. Cui, M. Neumann, and Y. Chen. An end-to-end deep learning architecture for graph classification. In *Proceedings of the AAAI conference on artificial intelligence*, volume 32, 2018.

[55] B. Zoph, V. Vasudevan, J. Shlens, and Q. V. Le. Learning transferable architectures for scalable image recognition. In *Proceedings of the IEEE conference on computer vision and pattern recognition*, pages 8697–8710, 2018.

A. Appendix Part I

A.1. Graph Attention Network

The Graph Attention Network (GAT) developed by [46] is a distinctive GNN architecture that features a unique attention mechanism inspired by natural language processing, specifically from the work [6]. This attention mechanism allows the model to focus on relevant parts of the input data during message-passing, enabling the GAT to learn the importance of each neighboring node for updating a node's representation.

Definition 25. The message-passing layers of the GAT architecture are defined as follows:

$$f_{\text{merge}}^{(t)} = \sigma(\alpha_{vv} \cdot f^{(t)}(v) + f_{\text{agg}}^{(t)}), \quad \text{and} \quad f_{\text{agg}}^{(t)} = \sum_{u \in \mathcal{N}(v)} \alpha_{vu} \cdot W^{(t)} \cdot f^{(t-1)}(u),$$

with the attention coefficient α_{vv} computed as follows:

$$\alpha_{vu} = \frac{\exp\Big(\text{LeakyReLU}\Big(\vec{a}^T \cdot \mathsf{concat}[W^{(t)} f^{(t-1)}(v),\ W^{(t)} f^{(t-1)}(u)]\Big)\Big)}{\sum_{k \in \mathcal{N}(v) \cup \{v\}} \exp\big(\text{LeakyReLU}\big(\vec{a}^T \cdot \mathsf{concat}[W^{(t)} f^{(t-1)}(v),\ W^{(t)} f^{(t-1)}(k)]\big)\big)},$$

where $\vec{a}$ is a learnable vector, $W^{(t)}$ a learnable matrix, and σ a non-linear activation function. Further, the LeakyReLU function is defined as follows:

$$\text{LeakyReLU}(x) := \begin{cases} x, & \text{if } x \geq 0 \\ m \cdot x, & \text{else} \end{cases},$$

where m is a learnable parameter and is referred to as "negative-slop". This value is in the context of the GAT usually initialized to $m := 0.2$.

B. Appendix Part II

B.1. Definition of the Normalized Shannon-Index

We used the following definition of the Normalized Shannon-Index.

Definition 26 (Normalized Shannon-Index)**.** The metric is computed as follows:

$$-\frac{1}{\log_2(|C|)} \cdot \sum_{i \in C} \frac{n_i}{n} \cdot \log_2(\frac{n_i}{n}) \tag{B.1.1}$$

where n is the total number of samples of the dataset, C is the set of all classes, and n_i is the number of samples of the class $i \in C$.

As an example, for the dataset PROTEINS the variables are set to be the following: $C = \{0, 1\}$ with $n_0 = 663$ and $n_1 = 450$, so that $n = 1113$, yielding a rounded value of 0.973.

B.2. Theoretical Maximum Accuracy Analysis

Table B.1.: An overview of the maximum theoretical classification accuracy achievable for each dataset based on the number of 1-WL iterations in percent. A hyphen "-" indicates that the maximum accuracy has converged with fewer iterations, implying that further iterations do not improve the accuracy. "OOM" denotes out of memory error.

	Datasets	**Iterations of the 1-WL algorithm**					
		0	1	2	3	4	5
Bioinformatics	DD	1.00	-	-	-	-	-
	ENZYMES	0.81	1.00	-	-	-	-
	KKI	1.00	-	-	-	-	-
	OHSU	1.00	-	-	-	-	-
	Peking_1	1.00	-	-	-	-	-
	PROTEINS	0.92	1.00	-	-	-	-
Small molecules	AIDS	1.00	1.00	-	-	-	-
	BZR	0.96	0.99	1.00	-	-	-
	COX2	0.93	0.96	0.99	1.00	-	-
	DHFR	0.92	0.95	1.00	1.00	-	-
	FRANKENSTEIN	0.63	0.77	0.88	0.89	0.89	-
	MUTAG	0.93	0.96	0.99	1.00	-	-
	NCI1	0.91	1.00	1.00	1.00	-	-
	NCI109	0.92	1.00	1.00	1.00	-	-
	PTC_MR	0.92	0.98	0.99	-	-	-
Social networks	COLLAB	0.61	0.98	-	-	-	-
	IMDB-BINARY	0.61	0.89	-	-	-	-
	IMDB-MULTI	0.44	0.63	-	-	-	-
	REDDIT-BINARY	0.84	1.00	-	-	-	-
	REDDIT-MULTI-5K	0.55	1.00	-	-	-	-
	REDDIT-MULTI-12K	0.36	OOM	OOM	OOM	OOM	OOM

B.3. Hyperparameter Configuration and Optimization

Overview of Hyperparameters: 1-WL+NN on the Classification Datasets

Table B.2.: Hyperparameters for 1-WL+NN models for the classification datasets. Highlighting the best-performing configuration when multiple options exist for a parameter.

Hyperparameter	**Dataset**		
	ENZYMES	IMDB-BINARY	MUTAG
Batch Size	32	32	32
Learning Rate	$X \sim U(0.0001, 0.1)$	$X \sim U(0.0001, 0.1)$	$X \sim U(0.0001, 0.1)$
Max Epochs	200	200	200
Optimizer	Adam	Adam	Adam
Scheduler	ReduceLROnPlateau	ReduceLROnPlateau	ReduceLROnPlateau
Number of 1-WL iterations	$\{\mathbf{1}, 2, 3, 4\}$	$\{\mathbf{1}, 2, 3, 4\}$	$\{\mathbf{1}, 2, 3, 4\}$
Use 1-WL-Convergence	False	False	False
MLP Activation Function	ReLU	ReLU	ReLU
MLP Normalization	BatchNorm	BatchNorm	BatchNorm
MLP Number of Layers	$\{2, \mathbf{3}, 4, 5\}$	$\{2, \mathbf{3}, 4, 5\}$	$\{2, \mathbf{3}, 4, 5\}$
MLP Dropout	$X \sim U(0, 0.2)$	$X \sim U(0, 0.2)$	$X \sim U(0, 0.2)$
Embedding Dimension	$\{\text{None}, 16, 32, 64, \mathbf{128}\}$	$\{\text{None}, \mathbf{16}, 32, 64, 128\}$	$\{\text{None}, 16, \mathbf{32}, 64, 128\}$
Pooling function	{Max, Mean, **Sum**}	{Max, **Mean**, Sum}	{Max, Mean, **Sum**}

Hyperparameter	**Dataset**		
	NCI1	PROTEINS	REDDIT-BINARY
Batch Size	33	32	32
Learning Rate	$X \sim U(0.0001, 0.1)$	$X \sim U(0.0001, 0.1)$	$X \sim U(0.0001, 0.1)$
Max Epochs	200	200	200
Optimizer	Adam	Adam	Adam
Scheduler	ReduceLROnPlateau	ReduceLROnPlateau	ReduceLROnPlateau
Number of 1-WL iterations	$\{1, 2, \mathbf{3}, 4\}$	$\{\mathbf{1}, 2, 3, 4\}$	$\{\mathbf{1}, 2, 3, 4\}$
Use 1-WL-Convergence	False	False	False
MLP Activation Function	ReLU	ReLU	ReLU
MLP Normalization	BatchNorm	BatchNorm	BatchNorm
MLP Number of Layers	$\{\mathbf{2}, 3, 4, 5\}$	$\{2, \mathbf{3}, 4, 5\}$	$\{2, \mathbf{3}, 4, 5\}$
MLP Dropout	$X \sim U(0, 0.2)$	$X \sim U(0, 0.2)$	$X \sim U(0, 0.2)$
Embedding Dimension	$\{\text{None}, 16, \mathbf{32}, 64, 128\}$	$\{\text{None}, 16, 32, \mathbf{64}, 128\}$	$\{\text{None}, 16, 32, 64, \mathbf{128}\}$
Pooling function	{Max, Mean, **Sum**}	{**Max**, Mean, Sum}	{Max, Mean, **Sum**}

Overview of Hyperparameters: GNN on the Classification Datasets

Table B.3.: Hyperparameters for GNN models for the classification datasets. Highlighting the best-performing configuration when multiple options exist for a parameter.

Hyperparameter	Dataset		
	ENZYMES	IMDB-BINARY	MUTAG
Batch Size	32	32	32
Learning Rate	$X \sim U(0.0001, 0.1)$	$X \sim U(0.0001, 0.1)$	$X \sim U(0.0001, 0.1)$
Max Epochs	200	200	200
Optimizer	Adam	Adam	Adam
Scheduler	ReduceLROnPlateau	ReduceLROnPlateau	ReduceLROnPlateau
GNN Architecture	{**GAT**, GCN, GIN}	{GAT, **GCN**, GIN}	{GAT, GCN, **GIN**}
GNN Activation Function	ReLU	ReLU	ReLU
GNN Dropout	$X \sim U(0, 0.2)$	$X \sim U(0, 0.2)$	$X \sim U(0, 0.2)$
GNN Hidden Dimension	{16, 32, **64**, 128}	{16, 32, **64**, 128}	{**16**, 32, 64, 128}
GNN Jumping-Knowledge	cat	cat	cat
GNN Number of Layers	5	5	5
MLP Activation Function	ReLU	ReLU	ReLU
MLP Normalization	BatchNorm	BatchNorm	BatchNorm
MLP Number of Layers	{2, **3**, 4, 5}	{2, 3, 4, **5**}	{2, **3**, 4, 5}
MLP Dropout	$X \sim U(0, 0.2)$	$X \sim U(0, 0.2)$	$X \sim U(0, 0.2)$
Pooling function	{Max, Mean, **Sum**}	{Max, **Mean**, Sum}	{Max, Mean, **Sum**}

Hyperparameter	Dataset		
	NCI1	PROTEINS	REDDIT-BINARY
Batch Size	{33, **129**}	32	32
Learning Rate	$X \sim U(0.0001, 0.1)$	$X \sim U(0.0001, 0.1)$	$X \sim U(0.0001, 0.1)$
Max Epochs	200	200	200
Optimizer	Adam	Adam	Adam
Scheduler	ReduceLROnPlateau	ReduceLROnPlateau	ReduceLROnPlateau
GNN Architecture	{GAT, GCN, **GIN**}	{GAT, GCN, **GIN**}	{GAT, **GCN**, GIN}
GNN Activation Function	ReLU	ReLU	ReLU
GNN Dropout	$X \sim U(0, 0.2)$	$X \sim U(0, 0.2)$	$X \sim U(0, 0.2)$
GNN Hidden Dimension	{16, 32, 64, **128**}	{16, 32, 64, **128**}	{**16**, 32, 64, 128}
GNN Jumping-Knowledge	cat	cat	cat
GNN Number of Layers	5	5	5
MLP Activation Function	ReLU	ReLU	ReLU
MLP Normalization	BatchNorm	BatchNorm	BatchNorm
MLP Number of Layers	{2, 3, **4**, 5}	{2, 3, **4**, 5}	{**2**, 3, 4, 5}
MLP Dropout	$X \sim U(0, 0.2)$	$X \sim U(0, 0.2)$	$X \sim U(0, 0.2)$
Pooling function	{**Max**, Mean, Sum}	{**Max**, Mean, Sum}	{**Max**, Mean, Sum}

Overview of Hyperparameters: 1-WL+NN on the Regression Datasets

Table B.4.: Hyperparameters for 1-WL+NN models for the regression datasets. Highlighting the best-performing configuration when multiple options exist for a parameter.

Hyperparameter	Dataset			
	ALCHEMY	ALCHEMY(10K)	ZINC	ZINC(10K)
Batch Size	25	25	25	25
Learning Rate	0.001	0.001	0.001	0.001
Max Epochs	1000	1000	1000	1000
Optimizer	Adam	Adam	Adam	Adam
Scheduler	ReduceLROnPlateau	ReduceLROnPlateau	ReduceLROnPlateau	ReduceLROnPlateau
Number of 1-WL iterations	$\{\mathbf{1}, 2, 3\}$	$\{\mathbf{1}, 2, 3, 4\}$	$\{1, 2, \mathbf{3}\}$	$\{1, \mathbf{2}, 3, 4\}$
Use 1-WL-Convergence	False	False	False	False
MLP Activation Function	ReLU	ReLU	ReLU	ReLU
MLP Normalization	BatchNorm	BatchNorm	BatchNorm	BatchNorm
MLP Number of Layers	$\{2, \mathbf{3}, 4, 5\}$	$\{2, 3, 4, 5, 6, \mathbf{7}\}$	$\{2, \mathbf{3}, 4, 5\}$	$\{2, \mathbf{3}, 4, 5\}$
MLP Dropout	$X \sim U(0, 0.2)$	$X \sim U(0, 0.2)$	$X \sim U(0, 0.2)$	$X \sim U(0, 0.2)$
Embedding Dimension	$\{16, \mathbf{32}, 64, 128, 256\}$	$\{16, 32, 64, 128, \mathbf{256}\}$	$\{16, 32, 64, 128, \mathbf{256}\}$	$\{16, 32, 64, 128, \mathbf{256}\}$
Pooling function	{Max, Mean, **Sum**}	{Max, Mean, **Sum**}	{Max, **Mean**, Sum}	{Max, Mean, **Sum**}

Overview of Hyperparameters: GNN on the Regression Datasets

Table B.5.: Hyperparameters for GNN models for the regression datasets. Highlighting the best-performing configuration when multiple options exist for a parameter.

Hyperparameter	Dataset			
	ALCHEMY	ALCHEMY(10K)	ZINC	ZINC(10K)
Batch Size	25	25	25	25
Learning Rate	0.001	0.001	0.001	0.001
Max Epochs	1000	1000	1000	1000
Optimizer	Adam	Adam	Adam	Adam
Scheduler	ReduceLROnPlateau	ReduceLROnPlateau	ReduceLROnPlateau	ReduceLROnPlateau
GNN Architecture	GIN	GIN	GIN	GIN
GNN Activation Function	ReLU	ReLU	ReLU	ReLU
GNN Dropout	0.0	0.0	0.0	0.0
GNN Hidden Dimension	256	256	256	256
GNN Jumping-Knowledge	cat	cat	cat	cat
GNN Number of Layers	5	5	5	5
MLP Activation Function	ReLU	ReLU	ReLU	ReLU
MLP Normalization	BatchNorm	BatchNorm	BatchNorm	BatchNorm
MLP Number of Layers	4	4	4	4
MLP Dropout	0.0	0.0	0.0	0.0
Pooling function	{Max, Mean, **Sum**}	{Max, Mean, **Sum**}	{Max, Mean, **Sum**}	{Max, Mean, **Sum**}

B.3.1. Impact of each Hyperparameter for 1-WL+NN

In this section, we present the results of our hyperparameter optimization for the 1-WL+NN framework on each classification dataset. We plot a random subset of the tested configurations where each line in the visualization represents a single configuration and is color-coded based on its accuracy relative to the other plotted configurations. Bright yellow lines indicate configurations that performed among the best, while dark purple lines represent configurations with the worst performance. The color coding gradually transitions between these two color endpoints, allowing for a clear visual representation of the performance spectrum. Note that a

value of -1 for the number of iterations of the 1-WL algorithm indicates the use of the standard version of the algorithm.

1-WL+NN Configurations on the ENZYMES Dataset

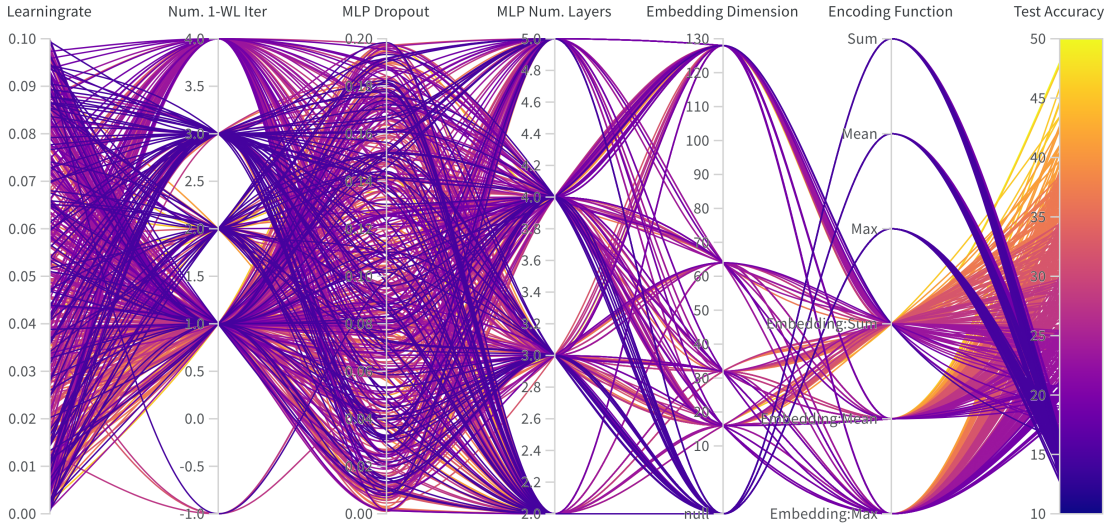

Figure B.1.: Overview of the effects of each hyperparameter on the accuracy of the corresponding configured 1-WL+NN model for the Enzymes dataset.

1-WL+NN Configurations on the IMDB-BINARY Dataset

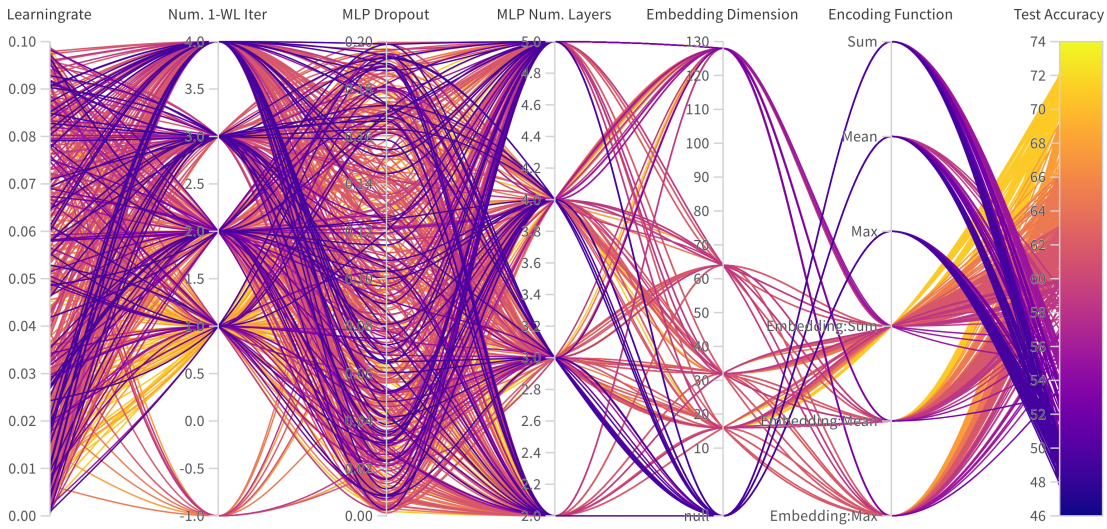

Figure B.2.: Overview of the effects of each hyperparameter on the accuracy of the corresponding configured 1-WL+NN model for the Imdb-Binary dataset.

1-WL+NN Configurations on the MUTAG Dataset

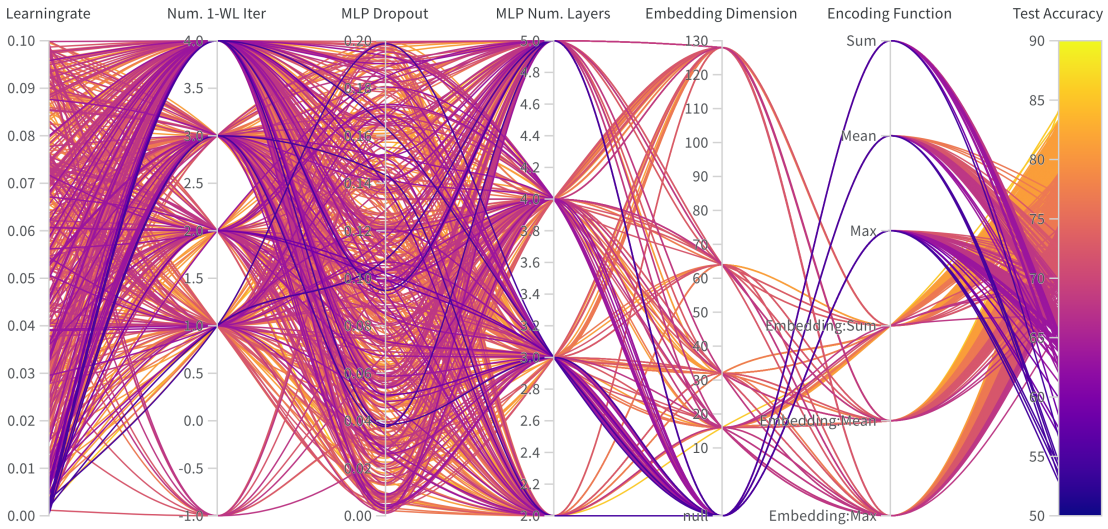

Figure B.3.: Overview of the effects of each hyperparameter on the accuracy of the corresponding configured 1-WL+NN model for the MUTAG dataset.

1-WL+NN Configurations on the NCI1 Dataset

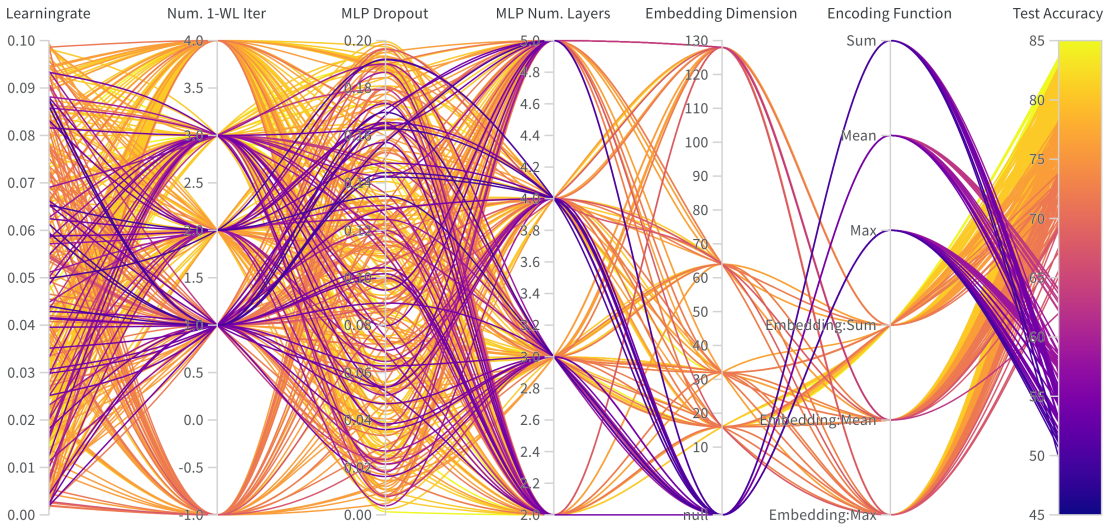

Figure B.4.: Overview of the effects of each hyperparameter on the accuracy of the corresponding configured 1-WL+NN model for the NCI1 dataset.

1-WL+NN Configurations on the PROTEINS Dataset

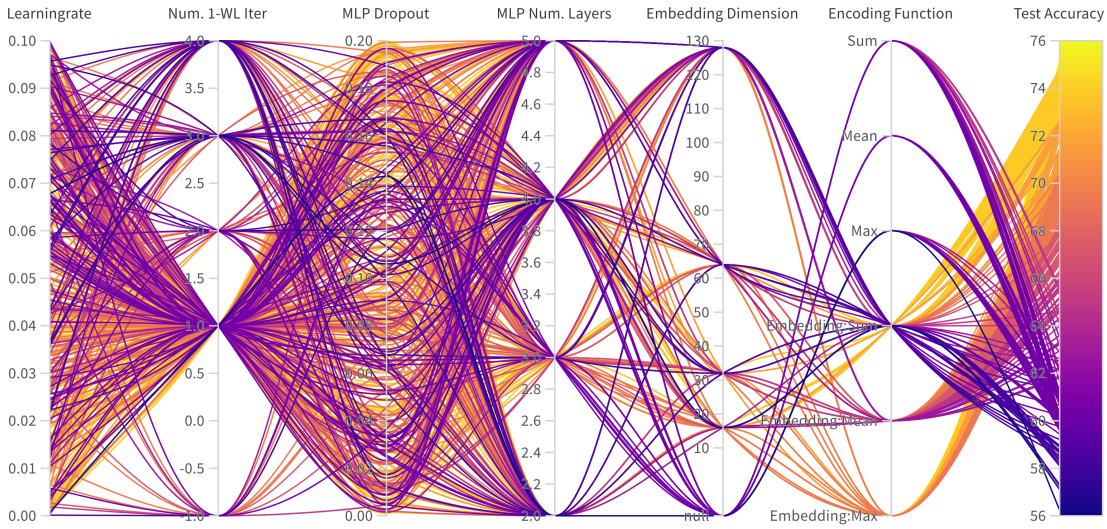

Figure B.5.: Overview of the effects of each hyperparameter on the accuracy of the corresponding configured 1-WL+NN model for the PROTEINS dataset.

1-WL+NN Configurations on the REDDIT-BINARY Dataset

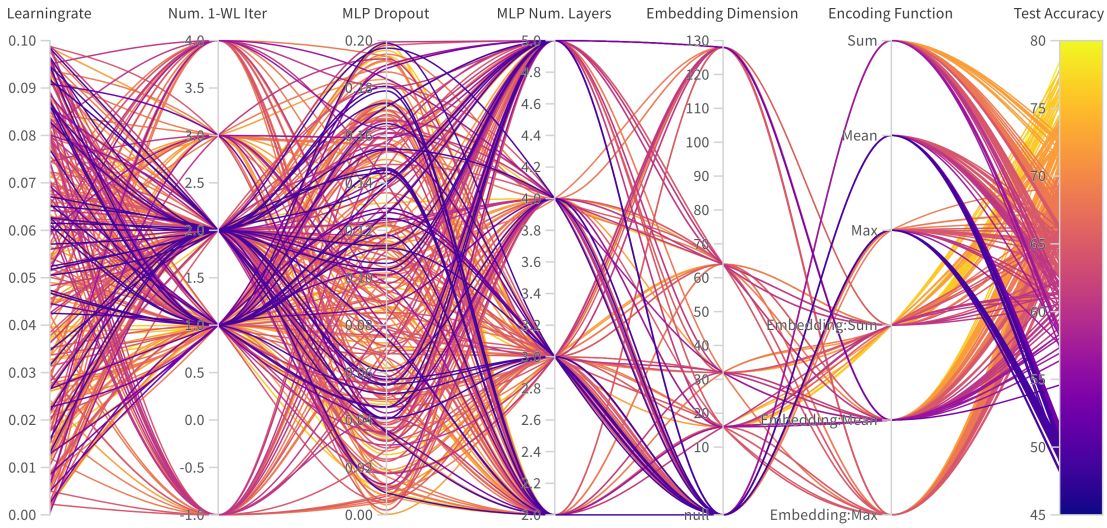

Figure B.6.: Overview of the effects of each hyperparameter on the accuracy of the corresponding configured 1-WL+NN model for the REDDIT-BINARY dataset.

B.3.2. Impact of each Hyperparameter for GNNs

In this section, we present the results of our hyperparameter optimization for the GNN framework on each classification dataset. We will use the same visualization explained and utilized in the previous section, customized to the hyperparameters of the GNN models.

GNN Configurations on the ENZYMES Dataset

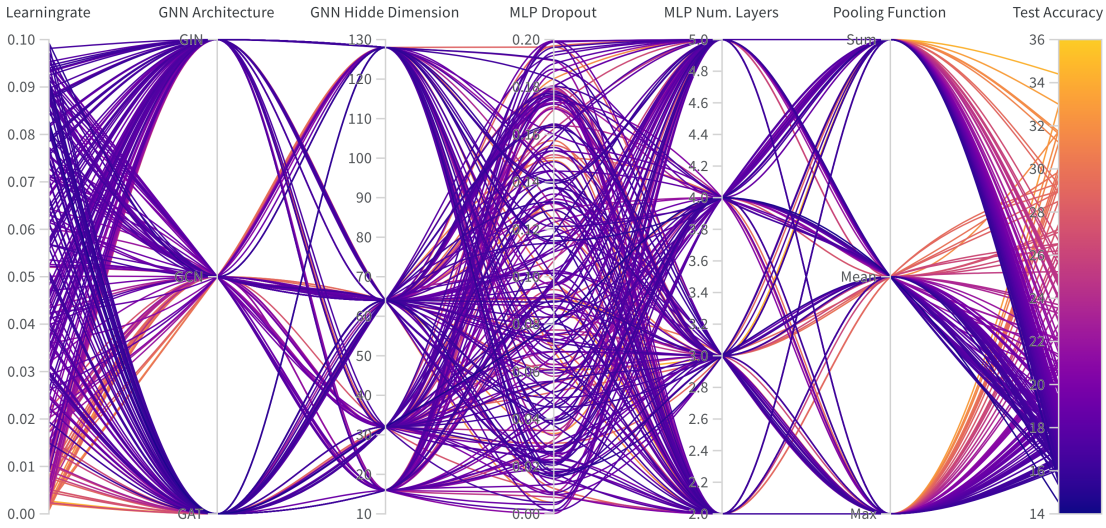

Figure B.7.: Overview of the effects of each hyperparameter on the accuracy of the corresponding configured GNN model for the ENZYMES dataset.

GNN Configurations on the IMDB-BINARY Dataset

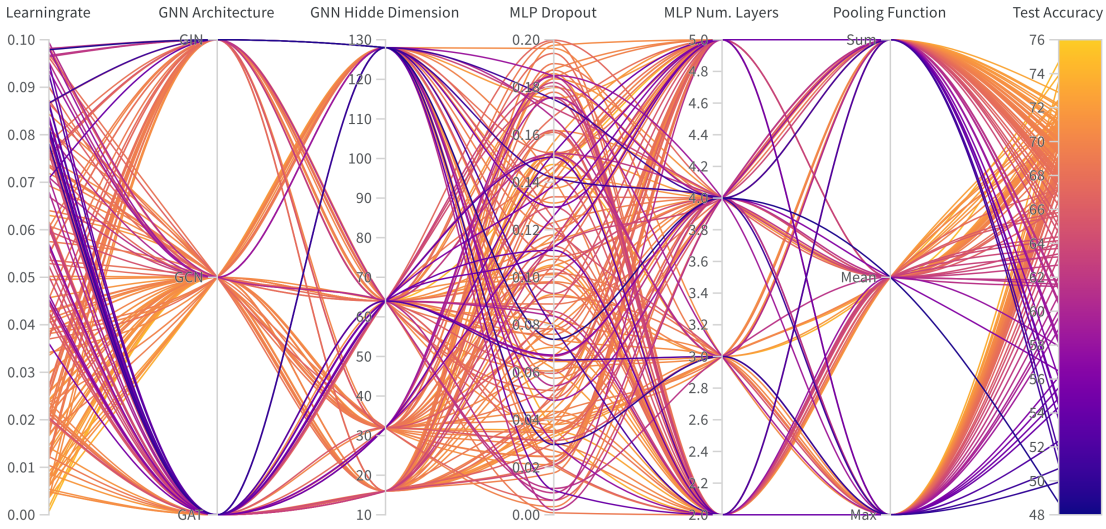

Figure B.8.: Overview of the effects of each hyperparameter on the accuracy of the corresponding configured GNN model for the IMDB-BINARY dataset.

GNN Configurations on the MUTAG Dataset

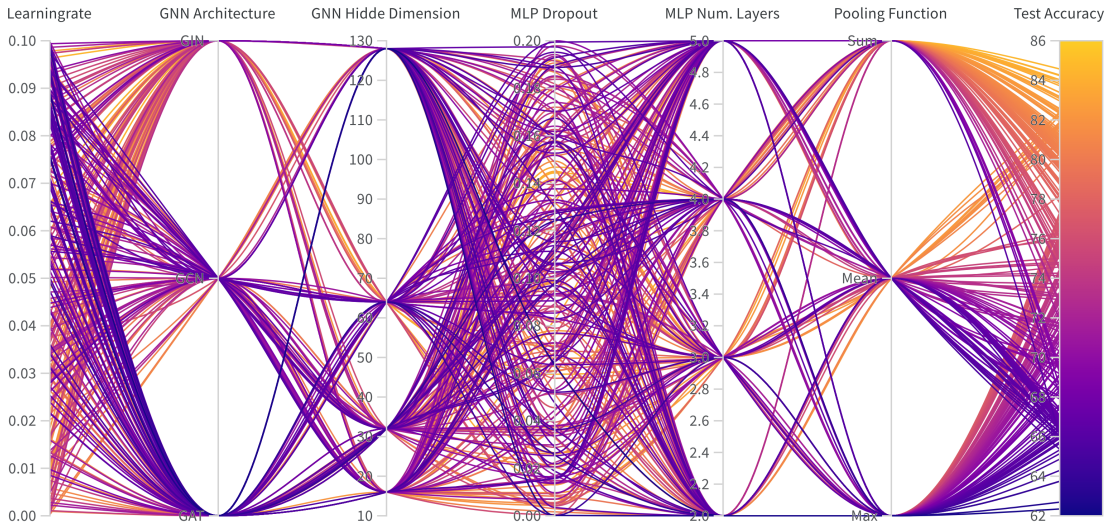

Figure B.9.: Overview of the effects of each hyperparameter on the accuracy of the corresponding configured GNN model for the MUTAG dataset.

GNN Configurations on the NCI1 Dataset

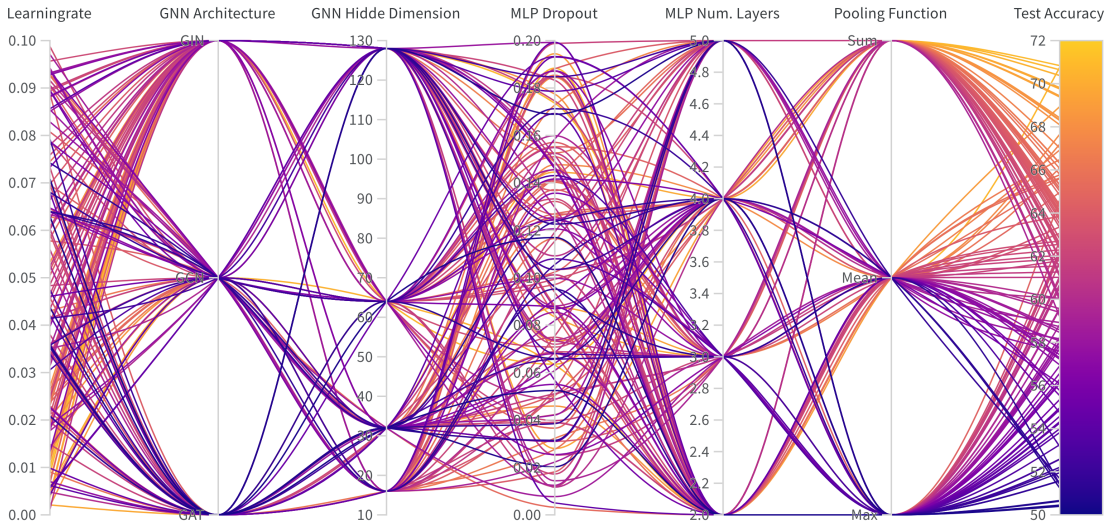

Figure B.10.: Overview of the effects of each hyperparameter on the accuracy of the corresponding configured GNN model for the NCI1 dataset.

GNN Configurations on the PROTEINS Dataset

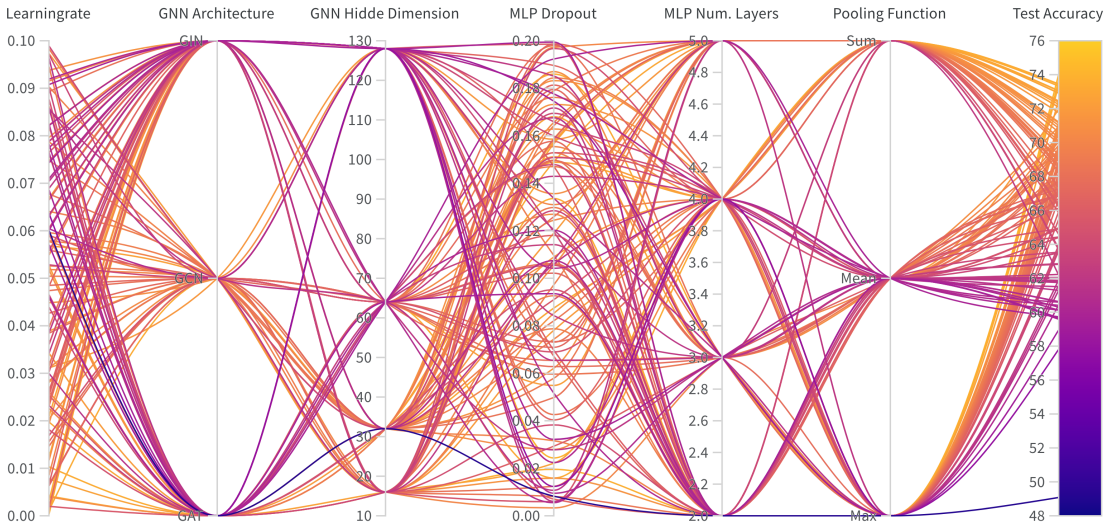

Figure B.11.: Overview of the effects of each hyperparameter on the accuracy of the corresponding configured GNN model for the PROTEINS dataset.

GNN Configurations on the REDDIT-BINARY Dataset

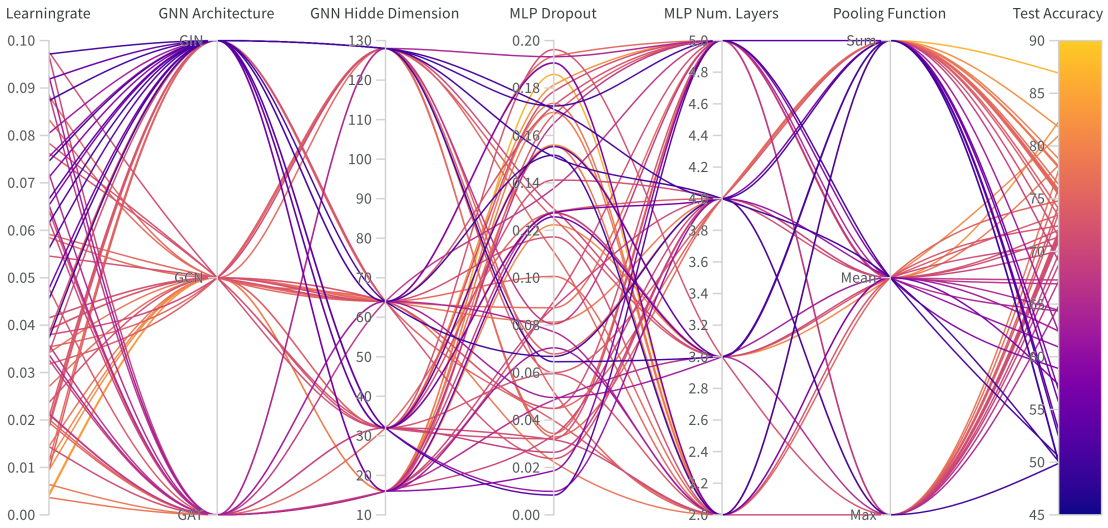

Figure B.12.: Overview of the effects of each hyperparameter on the accuracy of the corresponding configured GNN model for the REDDIT-BINARY dataset.

B.3.3. Overview of the Number of Configurations

Table B.6.: Overview of the number of different configurations tested for each model type and each dataset.

	Model	Dataset									
		Classification						Regression			
		Enzymes	Imdb-Binary	Mutag	Nci1	Proteins	Reddit-Binary	Alchemy	Alchemy(10k)	Zinc	Zinc(10k)
1-WL+NN	Max	86	70	150	26	35	40	0	0	0	0
	Mean	76	67	120	19	27	40	0	0	0	0
	Sum	85	67	130	14	29	41	0	0	0	0
	Embedding-Max	338	282	290	79	245	45	3	95	6	33
	Embedding-Mean	288	271	299	109	216	50	6	77	8	24
	Embedding-Sum	296	293	302	79	215	48	5	273	7	18
Graph Neural Networks	GAT:Max	17	17	36	11	10	6	0	0	0	0
	GAT:Mean	28	15	29	12	10	6	0	0	0	0
	GAT:Sum	26	17	37	15	16	6	0	0	0	0
	GCN:Max	31	22	37	17	10	9	0	0	0	0
	GCN:Mean	19	26	26	19	16	5	0	0	0	0
	GCN:Sum	30	29	27	17	14	10	0	0	0	0
	GIN:Max	21	17	28	25	20	3	1	1	1	1
	GIN:Mean	31	9	31	18	26	9	2	2	2	2
	GIN:Sum	26	9	36	20	11	9	1	1	1	1
1-WL-GNN	GAT:Max	2	4	1	9	4	2	0	0	0	0
	GAT:Mean	3	4	6	6	7	4	0	0	0	0
	GAT:Sum	5	5	6	9	4	4	0	0	0	0
	GCN:Max	2	6	4	12	6	3	0	0	0	0
	GCN:Mean	3	5	3	10	8	2	0	0	0	0
	GCN:Sum	6	2	3	5	5	3	0	0	0	0
	GIN:Max	3	4	4	9	7	5	0	0	0	0
	GIN:Mean	2	6	2	10	7	3	0	0	0	0
	GIN:Sum	4	2	4	11	4	4	0	0	0	0

B.4. Unique Color Count utilized by 1-WL Algorithm

Table B.7.: Overview of the number of unique colors in the colorings computed by the 1-WL algorithm when applied to each dataset. Specifically, we specified the number of iterations of the 1-WL algorithm. Additionally, the "# Nodes" column showcases the maximum number of unique colors that can appear in the colorings.

	Dataset	Number of 1-WL Iterations											
		0	1	2	3	4	5	6	7	8	9	10	# Nodes
Classification	Enzymes	2	231	10 416	15 208	16 029	16 450	16 722	16 895	17 026	17 130	17 204	195 80
	Imdb-Binary	1	65	2 931	3 595	3 595	3 595	3 595	3 595	3 595	3 595	3 595	19 773
	Mutag	2	33	174	572	1 197	1 766	2 167	2 403	2 511	2 560	2 579	3 371
	Nci1	2	292	4 058	22 948	44 508	58 948	68 632	75 754	81 263	85 590	88 968	122 747
	Proteins	2	297	20 962	35 676	37 940	38 653	38 926	39 064	39 141	39 180	39 203	43 471
	Reddit-Binary	1	566	71 893	244 529	317 728	333 258	335 961	336 412	336 490	336 506	336 507	859 254
Regress.	Alchemy	2	70	4 782	164 224	620 332	995 264	1 166 951	1 216 094	1 225 861	1 227 632	1 227 904	2 046 329
	Alchemy(10k)	2	70	2 764	33 903	76 822	98 394	104 687	105 907	106 109	106 149	106 166	121 422
	Zinc	2	773	288 74	290 473	1 000 917	1 977 437	2 921 087	3 690 341	4 270 959	4 681 881	4 945 363	5 775 257
	Zinc(10k)	2	392	9 818	61 198	132 862	185 699	216 210	233 484	242 866	247 688	249 971	278 179

Approximation Performance on the ENZYMES Dataset

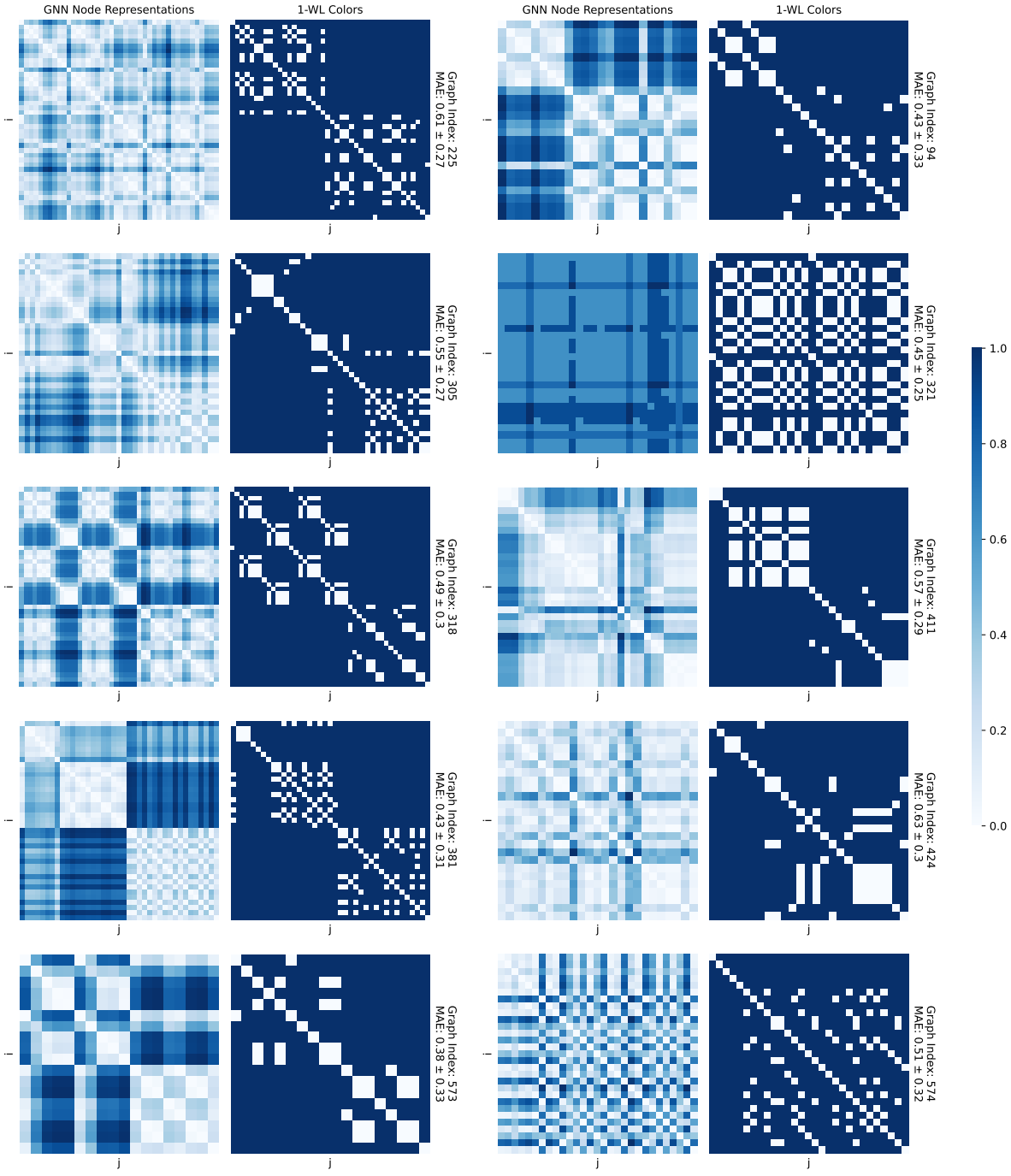

Figure B.13.: Visualizing the performance of the best performing GNN on the ENZYMES dataset in approximating node colors computed by the 1-WL algorithm. The ten graphs shown are randomly sampled from the GNN's test set. The average error for the entire test set is 0.49 ± 0.3.

Approximation Performance on the IMDB-BINARY Dataset

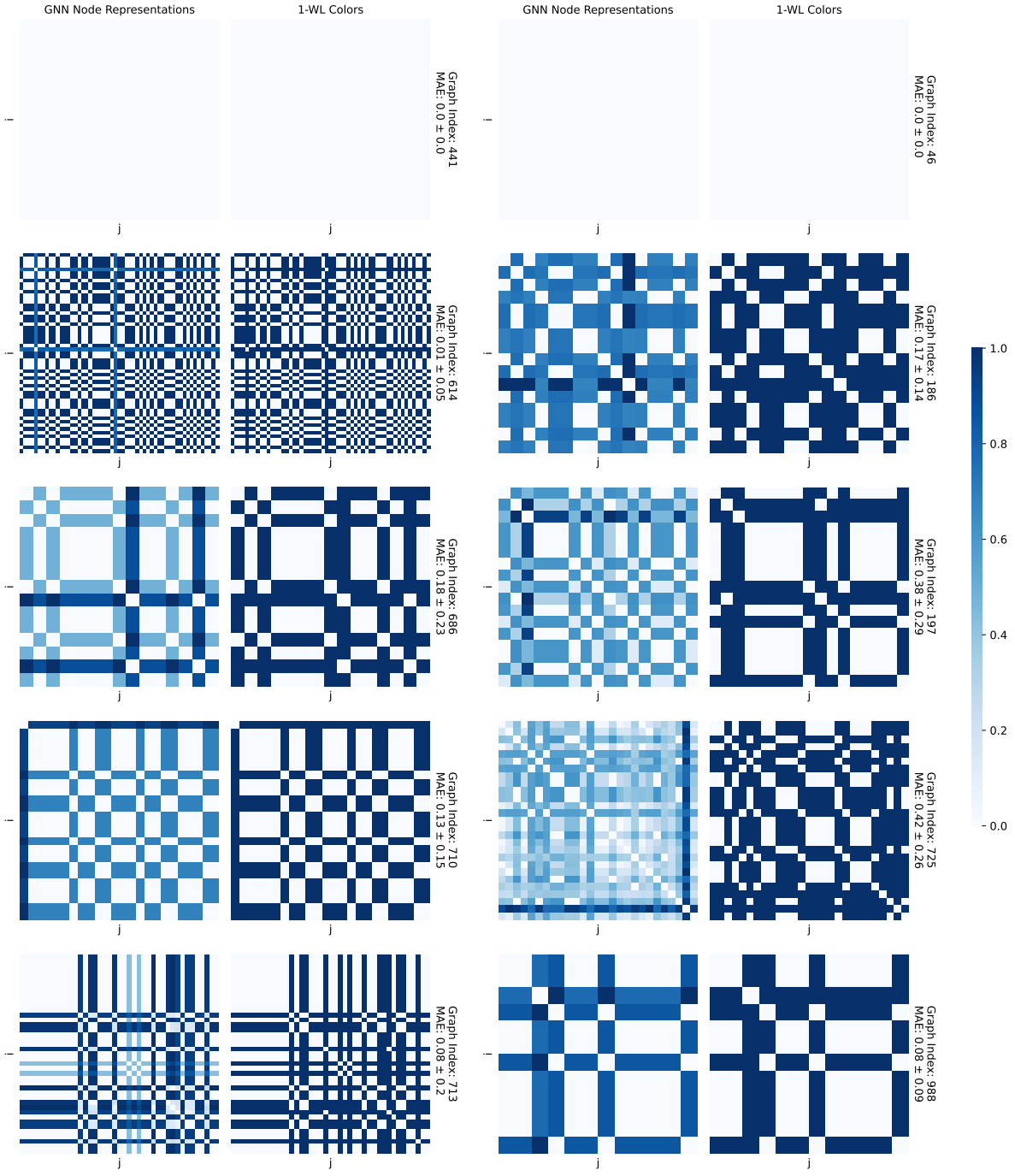

Figure B.14.: Visualizing the performance of the best performing GNN on the IMDB-BINARY dataset in approximating node colors computed by the 1-WL algorithm. The ten graphs shown are randomly sampled from the GNN's test set. The average error for the entire test set is 0.14 ± 0.15.

Approximation Performance on the MUTAG Dataset

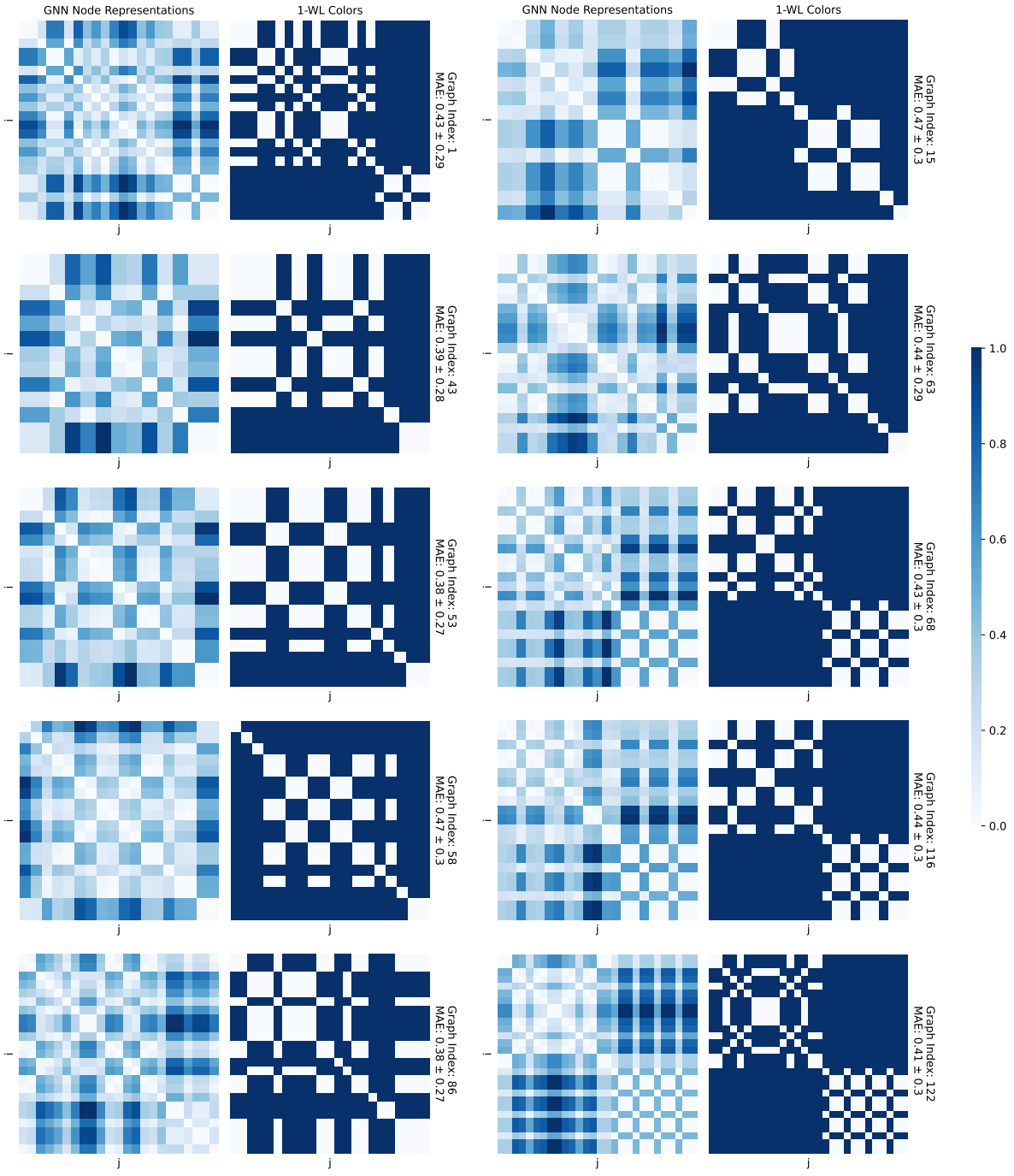

Figure B.15.: Visualizing the performance of the best performing GNN on the MUTAG dataset in approximating node colors computed by the 1-WL algorithm. The ten graphs shown are randomly sampled from the GNN's test set. The average error for the entire test set is 0.42 ± 0.29.

Approximation Capability on the NCI1 Dataset

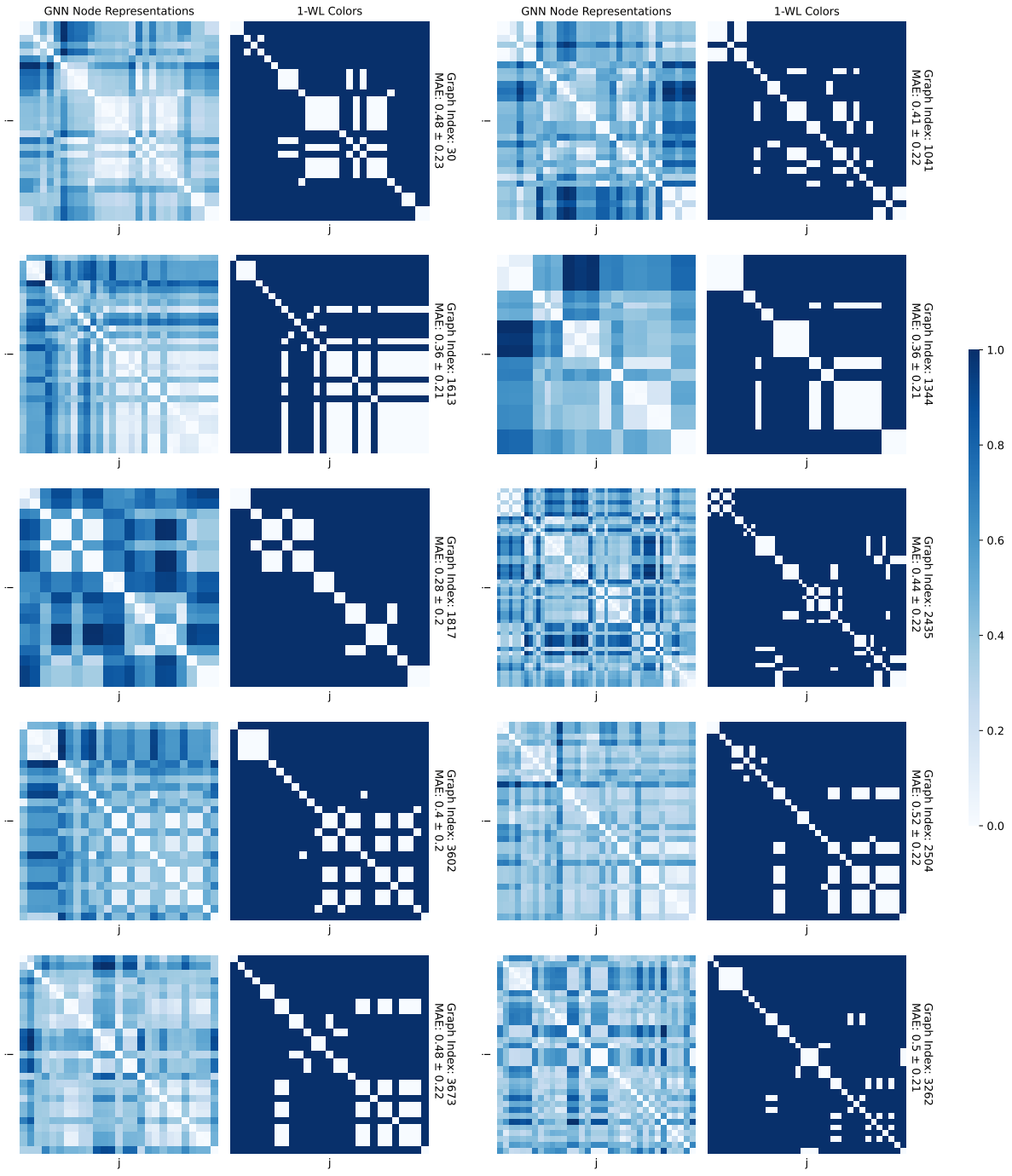

Figure B.16.: Visualizing the performance of the best performing GNN on the NCI1 dataset in approximating node colors computed by the 1-WL algorithm. The ten graphs shown are randomly sampled from the GNN's test set. The average error for the entire test set is 0.42 ± 0.22.

Approximation Capability on the NCI1 Dataset for 3 Iterations of the 1-WL Algorithm

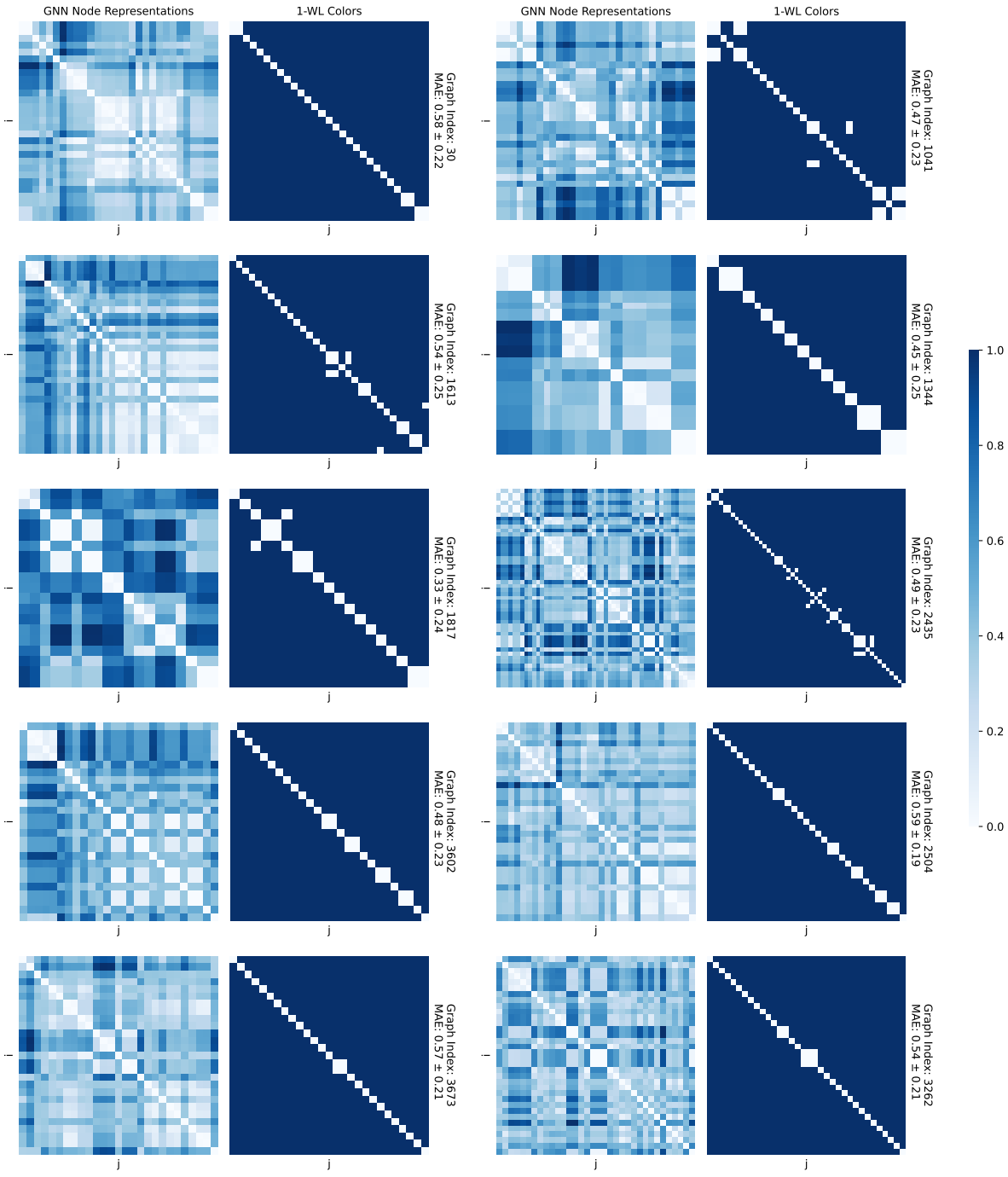

Figure B.17.: Visualizing the performance of the best performing GNN on the NCI1 dataset in approximating node colors computed by the 1-WL algorithm. The ten graphs shown are randomly sampled from the GNN's test set. The average error for the entire test set is 0.50 ± 0.24.

Approximation Performance on the PROTEINS Dataset

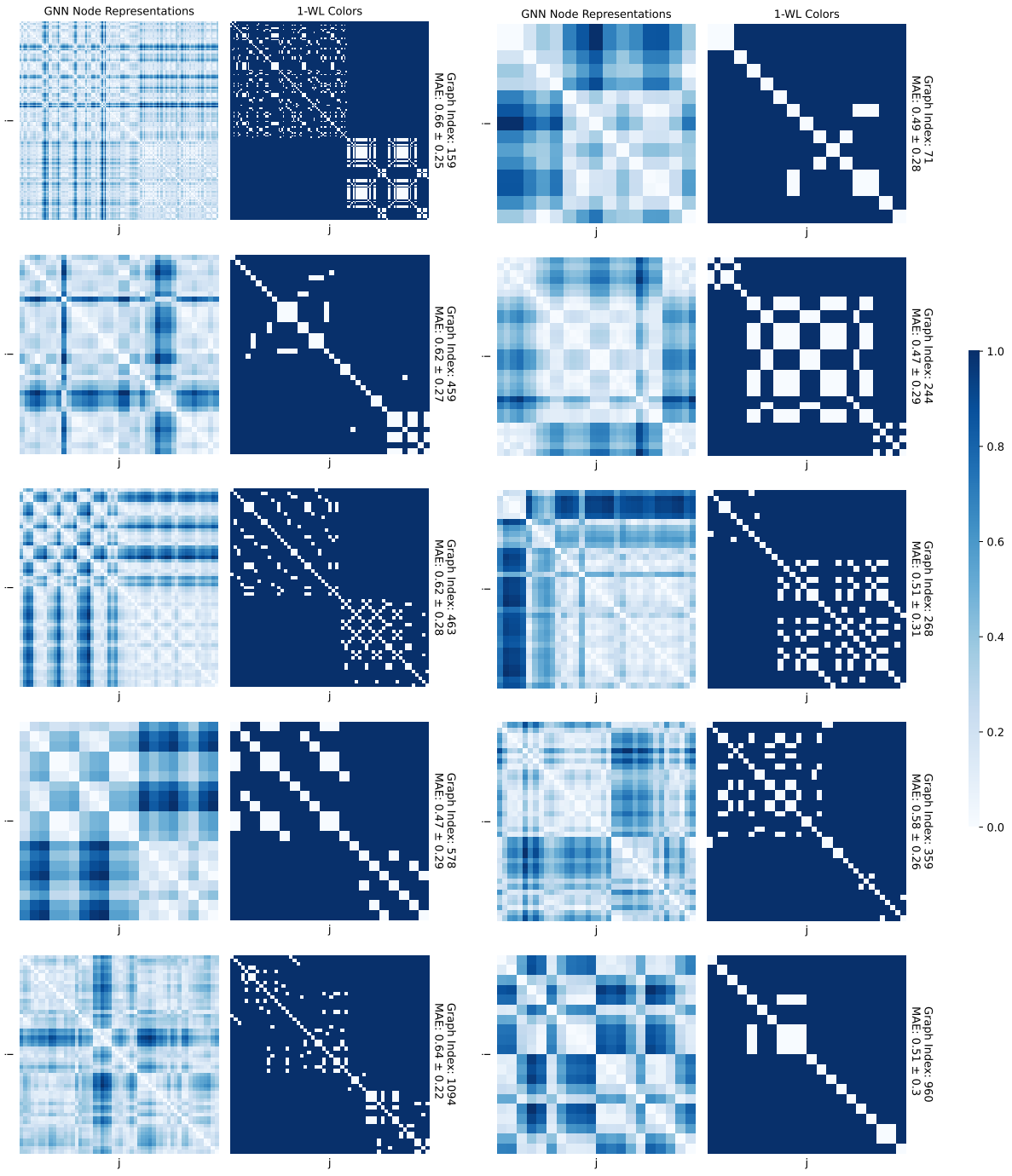

Figure B.18.: Visualizing the performance of the best performing GNN on the PROTEINS dataset in approximating node colors computed by the 1-WL algorithm. The ten graphs shown are randomly sampled from the GNN's test set. The average error for the entire test set is 0.49 ± 0.26.

Approximation Performance on the REDDIT-BINARY Dataset

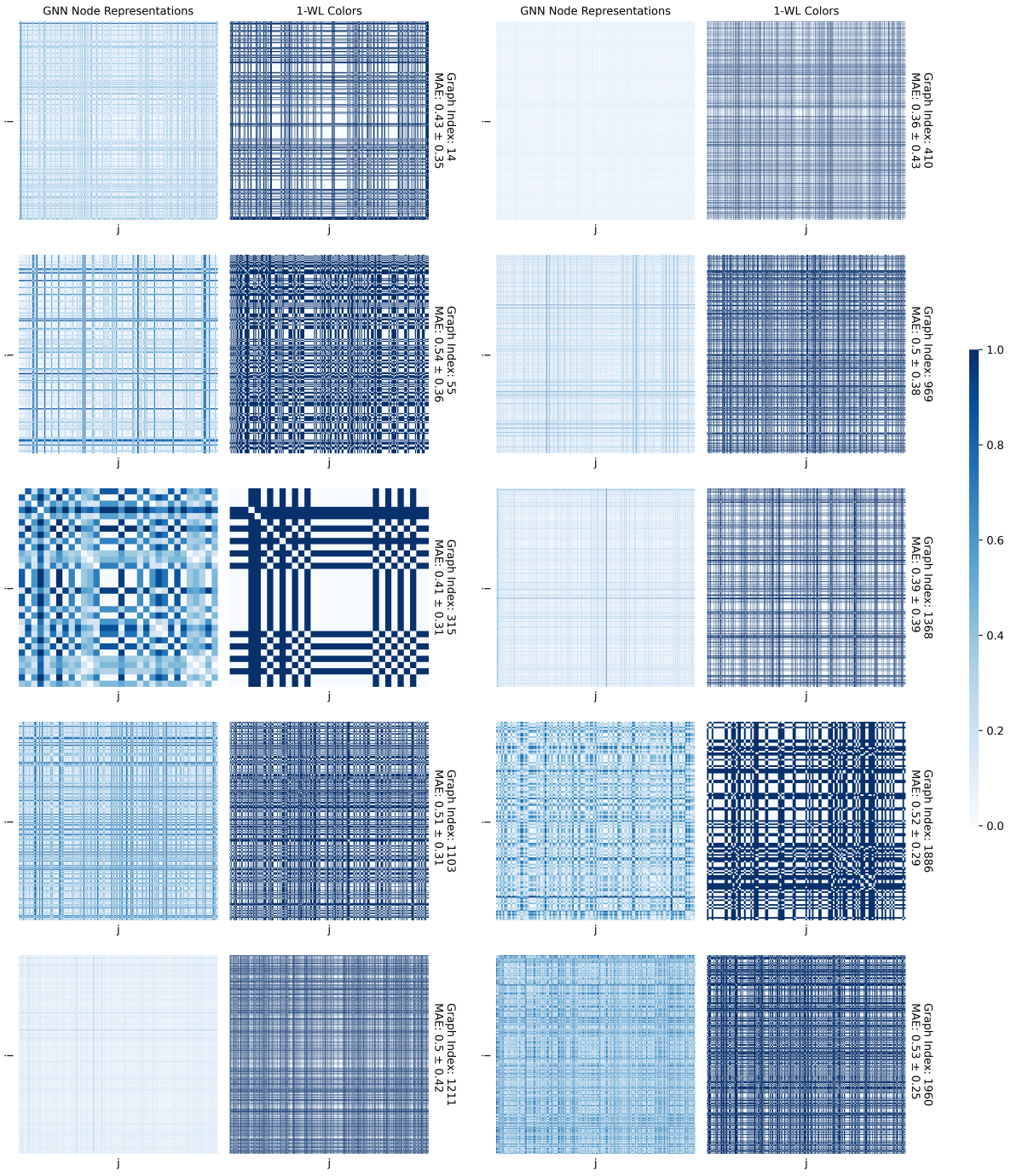

Figure B.19.: Visualizing the performance of the best performing GNN on the REDDIT-BINARY dataset in approximating node colors computed by the 1-WL algorithm. The ten graphs shown are randomly sampled from the GNN's test set. The average error for the entire test set is 0.48 ± 0.32.